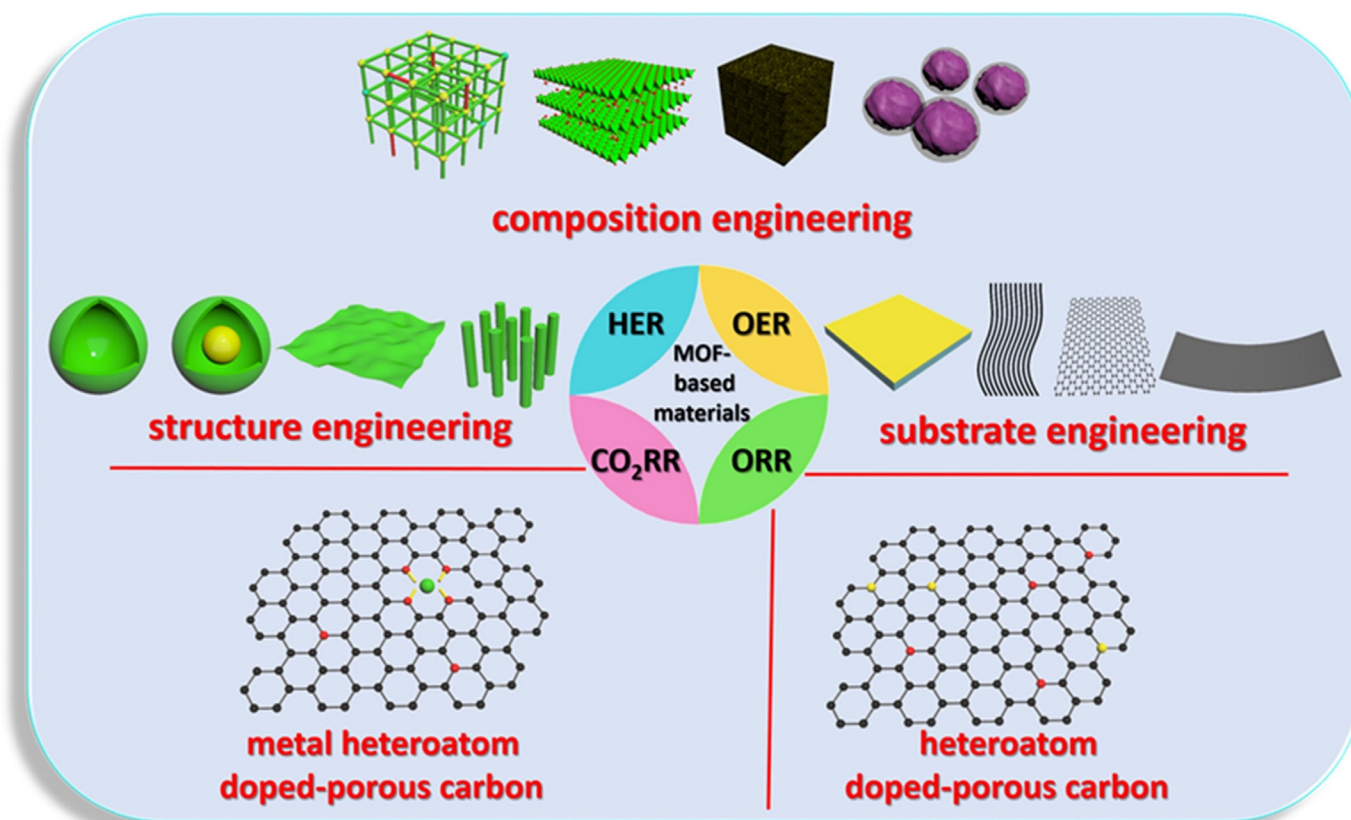


Special Issue **Recent Approaches to Design Electrocatalysts Based on Metal–Organic Frameworks and Their Derivatives**

Juan Liu<sup>+, [a]</sup> Shujin Hou<sup>+, [b]</sup> Weijin Li,<sup>[a]</sup> Aliaksandr S. Bandarenka,<sup>\*, [a, b]</sup> and Roland A. Fischer<sup>\*, [a]</sup>



**Abstract:** Rational design and synthesis of efficient electrocatalysts are important constituents in addressing the currently growing provision issues. Typical reactions, which are important to catalyze in this respect, include CO<sub>2</sub> reduction, the hydrogen and oxygen evolution reactions as well as the oxygen reduction reaction. The most efficient catalysts known up-to-date for these processes usually contain expensive and scarce elements, substantially impeding implementation of such electrocatalysts at a larger scale. Metal-organic frameworks (MOFs) and their derivatives containing affordable components and building blocks, as an emerging class of porous functional materials, have been recently attracting

a great attention thanks to their tunable structure and composition together with high surface area, just to name a few. Up to now, several MOFs and MOF-derivatives have been reported as electrode materials for the energy-related electrocatalytic application. In this review article, we summarize and analyze current approaches to design such materials. The design strategies to improve the Faradaic efficiency and selectivity of these catalysts are discussed. Last but not least, we discuss some novel strategies to enhance the conductivity, chemical stability and efficiency of MOF-derived electrocatalysts.

## 1. Introduction

Electrocatalysts are crucial for various renewable energy provision schemes. The latter involves several reactions such as hydrogen evolution reaction (HER),<sup>[1]</sup> oxygen evolution reaction (OER),<sup>[2]</sup> oxygen reduction reaction (ORR)<sup>[3]</sup> and carbon dioxide reduction reaction (CO<sub>2</sub>RR).<sup>[4]</sup> The present use of catalysts for HER, OER and ORR typically require elements, which are earth-scarce and often expensive.<sup>[5]</sup> While earth-abundant transition metals have shown promise in a number of electrocatalytic applications,<sup>[6]</sup> their direct use suffers from various undesirable effects such as aggregation, low efficiency and instability. Despite the fact that affordable metal electrodes such as copper, zinc and tin are usually utilized to catalyze electrochemical CO<sub>2</sub> reduction,<sup>[7]</sup> they often confronted with low Faraday efficiency and not acceptable selectivity. Rational design of electrocatalysts providing high efficiency and selectivity is nowadays a great challenge in this particular case.

Many efforts have been made during the last decades to design efficient HER, OER, ORR, and CO<sub>2</sub>RR electrocatalysts. These materials enable high current densities at low overpo-

tentials and low catalysts loadings with long-term stability and high selectivity in diverse electrochemical conversion systems.<sup>[5,8]</sup> Among the reported electrocatalysts, MOFs and MOF-derived materials have demonstrated their advantages through the uniquely controlled structure, high surface area, tunable pores, designable metal nodes and organic linkers to tailor the electrode surface morphology.<sup>[9]</sup> Generally, there are three main steps in an electrocatalytic process: i) adsorption of reactants at active surface sites; ii) formation of reaction intermediates and iii) desorption of the resulting products. Thus, the design strategies to improve efficiency and selectivity could focus on increasing the number of active sites and optimizing their adsorption properties (electronic structure). The merits of MOFs and MOFs derivatives would allow them to adjust the number of catalytic centers with high efficiency and optimize the electronic properties with relatively high predictability.


Herein, we will focus on the strategies to design MOF-based electrocatalysts with high efficiency and selectivity for HER, OER, ORR and CO<sub>2</sub>RR.


In the beginning, the approaches for increasing the density of the exposed active sites will be considered. Generally, the use of MOF-based materials can tailor the number of exposed catalytic centers due to their high and/or tunable surface area.<sup>[10]</sup> For instance, fabrication of MOFs as ultrathin nano-sheets or thin film can provide the opportunities to achieve high density of the exposed active sites.<sup>[11]</sup> On the other hand, utilization of nanostructured/porous supports<sup>[12]</sup> and downsizing/shaping the electrocatalysts<sup>[13]</sup> would also be a promising way to increase the number of exposed active sites. For example, Li and co-workers reported an example of preparing Co-based nanoparticles embedded in hollow N-doped carbon polyhedra for boosting the ORR/OER from pyrolysis-oxidation with Co-based MOF precursor.<sup>[14]</sup> These concepts offer the merits of high surface area and abundant hierarchical pores to increase the density of exposed active sites and accelerate the charge transfer. Afterwards, we will analyse strategies to increase the intrinsic activities of the MOFs and MOF-derivatives since the intrinsic activities of the electrocatalysts control the adsorption abilities of the catalysts surface towards reactants, reaction intermediates and products, and further determine


[a] Dr. J. Liu,<sup>†</sup> Dr. W. Li, Prof. Dr. A. S. Bandarenka, Prof. Dr. R. A. Fischer  
Department of Chemistry and Catalysis Research Center  
Technical University of Munich  
Lichtenbergstraße 4, 85748 Garching bei München (Germany)  
E-mail: bandarenka@ph.tum.de  
roland.fischer@tum.de

[b] S. Hou,<sup>†</sup> Prof. Dr. A. S. Bandarenka  
Department of Physics  
Technical University of Munich  
James-Frank-Straße 1, 85748 Garching bei München (Germany)

[†] These authors contributed equally to this work.

 The ORCID identification number(s) for the author(s) of this article can be found under:  
<https://doi.org/10.1002/asia.201900748>.

 © 2019 The Authors. Published by Wiley-VCH Verlag GmbH & Co. KGaA. This is an open access article under the terms of the Creative Commons Attribution-NonCommercial-NoDerivs License, which permits use and distribution in any medium, provided the original work is properly cited, the use is non-commercial and no modifications or adaptations are made.

 This manuscript is part of a special issue on Metal-Organic Frameworks and Their Applications. Click here to see the Table of Contents of the special issue.

the selectivity of the products. The intrinsic activities of the MOFs and MOF-derivatives are influenced by intrinsic characteristics, including electronic properties, conductivity, and stability, etc. In the following sections, the modulation of the metal noded/organic linkers,<sup>[15]</sup> loading nanoparticles/guest molecules into porous MOFs or

MOF-derivatives,<sup>[9b]</sup> rationally chosen of MOF as electrocatalysts and carbonizing the MOFs to conductive carbon-based materials,<sup>[16]</sup> will be discussed for improving the electronic properties and conductivities of the MOF-based catalysts and further optimizing the intrinsic activities of MOF-based catalysts. Regarding the construction of electrically conductive MOFs, we will guide the readers to the reported reviews.<sup>[17]</sup> Besides, The stability of the electrode materials is crucial for the long-term duration. Therefore, the stability of the MOFs on the electrode will be discussed in the corresponding section (strategy). While the discussion of the stability of the MOFs themselves (e.g. in water, etc.) also will be guided to the previous review.<sup>[18]</sup>

## 2. Design of MOF-based materials with high activity towards water splitting and oxygen reduction reaction

### 2.1. MOF-based electrocatalysts for the hydrogen evolution reaction

The typical electrochemical water splitting consists of two half-reactions: one is the hydrogen evolution reaction, and another

is the oxygen evolution reaction that occurs at the cathode and anode sides, respectively.<sup>[19]</sup>

In principle, HER is a two-electron transfer reaction; and in both acidic and alkaline conditions it can be described as given below:

In acidic media:



In neutral or alkaline media:



Electrochemical processes usually need sufficient energy to overcome activation energy barriers, which are associated with so-called overpotentials in electrochemistry. By utilization of

**Juan Liu** obtained her PhD from Fujian Institute of Research on the Structure of Matter (FJIRSM), Chinese Academy of Sciences (CAS) in 2017 under the supervision of Prof. Jian Zhang. Afterwards, she joined the group of Prof. Roland A. Fischer as a Post-doc in 2017. Currently, she is a Post-doc in collaboration with Prof. Roland A. Fischer at Technical University of Munich, Germany with the support of Sino-Germany (CSC-DAAD) Joint Post-doc Fellowship. Her research interests focus on the preparation of metal-organic frameworks for catalysis, particularly for using chiral metal-organic frameworks.



**Shujin Hou** received his bachelor's degree in chemical engineering and technology from Tianjin Polytechnic University in 2015. Subsequently, he went to East China Normal University to do his master thesis under the supervision of Prof. Likun Pan and obtained his master degree in material science and optoelectronics in 2018. Currently, he works in the Prof. Aliaksandr S. Bandarenka's group to pursue his PhD. degree with the support of CSC scholarship. His research interest focuses on the design and synthesis of MOFs and MOF-derived materials for enhanced electrocatalysis.



**Weijin Li** received his PhD degree from Fujian Institute of Research on the Structure of Matter (FJIRSM), Chinese Academy of Sciences (CAS) under the supervision of Prof. Rong Cao in 2015. After one-year (2015–2016) Post-doc in collaboration with Prof. Rong Cao at the FJIRSM, CAS, Prof. Xinchen Wang at Fuzhou University, Prof. Lasheng Long and Prof. Jun Tao at Xiamen University in the Collaborative Innovation Center of Chemistry for Energy Materials (2011-iChEM), he joined Prof. Roland A. Fischer's group in 2016 as a Post-doc with the support of Sino-Germany (CSC-DAAD) Joint Post-doc Fellowship (2016–2017) and Alexander von Humboldt Fellowship. His research interests focus on the development of MOF thin films for various devices and electrocatalytic applications.



**Aliaksandr S. Bandarenka** received his PhD from Belarusian State University in 2005. After a postdoc at the University of Twente, Netherlands and Technical University of Denmark, he joined the Center for Electrochemical Sciences (CES) at Ruhr University Bochum as a group leader (2010–2014). Currently, he is an Assistant Professor at the Department of Physics, Technical University of Munich, Germany. His research interests focus on the development of electrocatalysts, methodologies for characterization and modification of electrified solid/liquid interfaces, and interfacial charge transfer.



**Roland A. Fischer** received his Dr.rer.nat. from Technical University Munich (TUM) in 1989. After a postdoc at the University of California, Los Angeles he returned to TUM in 1990, where he obtained his Habilitation in 1995. He was Associate Professor at Heidelberg University (1996–1997) and Full Professor for Inorganic Chemistry at Ruhr-University Bochum (1997–2015). In 2016 he returned to TUM and took the Chair of Inorganic and Metal-Organic Chemistry. He has been elected Vice President of the Deutsche Forschungsgemeinschaft (DFG) in 2016. His research focuses on group 13/transition metal compounds and clusters, precursors for chemical vapor deposition (CVD) and the materials chemistry of metal-organic frameworks (MOFs).





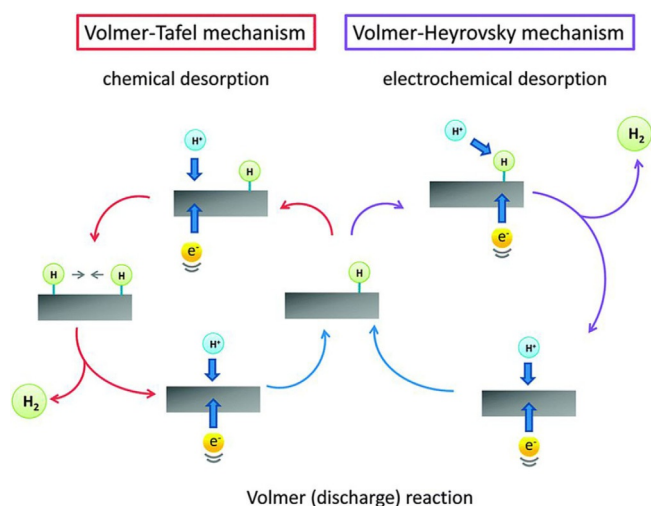
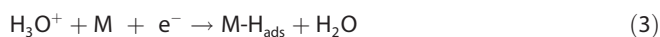


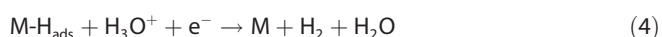
**Figure 1.** Schematic illustration of the hydrogen evolution mechanism in acidic media. Reproduced with permission from reference [20a]. Copyright 2014, Royal Society of Chemistry.

appropriate electrocatalysts, the overpotential can be reduced substantially and the reaction rate and efficiency can be increased. In acidic media, the HER is considered as a multi-step reaction [Eqs. (3)–(5)]. Depending on the applied potential and electrocatalyst surface, the HER can proceed through two possible reaction pathways, which can be in some cases distinguished experimentally (Figure 1).<sup>[20]</sup> The first step is known as the Volmer step:<sup>[20a,21]</sup> one electron is transferred through the interface, and one proton is adsorbed at the surface of the catalyst resulting in the adsorbed hydrogen atom [Eq. (3)]:



where M designate one surface adsorption site. The Volmer step can be followed by so-called

Heyrovsky step according to the following Scheme:



Alternatively, the Tafel step or chemical desorption can occur [Eq. (5)]:



Currently, Pt-based catalysts show the best performance for the HER in the absolute majority of cases.<sup>[22]</sup> However, their high cost and limited availability often question their high-scale applications.<sup>[23]</sup> Thus, the development of earth-abundant alternatives is of great importance. Over the past decade, numerous strategies and compounds have been explored to develop efficient and low price non-noble electrocatalysts for HER, such as transition metal compounds,<sup>[19,24]</sup> carbon-based or heteroatom-doped carbon materials<sup>[21a,25]</sup> and conducting polymers.<sup>[26]</sup> Recently, MOFs, which constructed by the coordination bonding of metal ions or clusters as inorganic building nodes and organic ligands as linkers, have attracted a quickly

growing interest as electrocatalysts or precursors to electrocatalysts owing to their high specific surface area, well-defined porous structures and readily accessible active sites.<sup>[27]</sup> The utilization of MOFs as active materials is possible to maximize the density of catalytically active sites and to optimize their binding strength to reaction intermediates.<sup>[28]</sup> MOFs have been proved to be a class of ideal templates or precursors for electrocatalytic reaction, due to their innate porosity and abundant carbon source from the organic ligands.<sup>[27b,28c,29]</sup> Tremendous efforts have been made to improve electrocatalytic performance of MOFs (Table 1) and MOFs-derived materials (Table 2), including the composition morphology engineering (hollow or yolk-shell structures,<sup>[30]</sup> 3D networks,<sup>[31]</sup> 2D nano-sheets,<sup>[32]</sup> 1D nanowires<sup>[33]</sup> and 0D nanoparticles or quantum dots<sup>[34]</sup>) and the substrate engineering.<sup>[34b,35]</sup> The conductivity of electrocatalysts is one of the parameters that largely influences the efficiency of electrocatalytic systems. However, most of the reported MOFs are semiconductors or insulators. In order to improve electrocatalytic performance, conductive MOFs are welcome. At this point, the strategy based on modulating the metal nodes and organic linker and further tailoring the structure, which denoted as structure engineering, is employed to build conductive MOFs.<sup>[17,36]</sup> Nishihara et al synthesized nickel bis(dithiolene) complex nanosheets via a liquid-liquid interfacial reaction to give the material with high conductivity of  $0.15 \text{ S cm}^{-1}$  at 298 K and a reversible redox activity, which could lead to applications in electrocatalytic processes.<sup>[36b]</sup> Afterwards, Marinescu et al achieved two-dimensional metal-organic surfaces through a coordination reaction between cobalt dithiolene and a trinucleating conjugated ligand (Figure 2).<sup>[37]</sup> The developed nanostructured material was used to catalyse the HER under fully aqueous conditions and reach  $10 \text{ mA cm}^{-2}$  current density with a relatively moderate overpotential of 0.34 V at pH 1.3. Furthermore, Marinescu et al modulated the metal nodes and organic linkers to achieve the synthesis of metal selenolate polymers via integrating benzene-1,2,4,5-tetraseselenolate with cobalt and nickel (Figure 2b and c).<sup>[38]</sup> The cobalt selenolate polymer can catalyse the HER, achieving a current density of  $10 \text{ mA cm}^{-2}$  at the overpotential of 343 mV at pH 1.3.

Based on the tailoring, the metal nodes and organic linkers, Feng et al have made great efforts in terms of immobilizing molecular metal dithiolene complexes on two-dimensional MOFs.<sup>[39]</sup> They demonstrated a reliable Langmuir–Blodgett (LB) method for the synthesis of two-dimensional supramolecular polymer single-layer sheets. The as-prepared triphenylene-fused nickel bis(dithiolene) complexes showed a  $10 \text{ mA cm}^{-2}$  HER current density at a slightly lower operating overpotential of 333 mV.<sup>[39b]</sup> Furthermore, they constructed a type of novel two-dimensional MOFs by incorporating organic ligands (2,3,6,7,10,11-triphenylenehexathiol and 2,3,6,7,10,11-triphenylenehexamine) with metal cobalt and nickel ions.<sup>[39a]</sup> These cobalt-based electrocatalysts demonstrated even lower operating overpotential of 283 mV to achieve an HER current density of  $10 \text{ mA cm}^{-2}$  in  $0.5 \text{ M H}_2\text{SO}_4$  aqueous solutions. Meanwhile, another strategy was elaborated by the same group to further improve HER performance via coupling the two-dimensional

**Table 1.** Typical examples of HER activities of pristine MOFs.

Material	Strategy used	Electrolyte	Substrate	Overpotential [mV] at 10 mA cm <sup>-2</sup>	Ref.
Cobalt dithiolene films MOS-1	(2D) structure engineering	H <sub>2</sub> SO <sub>4</sub> solution pH 1.3	glassy carbon	340	[37]
Cobalt dithiolene films MOS-2	(2D) structure engineering	H <sub>2</sub> SO <sub>4</sub> solution pH 1.3	glassy carbon	530	[37]
cobalt selenolate polymer	composition engineering	0.1 M NaOCl <sub>4</sub> pH 1.3	glassy carbon	343	[38]
THTNi 2DSP sheets	(2D) structure engineering	0.5 M H <sub>2</sub> SO <sub>4</sub> solution	glassy carbon	333	[39b]
THTNi 2DSP sheets	(2D) structure engineering	0.05 M KOH pH 15.3	glassy carbon	574	[39b]
THT-Co single-layer	(2D) structure engineering	0.5 M H <sub>2</sub> SO <sub>4</sub> solution	glassy carbon	323.0 ± 2.0	[39a]
THTA-Ni single-layer	composition engineering	0.5 M H <sub>2</sub> SO <sub>4</sub> solution	glassy carbon	315.0 ± 1.7	[39a]
THTA-Co single-layer	composition engineering	0.5 M H <sub>2</sub> SO <sub>4</sub> solution	glassy carbon	283.0 ± 1.5	[39a]
THTA-Co/G	substrate engineering	0.5 M H <sub>2</sub> SO <sub>4</sub> solution	graphene	230.0 ± 2.2	[39a]
POMOF ε(trim) <sub>4/3</sub>	composition engineering	1 M LiCl + HCl pH 1	carbon paste	–	[40]
Ni-BTT	composition engineering	0.1 M NaClO <sub>4</sub> pH 1.3	glassy carbon	470	[44]
NENU-500	composition engineering	0.5 M H <sub>2</sub> SO <sub>4</sub> solution	glassy carbon	237	[41]
NENU-501	composition engineering	0.5 M H <sub>2</sub> SO <sub>4</sub> solution	glassy carbon	392	[41]
NENU-499	composition engineering	0.5 M H <sub>2</sub> SO <sub>4</sub> solution	glassy carbon	570	[41]
NENU-5	composition engineering	0.5 M H <sub>2</sub> SO <sub>4</sub> solution	glassy carbon	585	[41]
ε(trim) <sub>4/3</sub>	composition engineering	0.5 M H <sub>2</sub> SO <sub>4</sub> solution	glassy carbon	515	[41]
HKUST-1	composition engineering	0.5 M H <sub>2</sub> SO <sub>4</sub> solution	glassy carbon	691	[41]
Ru-ε <sub>2</sub> (trim) <sub>2</sub>	composition engineering	0.1 M H <sub>2</sub> SO <sub>4</sub> pH 1	glassy carbon	617	[45]
ε(BTB) <sub>4/3</sub>	composition engineering	0.1 M H <sub>2</sub> SO <sub>4</sub> pH 1	glassy carbon	576	[45]
Co-ε(trim) (bpy) <sub>2</sub>	(1D) structure engineering	0.1 M H <sub>2</sub> SO <sub>4</sub> pH 1	glassy carbon	452	[45]
Co-ε(BTB) <sub>4/3</sub>	composition engineering	0.1 M H <sub>2</sub> SO <sub>4</sub> pH 1	glassy carbon	419	[45]
Ru-ε <sub>2</sub> (biphen) <sub>2</sub>	composition engineering	0.1 M H <sub>2</sub> SO <sub>4</sub> pH 1	glassy carbon	337	[45]
PPh <sub>4</sub> -ε <sub>2</sub> (trim) <sub>2</sub>	composition engineering	0.1 M H <sub>2</sub> SO <sub>4</sub> pH 1	glassy carbon	335	[45]
GO/Cu-MOF	substrate engineering	0.5 M H <sub>2</sub> SO <sub>4</sub> solution	glassy carbon	209 at 30 mA cm <sup>-2</sup>	[46]
NiFe-MOF/nickel foam	substrate engineering	0.1 M KOH solution	nickel foam	134	[32a]

**Table 2.** Activities of some MOF-derived materials towards the HER.

Material	Strategy used	Electrolyte	Substrate	Overpotential [mV] at 10 mA cm <sup>-2</sup>	Ref.
PtCoFe@CN	composition engineering	0.5 M H <sub>2</sub> SO <sub>4</sub> solution	glassy carbon	45	[47a]
Ni-0.2NH <sub>3</sub>	composition engineering	1 M KOH solution	glassy carbon	61	[34a]
Ni@graphene	composition engineering	1 M KOH solution	glassy carbon	240	[57]
CoP NRAs	composition engineering	0.5 M H <sub>2</sub> SO <sub>4</sub> solution	glassy carbon	181	[58]
Ni <sub>2</sub> P-CoP	composition engineering	0.5 M H <sub>2</sub> SO <sub>4</sub> solution	glassy carbon	105	[59]
Co <sub>0.85</sub> Se@NC	composition engineering	1 M KOH solution	glassy carbon	230	[60]
CoS <sub>2</sub> -(0.2–0.02)-12	composition engineering	1 M PBS buffer solution pH 7	FTO film	168	[50]
W-SAC(single atom catalyst)	composition engineering	0.1 M KOH/0.5 M H <sub>2</sub> SO <sub>4</sub>	glassy carbon	85/105	[28b]
Ni <sub>3</sub> ZnCo <sub>0.7</sub> -550	composition engineering	1 M KOH solution	glassy carbon	93	[61]
Zn <sub>0.30</sub> Co <sub>2.70</sub> S <sub>4</sub>	composition and structure engineering	0.5 M H <sub>2</sub> SO <sub>4</sub> /0.1 M phosphate buffer/1 M KOH	glassy carbon	80/90/85	[30b]
CoP hollow polyhedron	structure engineering	0.5 M H <sub>2</sub> SO <sub>4</sub> solution	glassy carbon	159	[53a]
hollow bimetallic Zn <sub>0.1</sub> Co <sub>0.9</sub> Se <sub>2</sub>	composition and structure engineering	0.5 M H <sub>2</sub> SO <sub>4</sub> solution	glassy carbon	140	[30a]
Co <sub>4</sub> Ni1P nanotubes	structure engineering	1 M KOH/1 M PBS/0.5 M H <sub>2</sub> SO <sub>4</sub>	rotating disk electrode	129/134/131	[33a]
Co-P@NC	structure engineering	0.5 M H <sub>2</sub> SO <sub>4</sub> solution	glassy carbon	98	[32b]
CoP/NCNHP hollow polyhedron	structure engineering	0.5 M H <sub>2</sub> SO <sub>4</sub> /1 M KOH	glassy carbon	140/115	[62]
CoS <sub>2</sub> @MoS <sub>2</sub> microcubes	structure engineering	0.5 M H <sub>2</sub> SO <sub>4</sub> solution	glassy carbon	239	[63]
CoS <sub>2</sub> NTA	substrate engineering	1 M KOH solution	carbon cloth	193	[55]
Co@NC/NF	substrate engineering	1 M KOH solution	nickel foam	240	[47b]
CoP/rGO-400	substrate engineering	0.5 M H <sub>2</sub> SO <sub>4</sub> /1 M KOH solution	reduced graphene oxide	105/150	[35b]
Co-Ni-Se/C/NF	substrate engineering	1 M KOH solution	nickel foam	90	[35a]
CoSe <sub>2</sub> /CF	substrate engineering	1 M KOH solution	carbon fibers	95	[34b]
NF@Ni/C-600	substrate engineering	1 M KOH solution	nickel foam	37	[64]

MOFs with graphene. Based on these results, the efficient electrochemical H<sub>2</sub> production might be ascribed to the unique

two-dimensional structure, conductive-conjugated organic ligands and the synergistic effect between metal, S and N.

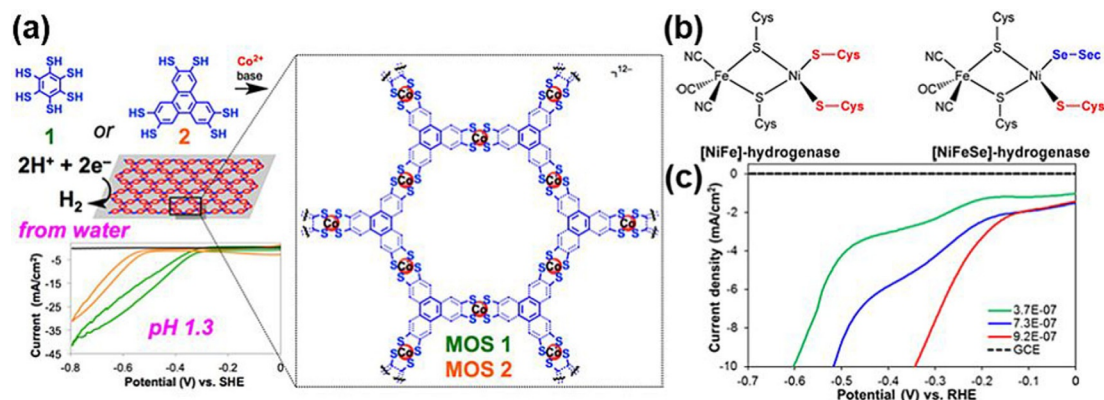


**Figure 2.** a) Illustration of synthesis of the two-dimensional cobalt dithiolenate catalyst for the HER. Reproduced with permission from reference [37]. Copyright 2014, American Chemical Society. b) and c) The active sites of [NiFe] and [NiFeSe] hydrogenases in metal selenolate polymers and corresponding voltammetric characterisation of these materials concerning the electrochemical hydrogen evolution activity. b) and c) Reproduced with permission from reference [38]. Copyright 2016, American Chemical Society.

Also, the introduction of polyoxometalates (POMs) into the MOF frameworks is another promising concept to improve HER activity. Nohra et al presented the first example using a type of novel polyoxometalate (POM)-based MOF for HER.<sup>[40]</sup> The reported  $(\text{TBA})_3[\text{PMo}^{\text{V}}_8\text{Mo}^{\text{VI}}_4\text{O}_{36}(\text{OH})_4\text{Zn}_4][\text{C}_6\text{H}_3(\text{COO})_3]_{4/3} \cdot 6\text{H}_2\text{O}$  ( $\epsilon$ (trim)<sub>4/3</sub>) (TBA = tetrabutylammonium) was synthesized by grafting triangular 1,3,5-benzene tricarboxylate linkers on the Zn- $\epsilon$ -Keggin inorganic building blocks, and the structure showed a high turnover number but the overpotential at a current density of  $10 \text{ mA cm}^{-2}$  for HER was not mentioned in the literature. Remarkably, another two novels POM based-MOFs (NENU-500 and NENU-501) with similar POM units and different organic fragments were reported for HER by Qin et al. in 2015.<sup>[41]</sup> As shown in Figure 3, they were tested for the HER activity in acidic aqueous solutions ( $0.5 \text{ M H}_2\text{SO}_4$ ), and NENU-500 exhibited the highest activity (with an overpotential of 237 mV at  $10 \text{ mA cm}^{-2}$ ) if compared with other MOFs discussed in this review. The high HER activity is probably ascribed to the redox-active sites from the POMs.

Apart from the pristine MOFs, the MOF-derivatives also attracted great attention for the HER. MOFs were applied as a sacrificial template by taking the advantages of their porous structures, controlled morphologies and easily tunable metal-ligand junctions.<sup>[27a,42]</sup> So far, a number of MOF-derived materi-

als have been developed via effective post-treatment under various experimental conditions.<sup>[43]</sup> To this approach, the catalysts conductivity can also be optimized.

Pyrolysis of MOFs to result in the carbon-supported electrocatalysts is one of the promising post-treatment techniques. The composition of the pyrolysis products can be controlled with relative ease by the MOFs precursors. We define the composition controllable process to convert MOFs to MOF-derivatives as "composition engineering". Based on the latter, the well-organised MOFs can be easily converted into carbon-supported transition metal nanohybrids with ultrahigh porosity, extraordinarily large surface area and high conductivity after thermal treatment of MOFs in an appropriate atmosphere.<sup>[28b,34a,47]</sup> The carbonization of MOFs into porous carbon skeletons are one of the promising pathways for accelerating electrons and ions transfer to improve the electrocatalytic activity. For instance, Chen et al demonstrated that the MOF-derived PtCoFe@CN electrocatalysts prepared by pyrolysis in a nitrogen atmosphere exhibit HER overpotential of 45 mV at  $10 \text{ mA cm}^{-2}$  (Figure 4).<sup>[47a]</sup> This rather remarkable activity was not only attributed to the modified electronic structures of the active sites resulting from the alloying of Pt with Co and Fe, but also originated from the good conductivity of N-doped carbon shells. Furthermore, Wang et al developed an efficient

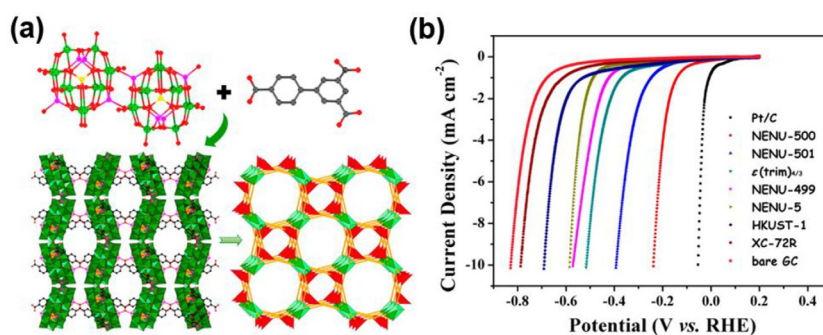


**Figure 3.** a) Schematics of the synthesis procedure for NENU-501 through the reaction of the dimeric Zn- $\epsilon$ -Keggin unit and the BPT3- fragment. b) HER activity assessment of different catalysts using the voltammograms recorded in  $0.5 \text{ M H}_2\text{SO}_4$ . Reproduced with permission from reference [41]. Copyright 2015, American Chemical Society.

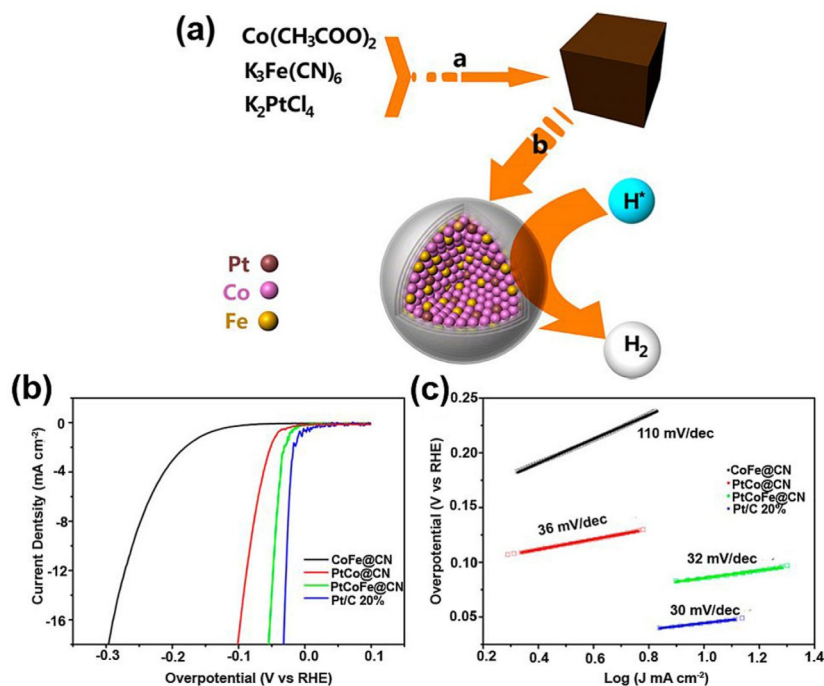


**Figure 4.** a) Schematic representation of the synthesis of the MOF-derived PtCoFe@CN electrocatalysts. b) and c) HER activity and Tafel plots for the various catalysts. Reproduced with permission from reference [47a]. Copyright 2017, American Chemical Society.

noble-metal-free catalyst for hydrogen evolution through the pyrolysis of a Ni-based MOFs ( $\text{Ni}_2(\text{bdc})_2\text{ted}$  (bdc = 1,4-benzenedicarboxylic acid; ted = triethylene-diamine)) in  $\text{NH}_3$ .<sup>[34a]</sup> The catalyst, composed of Ni nanoparticles and a surface-nitrified carbon layer coating, exhibits the overpotential of 61 mV at  $10 \text{ mA cm}^{-2}$ . They also reported the unique carbon-removal effect of  $\text{NH}_3$  during pyrolysis of MOFs that might lead this material to be one of the best for HER among the reported Ni-based noble metal-free HER catalysts.

Apart from the development of pure metal or alloy nanoparticles in carbon matrices, MOF-derived nanostructured transition metal carbides, nitrides, sulfides, phosphides and selenides have also been explored as the catalysts for HER owing to their special physical and chemical properties: (I) organic ligands-derived porous carbon skeletons play an important role in promoting fast electron transfer and ions diffusion; (II) homogeneously distributed transition metal hybrids in carbon matrix show smaller size and more accessible active sites; (III) various heteroatoms can significantly facilitate electrocatalytic process by optimizing the electronic structures of metal atom or species and improve electric conductivity.<sup>[27b, 43a]</sup> Among non-precious transition metal hybrids, the group IV-VI metal carbides and nitrides have attracted considerable attention due to their distinct electronic structure, which may help to easily adsorb and activate hydrogen.<sup>[28b, 48]</sup> For instance, Wu et al demonstrated a novel MOF-assisted strategy to synthesize porous  $\text{MoC}_x$  nano-octahedrons for hydrogen production (Figure 5a and b).<sup>[48a]</sup> In this work, they initially introduced polyoxometalates (POMs) guest into the pores of the MOFs host at ambient temperature, and then the as-prepared samples containing a substantial amount of Mo-based POMs were directly

in situ-converted into  $\text{MoC}_x\text{-Cu}$  during a heating process. Finally, ultrafine primary  $\text{MoC}_x$  nanocrystallites embedded in the porous carbon matrix were obtained through the removal of the metallic Cu with  $\text{Fe}^{3+}$  ions. Although the as-prepared  $\text{MoC}_x$  electrocatalyst showed higher overpotentials of 142 and 151 mV to achieve current density of  $10 \text{ mA cm}^{-2}$  in 0.5 M  $\text{H}_2\text{SO}_4$  and 1 M KOH, respectively, the Tafel slope of  $\text{MoC}_x$  electrocatalyst ( $59 \text{ mV dec}^{-1}$ ) is smaller than that of the Pt/C catalyst ( $113 \text{ mV dec}^{-1}$ ) with the same mass loading of the catalysts. Also, transition metal phosphides, sulfides and selenides have also been referred to as promising HER catalysts, because their hydrogen evolution on the surface active sites behave somewhat like at the hydrogenase or nitrogenase. Xu et al. used Co-MOF (ZIF-67) as the precursor and a template to synthesize porous CoP concave polyhedron electrocatalysts with a low-temperature multi-step calcination process.<sup>[49]</sup> The as-prepared sample showed an overpotential of 133 mV for obtaining at  $10 \text{ mA cm}^{-2}$  in 0.5 M  $\text{H}_2\text{SO}_4$  (Figure 5c and d). A Tafel slope of 51 mV per decade was calculated in that case. The better catalytic performance of porous CoP concave polyhedron should be associated with the porous structure, large surface area and highly conductive carbon network. Hod's group developed a facile experimental method to synthesize porous amorphous  $\text{CoS}_x$  by the electrochemical conversion of ZIF-67 MOF with various potential scan rates during the CV-cycling.<sup>[50]</sup> As shown in Figure 5e and f, the as-prepared  $\text{CoS}_x\text{-(0.2-0.02)-12}$ , obtained after an electrochemical conversion of ZIF-67 (12 growth cycles) with altered scan rates from 0.2 to  $0.02 \text{ V s}^{-1}$ , the overpotential of 168 mV at  $10 \text{ mA cm}^{-2}$  in neutral pH. This work proposed a facile and general strategy to converse MOFs into amorphous metal sulfides for electrocatalytic appli-



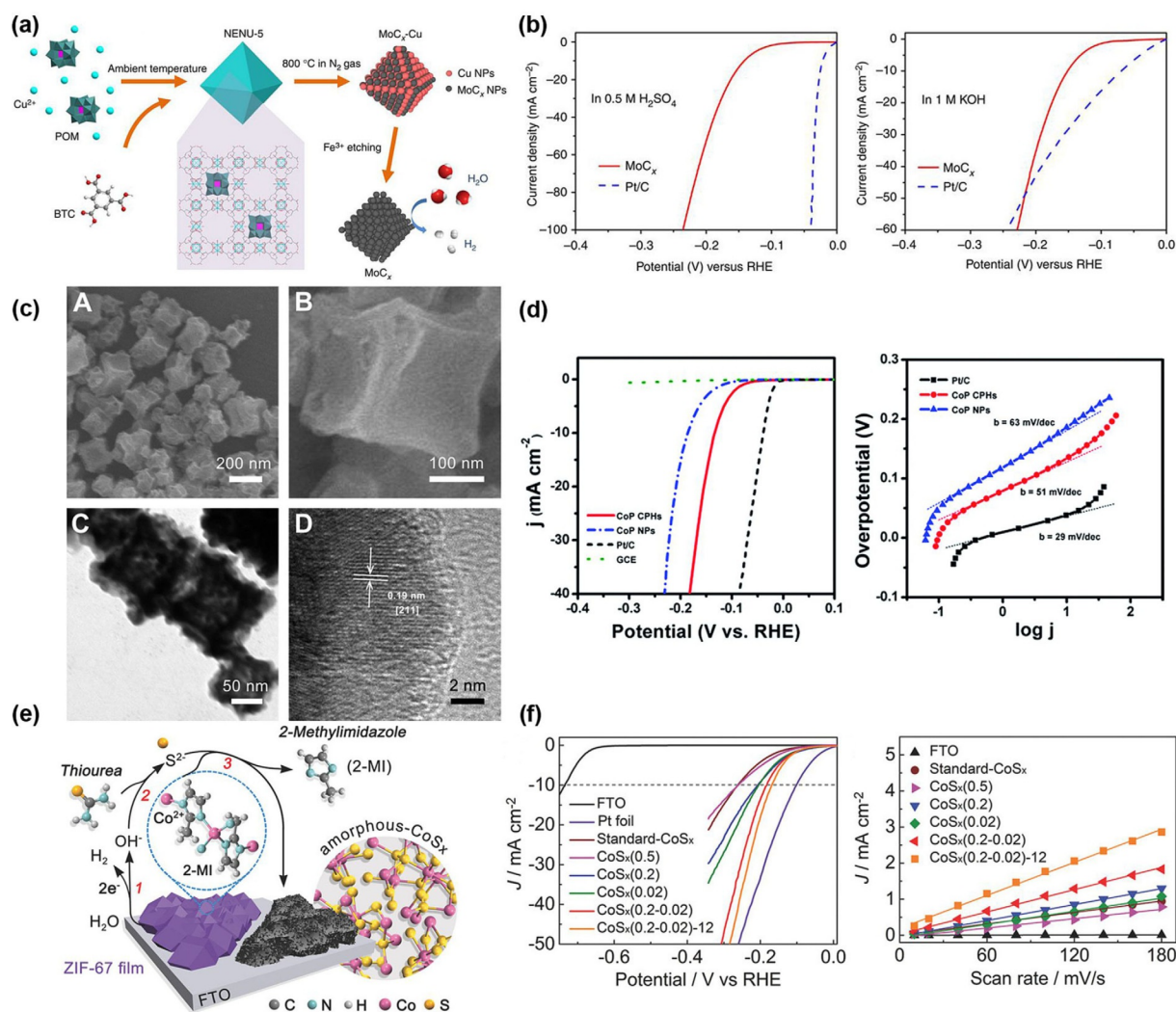


**Figure 5.** a) Schematics: synthesis of the MOF-derived  $\text{MoC}_x$ -Cu octahedrons and subsequent removal of metallic Cu via  $\text{Fe}^{3+}$  etching to produce porous  $\text{MoC}_x$ . b) Polarization curves for HER in both acid and alkaline solution. a) and b) reproduced with permission from reference [46]. Copyright 2015, Nature Publishing Group. c) SEM and TEM images of the as-obtained CoP CPHs. d) LSV curves and Tafel plots of Pt/C, CoP NPs and CoP CPHs. c and d) reproduced with permission from reference [49]. Copyright 2015, Royal Society of Chemistry. e) Schematic illustration showing the electrochemical conversion of ZIF-67 to porous amorphous  $\text{CoS}_x$  and f) the corresponding voltammetric curves and Tafel plots for the amorphous  $\text{CoS}_x$  compared with other related catalysts. Reproduced with permission from reference [50]. Copyright 2018, Wiley-VCH.

cations through a room-temperature electrochemical conversion.

Comparing to monometallic catalysts, bimetallic or multimetallic catalysts could provide the potential of enhanced activities and stability due to synergetic effects between different elements. Fundamental studies and theoretical calculations have proved that the introduction of more species should lead to a significant improvement of charge transfer and optimization of electronic structures at the surface of the catalysts.<sup>[30b, 34a, 51]</sup> MOF precursors enable relatively simple fabrication of multimetallic materials with controllable metal composition. For example, a series of nickel-cobalt bimetal phosphide nanotubes were synthesized by Yan et al. via a controllable low-temperature phosphorization strategy.<sup>[33a]</sup> Benefiting from the tunable chemical composition of MOF precursors, the obtained  $\text{Co}_x\text{Ni}_y\text{P}$  nanotubes with an optimized molar ratio of Co to Ni atoms show an overpotential of 129 mV at  $10 \text{ mA cm}^{-2}$ .

To date, most MOFs and MOF-derived materials usually deal with the microporous structures (smaller than 2 nm) and large particle sizes, which may seriously affect ion diffusion and the number of accessible active sites.<sup>[52]</sup> In order to address this issue, the structure or morphology engineering, which based on tuning the nanostructuring and morphologies of the catalysts, gives the possibilities to make full use of their functionalities via the construction of hollow or “yolk-shell” structures.<sup>[30, 53]</sup> For instance, Huang et al developed a simple MOF self-template strategy to synthesize hollow polyhedral nanocages of bimetallic sulfides by solvothermal reaction and thermal annealing (Figure 6 a).<sup>[30b]</sup> The characterization results demonstrated that the bimetallic sulfides can be easily obtained through an in situ reaction between the bimetallic MOFs and thioacetamide, and show promising electrocatalytic performance over a wide pH range (Figure 6 b and c). Particularly, in acidic media, the optimal HER catalyst, namely  $\text{Zn}_{0.30}\text{Co}_{2.70}\text{S}_4$ ,



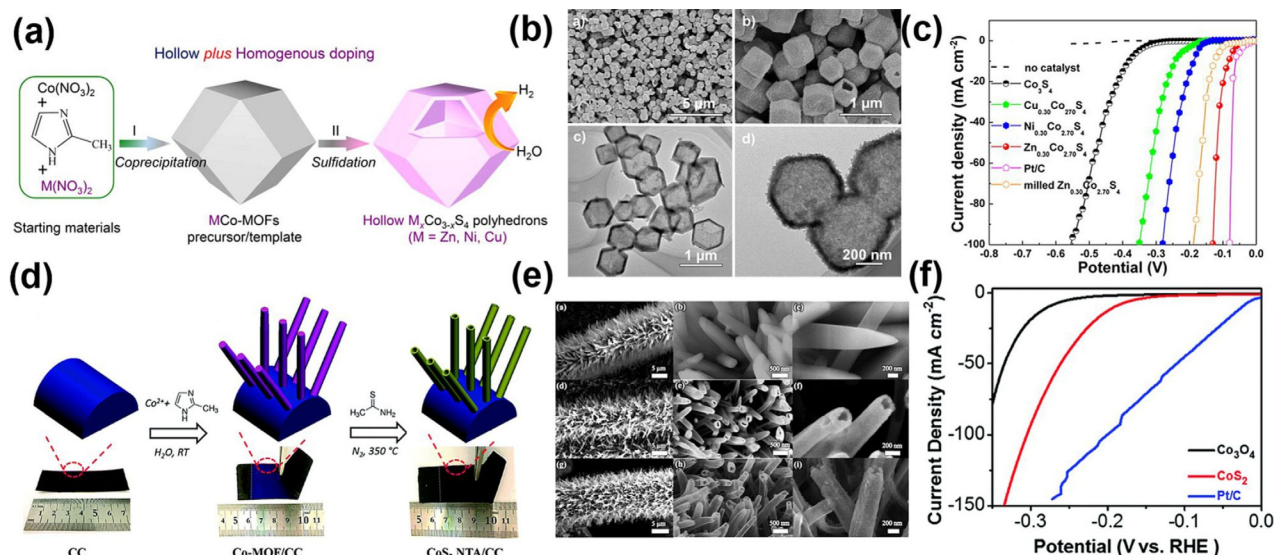


**Figure 6.** a) Sulfidation of bimetallic MOFs to produce hollow Co-based sulfide polyhedrals. b) SEM and TEM images of  $\text{Zn}_{0.30}\text{Co}_{2.70}\text{S}_4$ . c) Polarization curves of different catalysts for HER in 0.5 M  $\text{H}_2\text{SO}_4$ . a–c) Reproduced with permission from reference [30b]. Copyright 2016, American Chemical Society. d) Fabrication of  $\text{CoS}_2$  nanoarrays on the cloth substrate. e) Corresponding SEM images. f) Voltammetric curves for different HER catalysts. d–f) Reproduced from reference [55] with permission. Copyright 2017, Royal Society of Chemistry.

needs the overpotential of 80 mV at  $10 \text{ mA cm}^{-2}$  with the Tafel slope of  $47.5 \text{ mV dec}^{-1}$ . Alternative and at the same time promising avenues of the morphology engineering are to design 0D, 1D and 2D nanostructures or their self-assembled 3D networks as these structures generally possess large surface area, fast penetration of the electrolyte and more highly accessible active sites on their surface.<sup>[23,32b,54]</sup> Most likely, inspired by this avenue, Guan et al presented a template strategy to transform the uniform 1D Co-MOF on the carbon cloth substrate into unique hollow  $\text{CoS}_2$  tubular arrays via a sulfidation reaction with thioacetamide and a thermal treatment process (Figure 6d).<sup>[55]</sup> Thanks to the unique hollow tubular structure with an open space, the  $\text{CoS}_2$  nanoarrays showed the overpotential of 193 mV at the current density of  $10 \text{ mA cm}^{-2}$  and a Tafel slope of 88 mV per decade (Figure 6e and f). Remarkably, the long-term HER stability of  $\text{CoS}_2$  nanoarrays over 20 h at 200 mV overpotential with negligible degradation has been demonstrated.

Additionally, the rational selection of substrates, so-called substrate engineering, is one of most popular strategies for the development of MOF-derived catalysts by the direct growth of MOF precursors on conductive substrates, because simple using conductive substrates, e.g., graphite papers, carbon fibres, graphene, carbon nanotubes, glassy carbon, etc can significantly enhance the catalytic activities of the supporting materials.<sup>[27b,35,56]</sup> As an illustration, Jiao et al demonstrated the fabrication of a CoP/reduced graphene oxide (rGO) sandwich-type composite as a promising hydrogen-evolving catalyst through the MOF growth on both surfaces of graphene oxide (GO) and a subsequent low-temperature phosphating process (Figure 7).<sup>[35b]</sup> A sandwich-type structure of the resultant CoP/rGO guarantees a close contact between porous crystalline CoP and the conductive rGO, resulting in promising HER catalytic performance in both acidic and alkaline media. In

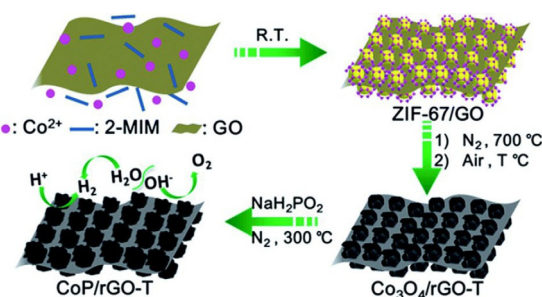


**Figure 7.** a) Schematic illustration of the formation process of the layered CoP/reduced graphene oxide (rGO) composite. Reproduced with permission from reference [35b]. Copyright 2016, Royal Society of Chemistry.

comparison with rGO, CoP and commercial Pt/C, CoP/rGO is expected to generate an HER current density of  $10 \text{ mA cm}^{-2}$  with an overpotential of 105 mV in acidic solutions, and corresponding Tafel slope of 50 mV per decade. Under alkaline conditions, the HER current density of CoP/rGO can reach the same current density at an overpotential of 150 mV and its Tafel slope can be as low as 38 mV per decade. CoP/rGO exhibits good electrochemical activity, which is attributed to the unique sandwich-type structure, the porous MOF-derived CoP and the high electrical conductivity of rGO substrate.

To avoid the MOF-based materials fall off from the electrode, binders (e.g., Nafion solution, Teflon particles, etc.) are usually used to glue the catalysts on the electrode surface.<sup>[57–59]</sup> Alternatively, porous substrates can trap the materials in the pores avoiding the leaching of the catalyst.<sup>[47b]</sup> As to the thin films, the substrates should be modified with some functional group such as -OH, or COOH to enhance the affinity of catalysts with the electrode surface.<sup>[50]</sup>

## 2.2. MOF-based electrocatalytic materials for the OER

Generation of hydrogen and oxygen through the electrochemical water splitting is considered as an efficient and sustainable method for the provision and storage of renewable energy.<sup>[21a,65]</sup> OER, as one of the half-reactions, requires high overpotential to complete the four electron-proton coupled reaction.<sup>[56a,66]</sup> Similar to HER, OER can also be carried out in both acidic and alkaline media, and its mechanisms (Figure 8) can be written as follows:<sup>[8,21b,56a,67]</sup>

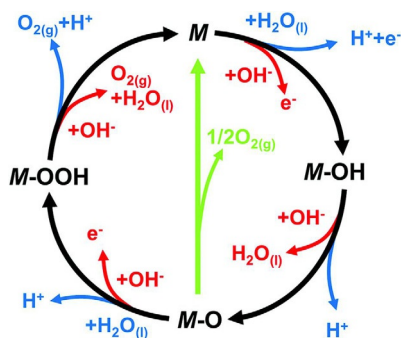
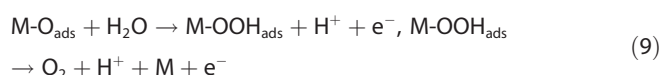
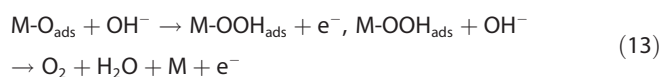
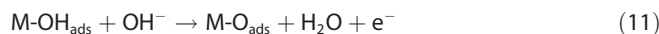


**Figure 8.** Schematic representation of the OER mechanisms at a solid electrode for acidic (blue line) and alkaline (red line) electrolytes. Reproduced with permission from reference [8]. Copyright 2017, Royal Society of Chemistry.

In acidic media:



In alkaline media:



Currently, noble metal-based functional electrodes, such as RuO<sub>2</sub> and IrO<sub>2</sub> demonstrate probably the best performance to catalyse the OER. However, high cost and low abundance of both Ru and Ir often question them for large-scale applications.<sup>[19,21a]</sup> MOFs, benefiting from their diverse structures and tunable properties can be a good alternative.<sup>[9c,27c,29b,43b]</sup> Beyond, the pristine MOFs were utilized as electrocatalysts for OER. MOFs are nowadays popular to serve as ideal precursors/templates to prepare porous carbon-based composites with more exposed active sites for OER.<sup>[27a,b,28a]</sup> In this section, the strategies based on the composition engineering, the structure and morphology engineering, and the substrate engineering to improve the oxygen evolution performance of MOFs (Table 3) and MOF-derived catalysts (Table 4) are discussed to enhance the binding abilities of catalysts to OER reaction intermediates [Eqs. (6)–(13)].

Although pristine MOFs still suffer from the inferior conductivity, tailoring desired metal clusters with functional organic links can give some possibilities to achieve remarkable improvement of catalytic performances toward the OER and broaden their potentials in the electrochemical applications.<sup>[68]</sup>

**Table 3.** Typical examples of pristine MOFs for the OER.

Material	Strategy used	Substrate	Overpotential [mV] at 10 mA cm <sup>-2</sup>	Ref.
Fe/Ni <sub>2.4</sub> /Co <sub>0.4</sub> -MIL-53	composition engineering	glassy carbon	219	[69]
Fe/Ni/Mn <sub>0.4</sub> -MIL-53	substrate engineering	nickel foam	238 at 100 mA cm <sup>-2</sup>	[69]
NiCo-UMOFNs	(2D) structure engineering	glassy carbon	250	[72]
Co-ZIF-9(III) nanosheets	(2D) structure engineering	glassy carbon	380	[11a]
NiFe-MOF/NF	(2D) structure and substrate engineering	nickel foam	240	[32a]
MAF-X27-OH	composition engineering	glassy carbon	387	[70]
MAF-X27-OH (Cu)	substrate engineering	Cu foil	292	[70]
([Co <sub>4</sub> (MoO <sub>4</sub> )(eim) <sub>6</sub> ]	composition engineering	glassy carbon	456	[71b]
ECD Fe/Ni-BTC@NF	substrate engineering	nickel foam	270	[73]
Ti <sub>3</sub> C <sub>2</sub> T <sub>x</sub> -CoBDC	(2D) substrate engineering	MXene phase	410	[74]
Co <sup>II</sup> Co <sup>III</sup> <sub>2</sub> (Im) <sub>12</sub>	substrate engineering	FTO	–	[75]
ZIF-67@NPC-2	substrate engineering	N-doped carbon	410	[76]
Fe <sub>3</sub> -Co <sub>2</sub> @GC	composition engineering	glassy carbon	283	[77]
Fe <sub>3</sub> -Co <sub>2</sub> @Cu	substrate engineering	Cu foam	237	[77]
Fe <sub>3</sub> -Co <sub>2</sub> @Ni	substrate engineering	nickel foam	225	[77]
Pb-TCPP	composition engineering	glassy carbon	470	[78]
UTSA-16	composition engineering	glassy carbon	408	[79]
Co-WOC-1	composition engineering	glassy carbon	390 at 1 mA cm <sup>-2</sup>	[80]
FeTPyP-Co	(2D) structure engineering	Au electrode	≈ 350 at 1 mA cm <sup>-2</sup>	[81]
Co/MIL-101(Cr)-O	composition engineering	glassy carbon	477	[82]

**Table 4.** Typical examples of MOF-derived electrocatalysts for the OER.

Material	Strategy used	Electrolyte [KOH]	Substrate	Overpotential [mV] at 10 mA cm <sup>-2</sup>	Ref.
Ni@NC-800	composition engineering	1 M	glassy carbon	280	[90]
Ni@graphene	composition engineering	1 M	glassy carbon	370	[57]
FeNi@N-CNT	composition engineering	1 M	glassy carbon	300	[83b]
SURMOFD	composition and substrate engineering	0.1 M	Au quartz	~ 0.8 mA μg <sup>-1</sup> at an overpotential of 300 mV	[85b]
CoNi hydroxide UNSs	composition and structure engineering	1 M	glassy carbon	324	[85a]
CoZn hydroxide UNSs	composition and structure engineering	1 M	glassy carbon	338	[85a]
(Ni <sub>2</sub> Co) <sub>0.925</sub> Fe <sub>0.075</sub> -MOF-NF	composition and substrate engineering	1 M	nickel foam	257	[92a]
Co <sub>3</sub> S <sub>4</sub> /EC-MOF	composition and substrate engineering	1 M	carbon cloth	226	[101]
t-Co <sup>II</sup> Co <sup>III</sup>	composition and substrate engineering	1 M	carbon cloth	240	[92b]
Zn-doped CoSe <sub>2</sub> /CFC	composition and substrate engineering	1 M	carbon fabric collector	356	[89]
CoOOH-NS	(2D) structure and substrate engineering	1 M	carbon paper	253	[92c]
Ni-MOF@Fe-MOF	composition engineering	1 M	glassy carbon	265	[92d]
NiCo-MOF@Fe-MOF	composition engineering	1 M	glassy carbon	275	[92d]
(Ni,Co)Se <sub>2</sub> /C-HRD	composition and substrate engineering	1	nickel foam	245	[53b]
Co@NC/NF	substrate engineering	1	nickel foam	390	[47b]
Co <sub>3</sub> O <sub>4</sub> C-NA	(1D) structure and substrate engineering	0.1 M	Cu foil	290	[93]
CoO <sub>x</sub> -ZIF	composition engineering	1 M	glassy carbon	3.18	[52b]
Ni <sub>2</sub> P-CoP	composition engineering	0.1 M	glassy carbon	320	[59]
Co-P/NC	composition engineering	1 M	glassy carbon	354	[96]
CoP <sub>3</sub> CPs/CFP	substrate engineering	1 M	carbon fiber paper	343	[88]
Ni-P porous nanoplates	(2D) structure engineering	1 M	glassy carbon	300	[94]
CoP hollow polyhedron	structure engineering	1 M	glassy carbon	400	[53a]
NC@Co-NGC DSNC	structure engineering	0.1 M	glassy carbon	410	[83a]
BNPC-1100	composition engineering	6 M	glassy carbon	320	[104]
N-PC@G-0.02	composition engineering	0.1 M	glassy carbon	400	[102a]

In this respect, Li et al investigated a series of bimetallic Fe/Ni-based MOFs with various tuned molar ratios of Fe/Ni, and then adopted them as efficient OER electrocatalysts (Figure 9a and b).<sup>[69]</sup> Fe/Ni<sub>2.4</sub>-MIL-53/C with the optimized Fe/Ni ratio exhibits an OER performance with an overpotential of 244 at 10 mA cm<sup>-2</sup>, which is better than that of commercial Ir/C catalyst (310 mV). Its Tafel slope is 48.7 mV per decade, revealing the rapid oxygen evolution kinetics. Furthermore, the introduction of the third metal ions (Co<sup>2+</sup> or Mn<sup>2+</sup>) can significantly enhance OER performance in comparison with bimetallic MOFs. Among the as-prepared trimetallic MOFs, Fe/Ni<sub>2.4</sub>/Co<sub>0.4</sub>-MIL-53 shows the best OER performance, with overpotentials as low as 219 mV at 10 mA cm<sup>-2</sup>. The well-defined atomic architecture, porosity and the synergy effect of third metal ions for trimetallic MOFs are the key factors to enable the excellent OER performance. Considering that the chemical structures of MOF-based electrocatalyst playing an important role for the OER process, Lu et al reported a kind of metal hydroxide mimicking MOFs through a post-synthetic ion exchange of a metal azolate framework [Co<sub>2</sub>(μ-Cl)<sub>2</sub>(bbta)] (MAF-X27-Cl, H<sub>2</sub>bbta = 1H,5H-benzo(1,2-d:4,5-d')bistriazole) for obtaining a material [Co<sub>2</sub>(μ-OH)<sub>2</sub>(bbta)] (MAF-X27-OH) (Figure 9c and d).<sup>[70]</sup> MAF-X27-Cl can be selected as an OER precursor because of its high chemical stability in acidic or strong alkaline solution. Electrochemical measurements showed that MAF-X27-Cl could only afford 0.028 mA cm<sup>-2</sup> at a high overpotential of 570 mV, while microcrystals of MAF-X27-OH could achieve 2.0 mA cm<sup>-2</sup> at a lower

overpotential of 489 mV at PH 7. In 1.0 M KOH solution, MAF-X27-OH showed much better catalytic activity (387 mV at 10 mA cm<sup>-2</sup>) than inorganic analogues Co(OH)<sub>2</sub> (421 mV) and Co<sub>3</sub>O<sub>4</sub> (445 mV). Synthesizing cobalt hydroxide chains contained open frameworks, such as MAF-X27-OH offer the possibility to achieve better electrochemical performances. Besides, the OER catalytic activities of 3d metal oxides/hydroxides can also be enhanced by introducing high-valence non-3d metals, such as W and Mo.<sup>[71]</sup> Moreover, Co<sup>II</sup> imidazolate frameworks have been widely regarded as the classical electrocatalysts for OER, but their catalytic activities for practical application are still questionable. Inspired by these strategies, Xu et al designed a series of non-3d metal modulation of cobalt imidazolate frameworks ([Co<sub>4</sub>(MO<sub>4</sub>)(eim)<sub>6</sub>] (denoted as Co<sub>4</sub>M, M = Mo or W, Heim = 2-ethylimidazole)) via integrating oxide units of non-3d metals into cobalt imidazolate frameworks (Figure 9e and f).<sup>[71b]</sup> Co<sub>4</sub>M performed remarkable enhanced OER performance, compared with Co<sub>4</sub>(eim)<sub>6</sub> in different neutral electrolytes. Especially in phosphate buffer solution (PBS, PH = 7), Co<sub>4</sub>Mo displayed a low onset potential of 1.50 V, and an overpotential of 388 mV at 2 mA cm<sup>-2</sup>, performing better than other Co-based compounds (400–700 mV) and commercial RuO<sub>2</sub> (395 mV). The same result can be obtained in CO<sub>2</sub>-saturated 0.5 M KHCO<sub>3</sub> electrolyte, Co<sub>4</sub>Mo merely required a low overpotential (210 mV) to achieve 1 mA cm<sup>-2</sup>. The further density functional theory (DFT) calculations proved that non-3d metals could significantly improve the OER performance of



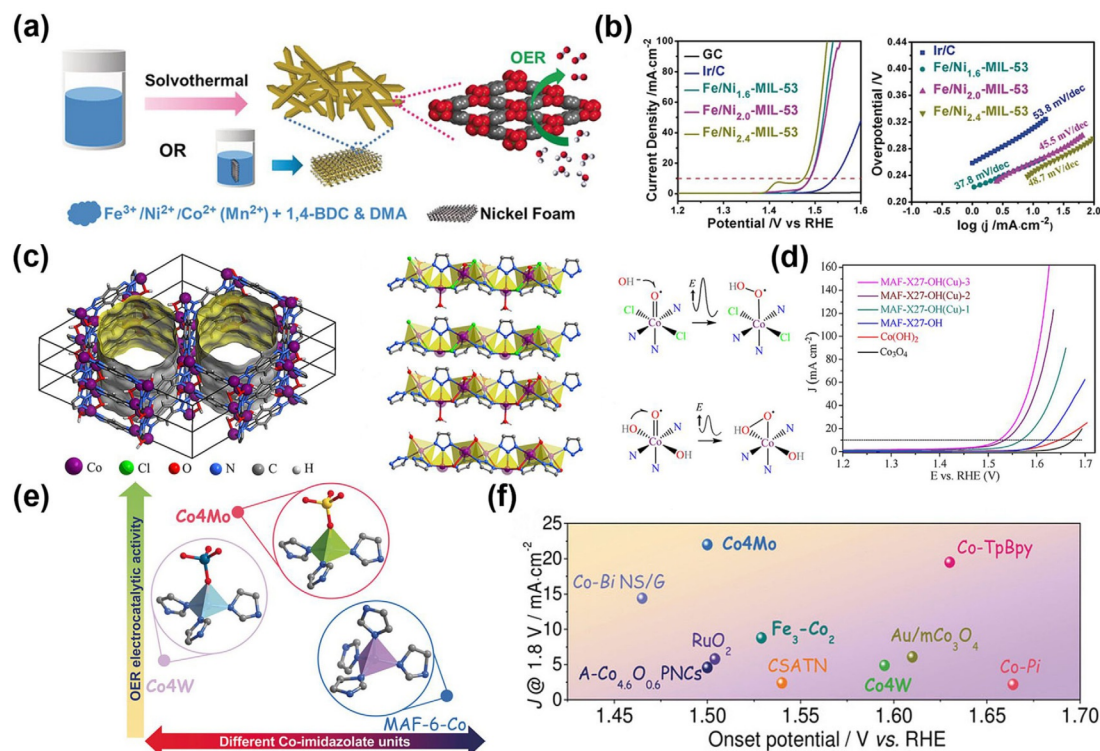


**Figure 9.** a) Schematic illustration of a synthetic process of Fe/Ni/Co(Mn)-MIL-53 and Fe/Ni/Co(Mn)-MIL-53/NF and b) corresponding voltammetric curves and Tafel plots of different electrodes. Reproduced with permission from reference [69]. Copyright 2018, Wiley-VCH. c) Three-dimensional coordination network and local coordination environments of MAF-X27-OH catalyst. d) Polarization curves of various materials for OER. c and d) Reproduced with permission from reference [70]. Copyright 2016, American Chemical Society. e) The relation between different Co-imidazolate units and OER electrocatalytic activity. f) Comparison of the current density at 1.8 V and onset overpotential with different OER catalysts. Reproduced with permission from reference [71b]. Copyright 2019, Wiley-VCH.

cobalt imidazolate frameworks through tailoring the electronic structure and reactant/product affinity of the cobalt centers.

Additionally, other attractive approaches for the activity improvement of pristine MOFs involve the structure engineering (e.g., ultra-thinning 2D MOFs and nanoarrays) and the substrate engineering (e.g., MXene, N-doped carbon, graphite foam, nickel foam and metal oxide). For example, a classic approach for the design and synthesis of ultrathin MOFs nanosheets under ultrasonication was reported by Zhao et al in 2016.<sup>[72]</sup> The as-prepared ultrathin NiCo-MOFs nanosheets (NiCo-UMOFNs) possessed a very low overpotential of 250 mV at  $10\text{ mA cm}^{-2}$ , even lower than that of commercial  $\text{RuO}_2$  (279 mV). Through the XAS analysis and DFT simulations, more exposed unsaturated metal atoms in the well-defined atomic architecture NiCo-UMOFNs played a critical role in the high electrocatalytic activity. Recently, Fischer and co-workers demonstrated a type of ultrathin 2D cobalt zeolite-imidazole framework (ZIF-9(III)) possessed efficient catalytic activities for OER, because of the unique physical and chemical properties.<sup>[11a]</sup> In detail, the bulk ZIF-9(III) phase can generate more 2D ZIF-9(III) nanosheets after the ultrasonication assisted liquid-phase exfoliation, and the resultant exfoliated nanosheets required a very low overpotential of 380 mV to achieve  $10\text{ mA cm}^{-2}$  in 1.0 M KOH, while bulk Co-ZIF-9(III) required 430 mV. The good OER electrocatalytic performance for 2D Co-ZIF-9(III) nanosheets may be attributed to the inherently higher electronic conduc-

tivity and more accessible nitrogen coordinated cobalt oxyhydroxide  $\text{N}_4\text{CoOOH}$  sites. Thus, ultra-thinning 2D MOFs derived with an exfoliated strategy can yield more active sites and lead to high efficient OER performance.

To maximize the exposure of active sites in pristine MOFs, substrate engineering is also an attractive strategy for the improvement of OER activities.<sup>[56a]</sup> For instance, Wang et al synthesized a series of M-BTC MOFs ( $M = \text{Ni}$  or  $\text{Fe}$ ,  $\text{BTC} = 1,3,5\text{-benzenetricarboxylic acid}$ ) on nickel foam by the electrochemical-deposition.<sup>[73]</sup> Strikingly, the optimized Fe/Ni-BTC@nickel foam with Fe/Ni molar ratio of 1/12 showed the smallest overpotential value of 270 mV for achieving  $10\text{ mA cm}^{-2}$ , together with the Tafel slope of  $47\text{ mV dec}^{-1}$ , which is even comparable to those of  $\text{IrO}_2$ ,  $\text{RuO}_2$  catalysts. It should be mentioned that the good catalytic performance should be originated from the synergy effect between Fe/Ni components and highly conductive nickel foam. Therefore, substrate engineering is of critical importance in guaranteeing the conductivity and providing large current density. However, the oxidation of nickel foam can produce high oxidation current. Thus, the intrinsic current density of the catalysts for OER still needs to be studied to distinguish the oxidation current of nickel foam and OER current.

Although recent tremendous progress in the field of OER has been witnessed based on these pristine MOFs, their catalytic activities are still limited to meet the increasing demand.<sup>[27b, 28a]</sup> MOF-derived electrocatalysts have shown promis-

ing advantageous characteristics such as highly conductive carbon network, porous nanostructures, large surface area, diverse heteroatoms doping (e.g., N, O, S, and P) and homogeneously distributed metal atoms or metal compounds, which are a benefit for OER.<sup>[27a,28a,42b,43b]</sup> In this section, the concepts based on the composition engineering, the structure or morphology engineering, and the substrate engineering for designing MOF-derived catalysts for improving the OER performance will be discussed.

The composition engineering allows the possibilities to design MOF-derived nanostructured transition metals,<sup>[47b,83]</sup> metal oxides,<sup>[52b,84]</sup> hydroxides,<sup>[85]</sup> carbides,<sup>[71d,86]</sup> nitrides,<sup>[87]</sup> sulfides,<sup>[51a,55,56b]</sup> phosphides,<sup>[35b,59,88]</sup> selenides,<sup>[35a,53b,60,89]</sup> and so on. Based on composition-engineered strategies, the OER performance of MOF-derived catalysts is significantly enhanced via creating more accessible active sites. As one kind of the typical derivatives, carbon encapsulating transition metals or alloys can be easily obtained through MOF-contained abundant metal ions and organic ligands under high temperature.<sup>[28a,c]</sup> Remarkably, metal or alloy nanoparticles incorporated in nitrogen-doped carbon materials show excellent electrocatalytic performance because of the catalytic sites of metallic nanoparticles and the intact metal protection effect of the outer carbon layers.<sup>[47b,57,83b,90]</sup> Xu et al directly used Ni-based MOF Ni<sub>2</sub>(bdc)<sub>2</sub>ted (bdc = 1,4-benzenedicarboxylic acid, ted = triethylenediamine) as the precursor to synthesize Ni nanoparticles encapsulated in few-layer nitrogen-doped graphene (denoted Ni@NC) (Figure 10a).<sup>[90]</sup> It was found that the temperature of annealing treatment played a critical role in the graphitization with the tunable carbon and nitrogen contents and further influenced their electrocatalytic activity. Benefiting from the synergistic effect between structure and composition, the Ni@NC-800 catalyst obtained under annealing temperature of 800 °C exhibited

the best OER performance, with a current density of 10 mA cm<sup>-2</sup> at an overpotential of 280 mV and a small Tafel slope of 45 mV dec<sup>-1</sup>, both of which are lower than those of other Ni@NC samples and IrO<sub>2</sub> catalyst (Figure 10b and c).

In practical use, electrocatalysts are usually operated in harsh conditions, such as strong acidic and alkaline solutions.<sup>[66a,91]</sup> However, most of the pristine MOFs cannot sustain their structure in harsh conditions.<sup>[9c,27c,42b]</sup> Taking this drawback as advantages, researchers developed MOF-derivatives by facile immersing pristine MOF into an alkaline environment.<sup>[85,92]</sup> Fischer et al used NiCo-based surface-mounted MOFs (SURMOF) thin films as precursors via one-step alkaline treatment for obtaining derived nickel/cobalt hydroxide electrocatalysts (Figure 11).<sup>[85b]</sup> The SURMOF-derived hydroxides grown on gold electrode exhibit outstanding performance and deliver a mass activity of ~0.8 mA μg<sup>-1</sup> at a defined overpotential of 300 mV, which is approximately 3.5 times higher than that of reported NiFe-, FeCoW-, or NiCo-based electrocatalyst as well as MOF-based nanosheets at the same overpotential. The outstanding OER mass activity should be ascribed to the high exposure of Ni- and Co-based active sites and ultrathin electrocatalyst coating on a highly conductive gold electrode. The developed strategies allow a potentially scalable methodology for the fabrication of high-performance SURMOF-derived hydroxide electrocatalysts and open a venue for preparing electrocatalysts with highly exposed active sites.

Based on the composition engineering strategy, heteroatoms can be introduced into various transition metal compounds by deriving pristine MOFs to MOF derivatives, such as metal oxides, carbides, nitrides, phosphides, sulfides and selenides. The heteroatoms doped MOF derivatives allow the possibility to control the particle sizes and conductivity of the transition metal compounds.<sup>[19,21b,66]</sup> The porous structures and

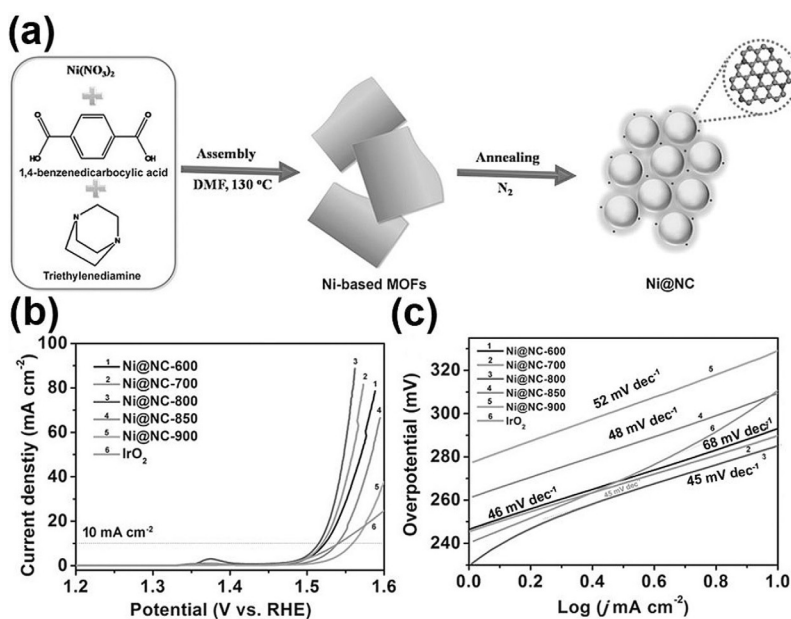


**Figure 10.** a) A schematic fabrication process for the Ni@NC catalysts derived from the Ni-based MOF precursors. b) and c) Electrochemical performance of all as-synthesized samples and IrO<sub>2</sub>. b) Voltammetric curves and c) the corresponding Tafel plots. Reproduced with permission from reference [90]. Copyright 2017, Wiley-VCH.

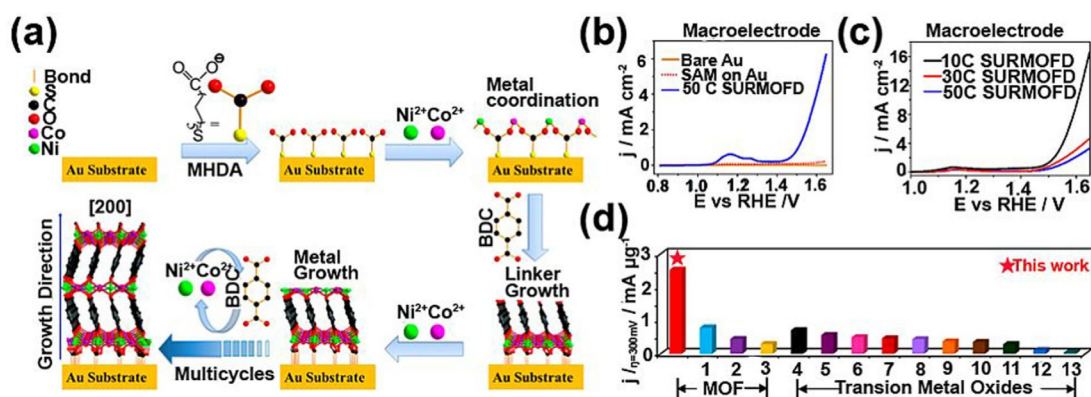


**Figure 11.** a) A schematics showing the fabrication process of the NiCo-based SURMOF thin films directly at the electrode substrate by a stepwise layer-by-layer (LBL) deposition method. b) and c) Polarization curves of SURMOF (10–50 cycles), SAMs on Au and the bare Au macro electrode for OER. d) Comparing the mass current density at the overpotential of 300 mV with some high active MOF and transition metal oxide catalysts. Reproduced with permission from reference [85b]. Copyright 2019, American Chemistry Society.

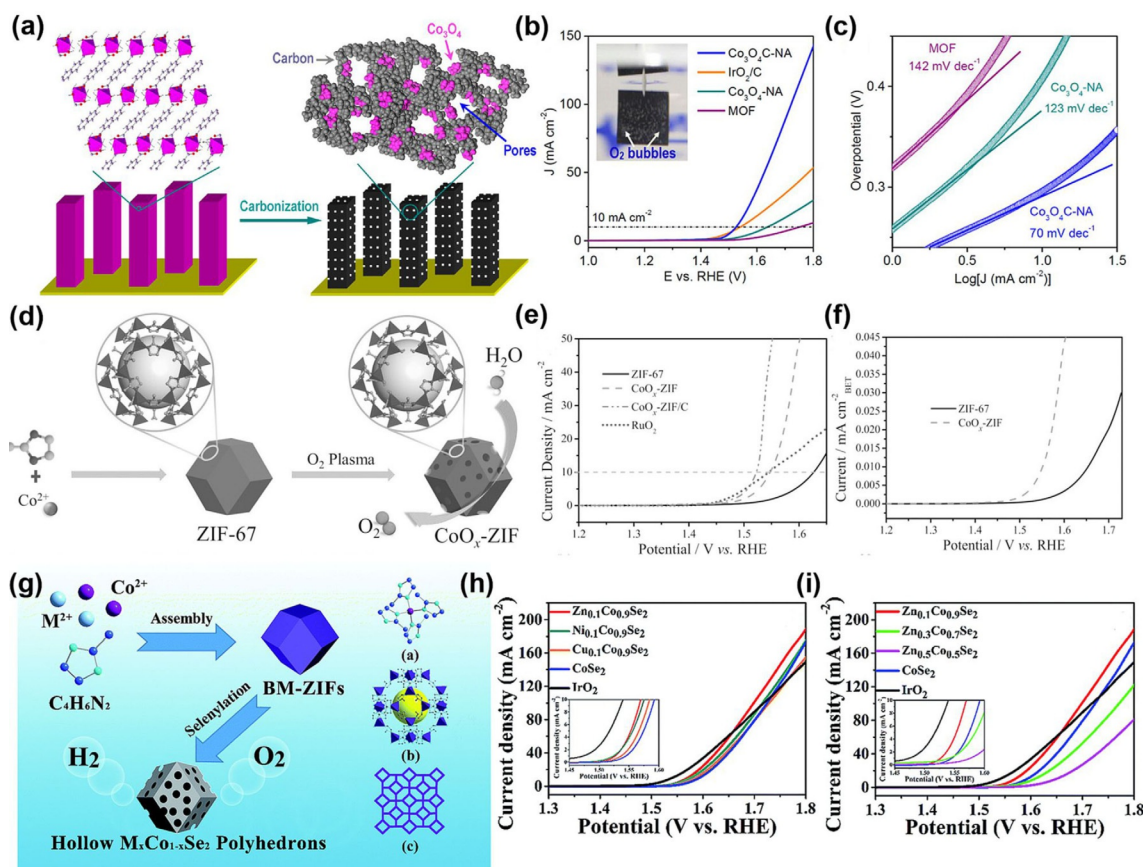


**Figure 12.** a) A schematic illustration showing the fabrication process of hybrid  $\text{Co}_3\text{O}_4$ -carbon porous nanowire arrays. b) and c) voltammetry curves and the derived Tafel plots of the different catalysts (inset in b: the optical image of  $\text{Co}_3\text{O}_4\text{C-NA}$  operating at 1.70 V with generated  $\text{O}_2$  bubbles). a–c) Reproduced with permission from reference [93]. Copyright 2014, American Chemical Society. d) The schematic fabrication process for  $\text{CoO}_x\text{-ZIF}$ . e) OER polarization curves of ZIF-67,  $\text{CoO}_x\text{-ZIF}$ ,  $\text{CoO}_x\text{-ZIF/C}$  and  $\text{RuO}_2$ . f) The normalized LSV curves of ZIF-67 and  $\text{CoO}_x\text{-ZIF}$  by BET surface area. d–f) Reproduced with permission from reference [52b]. Copyright 2017, Wiley-VCH. g) The synthesis of hollow  $\text{M}_x\text{Co}_{1-x}\text{Se}_2$  polyhedrons. Polarization curves of different transition metal-doped  $\text{CoSe}_2$  (h) and different molar ratio of  $\text{Zn}_x\text{Co}_{1-x}\text{Se}_2$  (i). g–i) Reproduced with permission from reference [30a]. Copyright 2017, Royal Society of Chemistry.

conductive carbon shells enable the derivatives to expose their active sites as much as possible.<sup>[27b,28a,43b]</sup> To illustrate this protocol, MOF-derived  $\text{Co}_3\text{O}_4$ -carbon porous nanowire arrays were designed by Qiao's group in 2014 (Figure 12 a–c).<sup>[93]</sup> The homo-

geneous distribution of metal oxide nanoparticles in porous carbon skeleton can be generated via a facile high-temperature pyrolysis strategy. This hybrid was employed as the OER catalyst and merely required an overpotential of 290 mV to de-



liver  $10 \text{ mA cm}^{-2}$ , which was lower than that of  $\text{IrO}_2/\text{C}$  ( $310 \text{ mV}$ ) and most of the highly active noble-metal OER catalysts. The unique nanowire structures and carbon incorporation derived from Co-based MOF promote good OER performance. Besides, Dou et al demonstrated a strategy to produce atomic-scale  $\text{CoO}_x$  species by applying  $\text{O}_2$  plasma to treat ZIF-67.<sup>[52b]</sup> The atomic-scale  $\text{CoO}_x$  species served as active sites in ZIF-67 show highly efficient OER activity, which is even better than  $\text{RuO}_2$  (Figure 12 d–f). As an alternatives electrocatalysts, transition metal phosphides have received extensive study as the efficient catalysts for HER and OER owing to their high activities and low costs.<sup>[33a,59,94]</sup> By modulating the MOF precursors, the carbon-incorporated transition metal phosphides can be facilely obtained via carbonization and phosphorization calculations in high temperature.<sup>[95]</sup> The prepared MOF-derived phosphides, such as  $\text{CoP}/\text{NC}$ ,  $\text{CoP}_3$  concave polyhedrons and  $\text{Ni}_2\text{P}-\text{CoP}$  have proven to show the enhanced catalytic performance.<sup>[59,88,94,96]</sup> For instance, You et al demonstrated the synthesis of MOF-derived porous Co-P/NC nanopolyhedrons for water splitting.<sup>[96]</sup> The prepared ZIF-67 derivatives show a high surface specific surface area and large mesopores, resulting in a remarkable catalytic performance for both HER and OER. The Co-P/NC catalysts with a loading amount of  $1 \text{ mg cm}^{-2}$  deliver  $10 \text{ mA cm}^{-2}$  at an overpotential of  $319 \text{ mV}$ . The superior electrocatalytic performance should be attributed to the 3D interconnected large mesopores, high specific surface area and some oxidized  $\text{CoO}_x$  species from the surface of  $\text{CoP}_x$ .

Additionally, transition metal sulfides and selenides have shown their promising application for the OER due to their good electron configuration and earth abundance.<sup>[97]</sup> Thus, a series of MOF-derived transition metal sulfides and selenides, such as  $\text{CoS}_2$ ,  $\text{Zn}_{0.1}\text{Co}_{0.9}\text{Se}_2$ ,  $\text{Co-Ni-Se}$ ,  $\text{Ni}_1\text{Co}_4\text{S}@C$  and  $\text{Co}_{0.85}\text{Se}@NC$ , have been explored.<sup>[30a,34b,35a,51a,53b,60,89]</sup> For example, Wang et al developed an in situ transformation approach to design a hollow porous  $\text{M}_x\text{Co}_{1-x}\text{Se}_2$  ( $M = \text{Fe, Co, Ni}$  etc) polyhedron through a straightforward solvothermal selenylation process.<sup>[30a]</sup> The hollow resultant,  $\text{Zn}_{0.1}\text{Co}_{0.9}\text{Se}_2$  with the optimized molar ratio, shows an outstanding OER performance, giving  $10 \text{ mA cm}^{-2}$  at an overpotential of  $340 \text{ mV}$  with a Tafel slope of  $43.2 \text{ mV dec}^{-1}$ , superior to  $\text{IrO}_2$  catalyst ( $64.0 \text{ mV dec}^{-1}$ ) (Figure 12 g–i). The MOF-derived bimetallic selenide generates remarkable catalytic activity owing to the hollow porous structures, more exposed active sites, high conductivity and the synergistic effect of Zn and Co.

In addition to the composition engineering, structure or morphology is another crucial factor in affecting the efficiency of MOF-derived electrocatalysts for OER.<sup>[27b,56a,98]</sup> Well-defined structure or morphology, such as hollow structures, yolk-shell structures, 3D networks, 2D nanosheets, 1D nanowires and 0D nanoparticles, exhibit high specific surface area with a large number of actives sites.<sup>[31a,99]</sup> Taking advantages of MOFs, a variety of porous nanostructures based on MOF-derived materials have been widely explored in the last decade.<sup>[30b,53a,85a,95]</sup> For example, Yu et al indicated that various porous carbon-coated nickel phosphides (Ni-P), NiO and  $\text{Ni(OH)}_2$  nanoplates can be easily synthesized via employing Ni-Ni Prussian blue analogue (PBA) nanoplates as the templates (Figure 13).<sup>[94]</sup> These MOF-de-

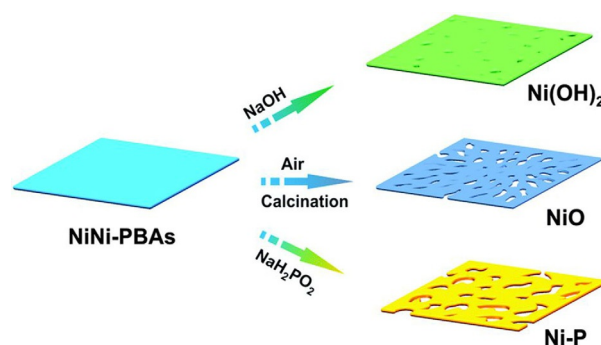


**Figure 13.** schematics of the transformation of NiNi-PBAs to  $\text{Ni(OH)}_2$ , NiO and Ni-P porous nanoplates. Reproduced with permission from reference [94]. Copyright 2016, Royal Society of Chemistry.

ived materials, especially Ni-P nanoplates show highly active for OER, which is ascribed to the incorporation of amorphous carbon, the porous nanostructure and lots of exposed active sites. The Ni-P nanoplate electrode exhibits remarkable OER activity with a low overpotential of  $300 \text{ mV}$  at  $10 \text{ mA cm}^{-2}$ , which is lower than that of  $\text{Ni(OH)}_2$  ( $360 \text{ mV}$ ) and NiO ( $430 \text{ mV}$ ). Moreover, Liu et al<sup>[83a]</sup> controlled pyrolysis of core-shell ZIF-8@ZIF-67 crystals and obtained the double-shelled NC@Co-NGC nanocages, consisting of Co-N-doped graphitic carbon (Co-NGC) outer shells and N-doped microporous carbon (NC) inner shells, which display superior electrocatalytic activities for OER and ORR. The results prove that designing unique nanostructures can promote the improvement of diffusion kinetics and exposure of active sites.

Electroactivity is highly dependent on the conductivity of electrocatalysts.<sup>[56a]</sup> Direct growth of MOF precursors on conductive substrates, such as graphite papers, carbon fibres, graphene, carbon nanotubes, glassy carbon, fluorine-doped tin oxide, nickel foam and metal films, offers the possibilities to improve the conductivity, stability and catalytic activity of MOFs based electrocatalysts. Tremendous research efforts have been devoted to substrate engineering for the activity improvement of MOF-derived electrocatalysts.<sup>[9c,56a,98,100]</sup> A typical example of the substrate engineering was reported by Liu et al.<sup>[101]</sup> They firstly prepared well-aligned MOFs on conductive carbon cloth (CC) via a vapour-phase method, and then produced  $\text{Co}_3\text{S}_4$  species on the surface of MOFs through an on-site controlled vulcanization method. The resultant  $\text{Co}_3\text{S}_4/\text{EC-MOF}$  reached an enhanced catalytic activity at  $10 \text{ mA cm}^{-2}$  with a low overpotential  $226 \text{ mV}$ . The great enhancement of OER performance for  $\text{Co}_3\text{S}_4/\text{EC-MOF}$  is not only ascribed to the synergy effect of the  $\text{Co}_3\text{S}_4$  species and Co-MOF through N–S/N–Co bonds, but also the increased the charge transfer and conductivity through the substrate of carbon clothes. It is obvious that substrate engineering plays a key role in the development of highly efficient OER electrocatalysts.

Metal-free electrocatalysts developed by MOFs have the characteristics of numerous structural defects, ultrahigh specific surface area and doping amount of heteroatoms, which could enhance the OER performance.<sup>[21a,27b,28a,c]</sup> Keeping these in mind, N, P, S, and B heteroatoms were effectively introduced into MOF-derived porous carbons by utilization of the heteroa-

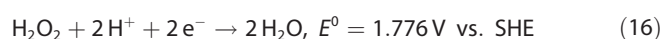
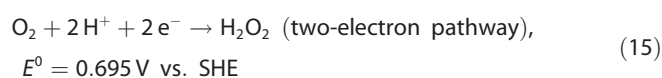
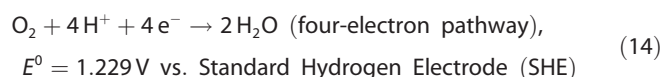
tom-containing organic units or chemical replacement in post-treatment, and change the electronic structure of carbons, which can further create more active sites for catalytic reactions.<sup>[102]</sup> For instance, some N-containing MOFs have been used as precursors to produce porous carbon with high N content and total pore volumes.<sup>[103]</sup> Thanks to the Zn-MOF containing Zn, N, and B, the B-N dual-doped and metal-free ORR/OER bifunctional ORR/OER electrocatalysts can be easily synthesized via a one-step pyrolyzing reaction under H<sub>2</sub>-containing atmosphere.<sup>[104]</sup> The as-prepared catalyst showed remarkable OER and ORR catalytic activities, as well as the cycling stability due to its high porosity and large content of pyridinic N. The 10 mAcm<sup>-2</sup> can be achieved using the B-N dual-doped carbon as the catalyst at an overpotential of 320 mV for the OER. The results show that the strategy of prepared MOF derived heteroatom-doped porous carbons are promising for developing OER catalysts with low-cost, high efficiency and long-term stability.

### 2.3. Design MOF-based electrocatalysts for the oxygen reduction reaction

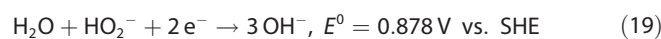
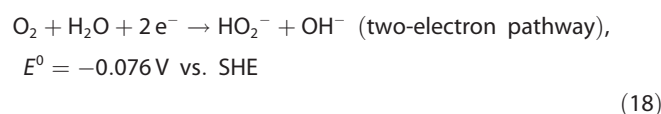
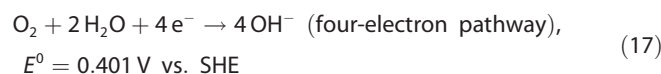
With the development of various energy storage and conversion techniques, many clean and sustainable energy devices have aroused widespread attention, including water splitting, fuel cells, and metal-air batteries, etc.<sup>[42a,105]</sup> Among these devices, the ORR is the indispensable reaction during the discharging process at the cathode of the fuel cells and metal-air batteries devices. However, ORR usually suffers the sluggish kinetics of multi-electron transfer.<sup>[106]</sup> Presently, the noble-metal based electrocatalysts are the main electrocatalysts used for ORR. Due to the scarcity and high cost of noble metal, it is crucial to explore earth-abundant and cost-effective ORR catalysts for the urgent demands of clean power supplies in the flourishing human society. A series of alternative electrocatalysts with earth abundance and high activity for ORR have been explored, such as carbon-based non-precious metals or alloys, transition metal hydrides and heteroatom doped porous carbon.<sup>[1a,107]</sup> Among these electrocatalysts, MOF-based nanomaterials have been proved to serve as distinctive electrocatalysts for ORR over the past decade due to their large surface area, tunable chemical composition and pore structure.<sup>[106b,108]</sup>

In both alkaline and acidic media, the ORR probably shows a two- or four-electron pathway. Generally, the two-electron reduction pathway produces peroxide species as the reaction intermediates, followed by either further reduction, while oxygen can be directly transferred into water or OH<sup>-</sup> through a more efficient four-electron reduction pathway.<sup>[107,109]</sup>

In acidic solutions:



In alkaline solutions:



According to the ORR process [Eqs. (14)–(19)], the conductivity and binding strength to reaction intermediates of electrocatalysts are two key parameters for designing efficient catalysts. MOF-based materials have shown remarkable ORR performance via modulating the abundant metal ions or functional organic ligands, tuning the porous structure, and developing various post-processing techniques of MOFs precursors.<sup>[110]</sup> In this section, the concepts of development of MOF-based materials are discussed from the aspects of the composition engineering, the structure and morphology engineering, and substrate engineering (Table 5 and Table 6).

By tailoring the metal nodes and organic ligands, MOFs could exhibit good performance for the ORR.<sup>[42b,43b]</sup> Mao et al demonstrated that water-stable Cu-bipy-BTC MOF (bipy = 2,2'-bipyridine, BTC = 1,3,5-tricarboxylate) can be used as the electrocatalyst towards ORR with a four-electron reduction pathway.<sup>[111]</sup> The Cu-bipy-BTC MOF coated on a glassy carbon disk electrode can produce ORR at -0.10 V versus Ag/AgCl and quickly reach a steady current at -0.25 V versus Ag/AgCl. Based on the same concept, Jahan et al reported a graphene-metalloporphyrin (denoted G-dye-FeP<sub>n</sub>) MOF as an ORR catalyst through integrating functionalized graphene oxide and iron-porphyrin (Figure 14).<sup>[112]</sup> The as-prepared (G-dye 50 wt %-

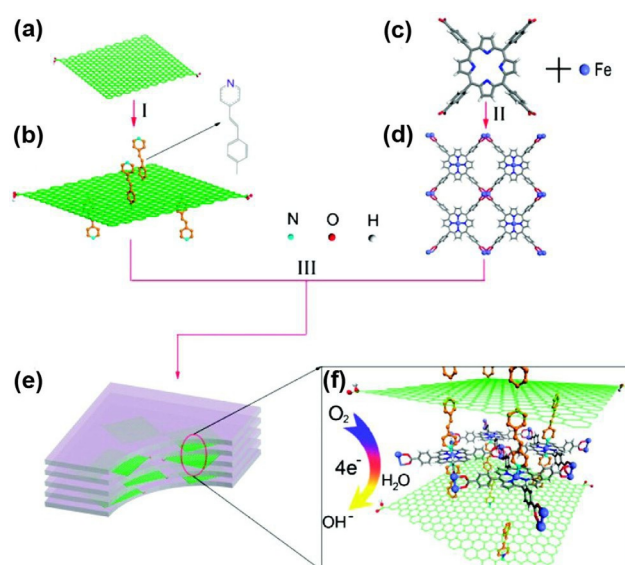


**Figure 14.** Synthetic routes of graphene-porphyrin MOF (e and f) via integrating G-dye (b), iron-porphyrin (d). Reproduced with permission from reference [112]. Copyright 2012, American Chemical Society.

**Table 5.** Typical examples of pristine MOFs for ORR.

Material	Strategy used	$E_{\text{onset}}$ [V vs. RHE]	$E_{1/2}$ [V vs. RHE]	$j_{\text{lim}}$ [mA cm <sup>-2</sup> ]	$n^{[a]}$ [E vs. RHE]	Substrate	Ref.
(G-dye-FeP) <sub>n</sub> MOF	composition engineering	0.93	–	–0.63	3.82 (0.32 V)	GC-RDE	[112]
Cu-bipy-BTC	composition engineering	0.87	≈ 0.8	–0.26	3.8 (0.40 V)	GC-RDE	[111]
(GO 8 wt %) Cu-MOF	composition engineering	0.29	–	–5.3	–	GC-RDE	[46]
NPC-4/rGO	structure engineering	0.84	–	–	1.8 (0.67 V) 3.2 (0.37 V)	GC-RDE	[117]
PCN-222-G-py (25 wt %)	composition engineering	–	–	–0.9	–	GC	[118]
Co/MIL-101(Cr)-R	composition engineering	0.92	0.64	–6	≈ 3.9	GC-RDE	[82]
ε-MnO <sub>2</sub> /MOF(Fe)	composition engineering	0.84	0.64	–5.56	3.8 (0.55 V)	GC-RDE	[116]
nano-CuS(28 wt %) @Cu-BTC	composition engineering	0.91	–	–	3.82 (0.55 V)	GC-RDE	[119]
Ni <sub>3</sub> (HITP) <sub>2</sub>	composition engineering	0.82	–	–	2.25 (0.767 V)	GC-RDE	[114]
Co-Al-PMOF	composition engineering	0.75	–	–0.6	2.9 (0.55 V)	GC-RDE	[120]
(Co(bpdc)(H <sub>2</sub> O) <sub>4</sub> )/GF	structure engineering	0.78	0.7	–2.7	–	graphite foam	[121]

[a] *n* represents the number of electrons transfer.

**Table 6.** Typical examples of MOF-derived materials for the ORR.

Material	Electrolyte	$E_{\text{onset}}$ [V vs. RHE]	$E_{1/2}$ [V vs. RHE]	$j_{\text{lim}}$ (mA cm <sup>-2</sup> )	$n^{[a]}$ [E vs. RHE]	Ref.
Fe-ISAs/CN	0.1 M KOH	0.986	0.9	≈ 6.1	3.9	[122e]
P-CNCo-20	0.1 M KOH	0.93	0.85	6.00	3.9	[129]
COP-TPP(Fe)@MOF-900	0.1 M KOH	0.99	0.932	≈ 4.7	3.95 at 0.6 V	[122f]
Co-N-C@F127	0.5 M H <sub>2</sub> SO <sub>4</sub>	0.95	0.84	≈ 3.9	4	[124a]
NC@Co-NGCDSNC	0.1 M KOH	0.92	0.82	–	4	[83a]
FeNC-20-1000	0.1 M HClO <sub>4</sub>	1.04	0.88	≈ 6.2	3.99	[122c]
Co <sub>2</sub> N-CNF	0.1 M KOH	0.888	0.815	5.71	3.8	[130]
Co-N-C	0.1 M KOH	0.982	0.871	5.35	3.94–3.98	[131]
NC900	0.1 M KOH	0.83	–	4.9 at 0.1 V	3.3	[132]
PNPC-1000	0.1 M KOH	0.89	–	6.9	3.82	[103a]
NPCTC-850	0.1 M KOH	0.92	0.83	5.35	3.88–3.92 at 0.4–0.7 V	[133]
N-PC@G-0.02	0.1 M KOH	1.01	0.80	–	3.93	[102a]
MOFCN900	0.1 M KOH	0.035 vs. Hg/HgO	–	≈ 4.1	3.12	[134]
MZ8-S-P	0.1 M KOH	0.964	0.855	5.89	4.02–4.07 at 0.2–0.8 V	[99b]
NHPC <sub>1,3</sub> -900	0.1 M KOH	–	0.87	5.7	close to 4	[54a]
NGPC-1000-10	0.1 M KOH	0.953	0.772	4.69	3.81	[127]
NS(3:1)-C-MOF-5	0.1 M KOH	–0.005 vs. Ag/AgCl	–	3.2	3.4–3.8 at 0.57–0.07 V	[128b]
P-N-carbon-950	0.1 M KOH	–	0.80	4.86	3.82	[128c]
NPS-C-MOF-5	0.1 M KOH	–0.006 vs. Ag/AgCl	–	–	3.6	[128a]

[a] *n* represents the number of electrons transfer.

FeP)<sub>n</sub> MOF exhibited a well-defined cathodic peak at –0.23 V versus Ag/AgCl in CV, which indicates its origin to ORR. The oxygen reduction current density at the onset potential of (G-dye 50 wt %-FeP)<sub>n</sub> MOF can reach –6.2 mA cm<sup>-2</sup> with a good durability. The high ORR activity and 4-electron reduction pathway are ascribed to the synergistic effect between r-GO, pyridinium linker and porphyrin in the MOF frameworks.

Research also devoted to improving the conductivity of MOFs for ORR.<sup>[36a,c,113]</sup> Miner et al demonstrated an intrinsically conductive MOF, Ni<sub>3</sub>(HITP)<sub>2</sub> (HITP = 2, 3, 6, 7, 10, 11-hexamino-triphenylene), exhibiting good electrical conductivity ( $\sigma = 40 \text{ S cm}^{-1}$ ) with outstanding ORR activity, which is comparable with the most non-platinum electrocatalysts (Figure 15).<sup>[114]</sup> In oxygen-saturated 0.1 M KOH solution, Ni<sub>3</sub>(HITP)<sub>2</sub> thin film on glassy carbon electrode showed a low onset potential ( $j =$

50 mA cm<sup>-2</sup>) of 0.82 V. After 8 h durability test via steady-state potentiostatic measurements at 0.77 V, Ni<sub>3</sub>(HITP)<sub>2</sub> delivered a high ORR stability and kept 88% of the initial current density after the test. Through calculating the inverse of the slope of Koutecky-Levich (K-L), the total number of transferred electrons was determined to be  $n = 2.25$ , indicating that oxygen tended to be converted into HO<sub>2</sub><sup>-</sup> on Ni<sub>3</sub>(HITP)<sub>2</sub> during ORR. Rationally designing MOF with conductive properties will facilitate the development of pristine MOF-based catalysts.

Apart from designing conductive MOFs as catalysts, the integration of transition metal hybrids with water-stable MOFs can also enhance catalytic activities and stabilities.<sup>[101,115]</sup> For example, Wang et al synthesized a hybrid electrocatalyst consisting of ε-MnO<sub>2</sub> and a MOF(Fe) support towards ORR.<sup>[116]</sup> Compared with the MOF-free ε-MnO<sub>2</sub> and MOF(Fe), the resulting ε-MnO<sub>2</sub>/



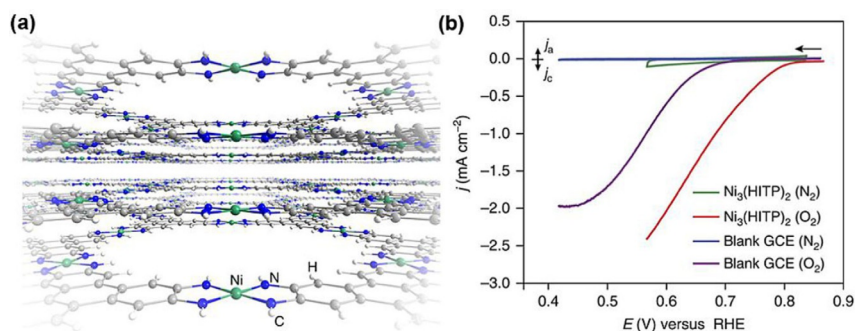


**Figure 15.** a) A schematic representation of the conductive two-dimensionally layered  $\text{Ni}_3(\text{HITP})_2$ . b) LSV scans ( $5 \text{ mV s}^{-1}$ ) for the  $\text{Ni}_3(\text{HITP})_2$  catalyst and blank GCE under  $\text{N}_2$  versus  $\text{O}_2$  atmosphere. Reproduced with permission from reference [114]. Copyright 2016, Nature Publishing Group.

MOF(Fe) composite on the glassy carbon rotating disk electrode (GC-RDE) exhibited significantly enhanced performance for ORR, possessing a more positive onset ORR potential ( $0.84 \text{ V}$  at  $-0.10 \text{ mA cm}^{-2}$ ), a higher half-wave potential ( $0.64 \text{ V}$ ), a larger kinetic current density ( $-3.16 \text{ mA cm}^{-2}$  at  $0.65 \text{ V}$ ) and a similar diffusion-limited current density ( $-5.56 \text{ mA cm}^{-2}$ ). Based on K-L plots, the electron transfer number for the  $\epsilon\text{-MnO}_2/\text{MOF}(\text{Fe})$  composite was calculated to 3.7–3.9 and unchanged with the overpotentials, suggesting that the oxygen reduction was via an apparent 4-electron process. Moreover, the  $\epsilon\text{-MnO}_2/\text{MOF}(\text{Fe})$  showed an excellent ORR stability and finally maintained a 77.5% of the initial current density at after 20000 s, which may be attributed to the high specific surface area and the strong interactions between  $\epsilon\text{-MnO}_2$  and MOF(Fe).

MOF-derived carbon-based non-precious metal nanocatalysts are regarded as a class of outstanding ORR catalysts for the low cost, porous structure and high conductivity. Recently,

a part of MOF-derived metal heteroatom-doped porous carbon with heteroatom doping show superior ORR performances than commercial 20% Pt/C in alkaline solution.<sup>[122]</sup> In these works, some pristine MOFs consisting of heteroatom-containing ligands (such as N, P, S, C, etc.) and metal sources (such as Fe, Co, Ni, etc.) could be transformed into metal heteroatom-doped porous carbon catalysts through a direct carbonization method.<sup>[122d, 123]</sup> Using the method, a class of catalysts with  $\text{M-N}_4$  or  $\text{M-N}_x$  (metal-nitrogen) structure, known as active sites, have attracted huge research interest as alternatives to noble metals.<sup>[124]</sup> For example, Li et al have made great efforts in terms of  $\text{M-N}_4$  structure for ORR, they synthesized the atomic dispersion of Co atoms with N-coordination as the ORR catalyst via one-step pyrolysis of a type of Zn/Co bimetallic MOF (Figure 16).<sup>[122d]</sup> When heating temperature above  $800^\circ\text{C}$ , the low boiling point Zn atoms would be selectively evaporated away. Meanwhile, Co units were reduced to Co single atoms by carbonization of the organic linkers. The as-prepared Co single

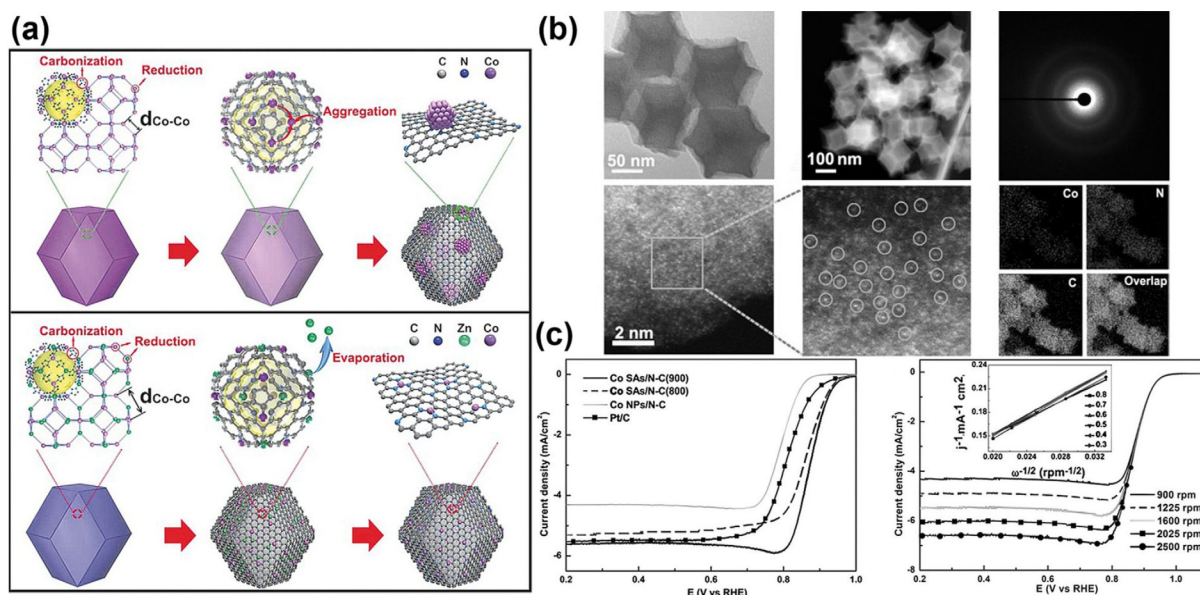


**Figure 16.** a) Schematic illustration of tuning the atomic dispersion of Co atoms in the N-doped porous carbon through the evaporation of Zn. b) TEM, HAADF-STEM and EELS mapping images of Co SAs/N-C(800). c) Voltammetric curves for different catalysts obtained  $\text{O}_2$ -saturated  $0.1 \text{ M KOH}$  together with the RDE polarization curves for the Co SAs/N-C(900) catalyst recorded at different rotation rates. Reproduced with permission from reference [122d]. Copyright 2016, Wiley-VCH.

atoms/nitrogen-doped porous carbon (Co SAs/N-C)-900 exhibited the almost same onset potential as Pt/C at 0.982 V, and a more positive half-wave potential (0.881 V) than that of Pt/C (0.811 V). According to K-L plots, its kinetic current density at 0.8 V can reach  $21.2 \text{ mA cm}^{-2}$  with a small Tafel slope of  $75 \text{ mV dec}^{-1}$ . The superior ORR performance should be related to Co-N-C sites, atomic dispersion and N-doped porous carbon support. Apart from Co-N-C structure, Liu et al demonstrated that Zn/Fe bimetallic ZIF-derived Fe-N-C hybrid exhibited excellent ORR activity.<sup>[122c]</sup> The as-obtained hybrid FeNC-20-1000 displayed the best catalytic activity, with a higher onset potential (1.04 V) than that of Pt/C (0.97 V) and a half-wave potential of 0.88 V. Based on the corresponding K-L plots, the electron transfer number was calculated to 3.99 with a catalysis loading of  $0.75 \text{ mg cm}^{-2}$  and its Tafel slope was  $49 \text{ mV dec}^{-1}$ , which was even lower than that of Pt/C ( $61 \text{ mV dec}^{-1}$ ). With the optimized annealing temperature, FeNC-20-1000 derived from bimetallic Zn/Fe-ZIFs delivered an enhanced mass-transport efficiency and the highest ORR catalytic activity. Besides, Wang et al reported a novel metal heteroatom-doped porous carbon with Fe-Co dual sites embedded in N-doped carbon nanotubes through the processes of adsorption and pyrolysis.<sup>[123b]</sup> The MOF-derived catalyst (Fe,Co)/CNT exhibited an outstanding ORR activity, with an onset potential of 1.15 V and a half-wave potential of 0.954 V in  $\text{O}_2$ -saturated 0.1 M KOH. Also, the (Fe,Co)/CNT achieved a much higher turnover frequency ( $0.105 \text{ s}^{-1}$ ) than that of the single-site Fe/CNT-C ( $0.0049 \text{ s}^{-1}$ ) and the single-site Co/CNT-C ( $0.00036 \text{ s}^{-1}$ ). Its K-L plots at various rotating speeds proved a nearly four-electron ORR pathway, and the kinetic current density at 0.9 V was  $17.51 \text{ mA cm}^{-2}$ , suggesting the best ORR performance.

In terms of the carbon-incorporated transition metal complexes, great efforts have also been devoted to exploring MOF-derived nanostructured metal or alloy, metal oxides, carbides, sulfides and selenides.<sup>[33b, 60, 71d, 86b, 93, 100, 125]</sup> For example, Ma and co-workers developed  $\text{Co}_3\text{O}_4\text{C-NA}$  electrocatalysts, which showed a half-wave potential of 0.78 V together with a Tafel slope of  $89 \text{ mV dec}^{-1}$ .<sup>[93]</sup> Further, the electron transfer number was calculated to 3.85–3.96 via the RRDE measurements. The hybrid porous nanowire arrays exhibited a state-of-the-art ORR activity and a desirable four-electron pathway owing to the unique nanowire arrays and in situ carbon incorporation. Apart from metal oxides, Guan et al proposed a dual-MOF confined-pyrolysis method to synthesize  $\text{Fe}_3\text{C}$  nanoparticle-embedded N-doped carbon nanotube assemblies ( $\text{Fe}_3\text{C@N-CNT}$  assemblies).<sup>[86b]</sup> The electrocatalytic activity and kinetics of the resulting sample were investigated in  $\text{O}_2$ -saturated 0.1 M KOH solution, and the electron transfer number was determined in the range of 3.95–3.98 by the K-L plots, suggesting oxygen can be directly reduced to  $\text{OH}^-$  using the  $\text{Fe}_3\text{C@N-CNT}$  assemblies as electrocatalysts. Remarkably, the sample shows a more positive half-wave potential of 0.85 V than that of commercial Pt/C (0.83) and a small Tafel slope of  $\approx 78 \text{ mV dec}^{-1}$ . The superior electrocatalytic activity of the as-prepared  $\text{Fe}_3\text{C@N-CNT}$  assemblies might be related to highly active chemical composition and robust structure. A great number of previous works in exploring the high activity of catalysts pay more attention to

active sites and nanostructures, but the intrinsic drawbacks of poor charge transport for most compounds have a crucial impact on catalytic performance. Transition metal sulfides and selenides with high conductivity, remarkable stability and efficient catalytic activity have caused widespread concern.<sup>[97]</sup> Meng et al constructed N-doped carbon-wrapped ultrafine  $\text{Co}_{0.85}\text{Se}$  nanocrystals for ORR via a one-step carbonization-selenylation calcinations in high temperature (Figure 17 a).<sup>[60]</sup> Benefiting from the synergistic contributions by coupling  $\text{Co}_{0.85}\text{Se}$  nanocrystals and highly conductive N-doped carbon layers, the resultant  $\text{Co}_{0.85}\text{Se@NC}$  afforded an excellent ORR performance with a sharp onset potential at 0.912 V and a desirable electron-transfer number in the range of 3.98–4.03 within the potential range from 0.272–0.572 V, indicating the four-electron pathway for ORR process (Figure 17 b and c). All the above investigations indicate that exploring MOF-derived carbon-incorporated transition metal complexes provides an important route to design high-performance electrocatalysts for ORR.

Alternatively, developed heteroatom-doped metal-free porous carbon can also improve the electrical conductivities, stabilities, tolerance to acidic/alkaline conditions, abundance, and low cost of MOF-based materials.<sup>[126]</sup> The rich N-contained ligand in MOF framework offers the MOF derivatives unique electron structure and high conductivity. For example, Zheng et al reported the first example of MOF-derived metal-free ORR electrocatalyst via a carbonization procedure of ZIF-7 and glucose mixture.<sup>[110b]</sup> The resulting N-doped porous carbon showed porous structures and high specific surface area. The corresponding electrocatalytic activity was measured in  $\text{N}_2$  or  $\text{O}_2$  gas saturated 0.1 M KOH aqueous solution, and the N-doped porous carbon exhibited outstanding ORR performance with the onset potential of 0.86 V, half-wave potential of 0.7 V and the limiting current density of  $-4.59 \text{ mA cm}^{-2}$ . Based on the K-L equation, the number of electron transfers at 0.3 V was calculated to 3.68, which was close to commercial 20% Pt/C. In this work, Zn nodes played a critical role in the activation of carbon for the formation of micropores by evaporation etching at  $950^\circ\text{C}$ . Hong et al also studied N-doped graphitic porous carbons (NGPCs) as the metal-free electrocatalysts for ORR through using a zeolite-type MOF as the carbon and nitrogen precursors.<sup>[127]</sup> Compared with commercial Pt/C, the optimized NGPC-1000-10 exhibited high electrocatalytic performance for ORR with slightly negative activities on onset potential (0.95 V) and half-wave potential (0.77 V), which were mainly attributed to the synergistic effects of high specific surface area, the high degree of graphitization and porous structures. What is more, the number of electron transfers was an almost constant (3.81 at 0.62 V) over the potential range from 0.72 to 0.37 V. The corresponding kinetic current density was  $14.2 \text{ mA cm}^{-2}$ , even comparable to that of commercial Pt/C ( $19.9 \text{ mA cm}^{-2}$ ).

Apart from single-atom doping, the incorporation of multi-nonmetallic heteroatoms (such as N, S, P, B, etc.) into the carbon lattice is one of the promising strategies to tailor electrocatalytic property by the combination of the synergistic effect among different dopant.<sup>[128]</sup> Li et al indicated that N and S co-doped porous carbons could be easily converted to derivatives using MOF-5, urea and DMSO as the template, N and S

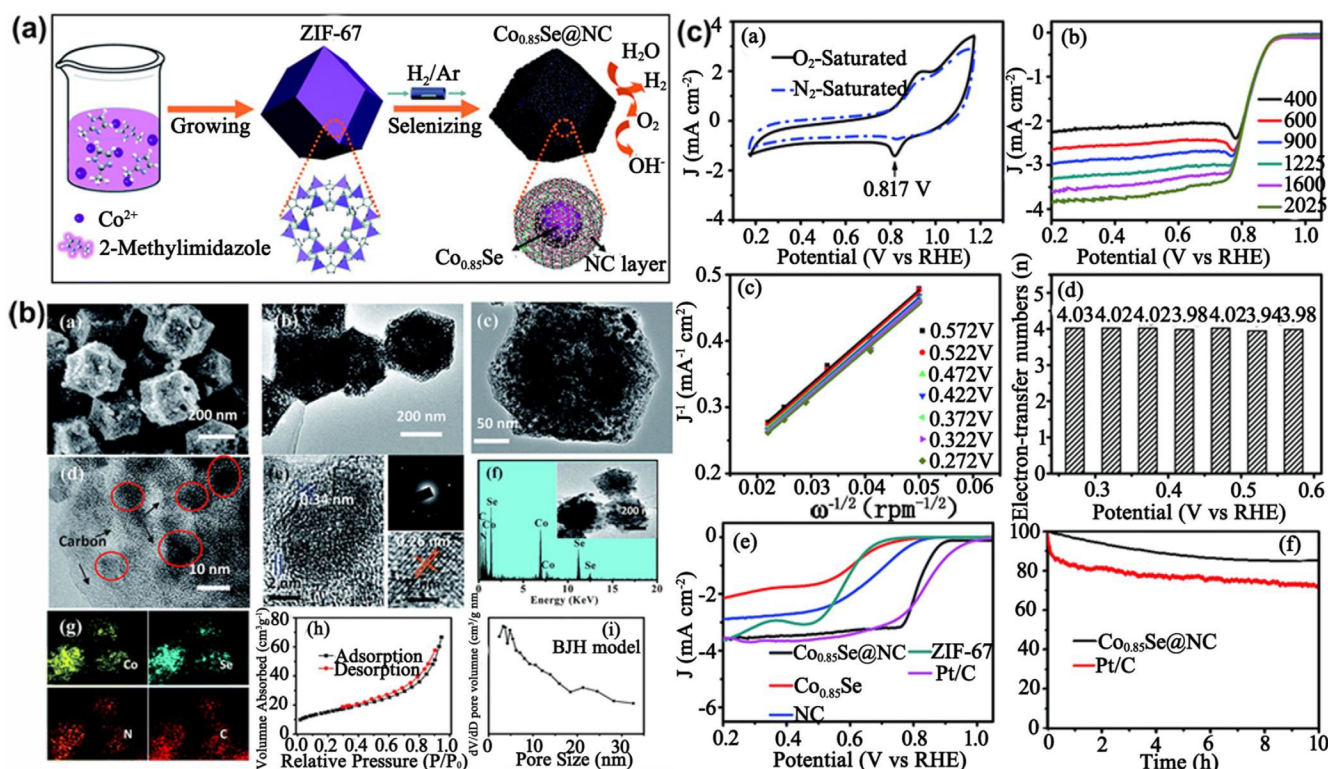


**Figure 17.** a) Schematic illustration of the synthesis process of  $\text{Co}_{0.85}\text{Se}@\text{NC}$ . b) FE-SEM, TEM, HRTEM images, SAED pattern, EDS spectrum, the corresponding EDS elemental maps,  $\text{N}_2$  adsorption-desorption isotherms and corresponding pore size distribution curve of the  $\text{Co}_{0.85}\text{Se}@\text{NC}$  sample. c) ORR electrocatalysis in 0.1 M KOH. Reproduced with permission from reference [60]. Copyright 2017, Royal Society of Chemistry.

precursors, respectively.<sup>[128b]</sup> The onset potential of the obtained N and S co-doped porous carbons was at about  $-0.005$  versus Ag/AgCl, which was more positive than that of single-atom doping catalysts and even comparable to commercial Pt/C catalyst. From the slopes of the K-L plots, the electron transfer number of N and S co-doped porous carbons was calculated to be 3.4–3.8 at a potential range of  $-0.4$  to  $-0.9$  V versus Ag/AgCl, indicating the high ORR activity via a 4-electron transfer pathway. The enhanced catalytic performance is mainly attributed to the destruction of electroneutrality of the carbon matrix through the doped atoms with different electronegativities.

### 3. MOF-based electrocatalysts for $\text{CO}_2$ reduction

Carbon dioxide has been one of the arch-criminals of global warming aggravated the desertification and sea-level rise due to the combustion of fossil fuel and hydrocarbon materials.<sup>[135]</sup> Great efforts have been made by governments and researchers by reducing the  $\text{CO}_2$  emission, capturing and reusing of  $\text{CO}_2$ .<sup>[136]</sup> Conversion of  $\text{CO}_2$  into valuable chemical compounds, intermediate industry products and green fuel not only can prevent severe global warming but also can relieve energy crisis. There are plentiful approaches for  $\text{CO}_2$  conversion, for example, electrochemical,<sup>[137]</sup> biochemical,<sup>[138]</sup> photochemical,<sup>[139]</sup> chemical and hydrothermal,<sup>[140]</sup> to name just a few.

The electrochemical conversion of  $\text{CO}_2$  into value-added carbon products have been attracting as one of the promising approaches due to the following advantages: (I) The  $\text{CO}_2$  electrochemical reduction process can be in situ monitored by electrochemical workstation; (II) The reaction is carried out under mild conditions, which is controllable; (III) The reaction products can be adjusted by operation parameters, such as electrode potential, electrolytes, and reaction temperature, etc; (IV) The driving force of electric power for  $\text{CO}_2$  reduction can use renewable energy sources such as wind, hydro and solar power. Depending on the catalysts, applied potential, supporting electrolyte and reaction temperature, the electrochemical conversion of  $\text{CO}_2$  produces various products such as CO,  $\text{CH}_4$ ,  $\text{C}_2\text{H}_4$ , HCOOH,  $\text{H}_2\text{C}_2\text{O}_4$ , methanol and ethanol, which follows the reaction approaches involving two, four, six, and eight electrons transfer.<sup>[141]</sup> (Table 7) Metal-organic frameworks allow for producing the desired product via rationally controlled metal nodes, well-design organic linker, and flexible electrode preparation.<sup>[29b, 142]</sup> However, to design MOFs or MOFs derivatives as electrocatalysts with a good compromise of high Faradaic efficiency and selectivity is still a challenge. Several reviews have been published concerning the MOFs and MOFs derivatives for electrochemically reducing  $\text{CO}_2$  into different products.<sup>[9c, 29, 141–143]</sup> However, the comprehensive discussion of the design strategies of MOFs and MOFs derivatives for  $\text{CO}_2$  electrochemical reduction has not been studied yet. In this section, we will focus on the design concepts of MOFs and MOFs



**Table 7.** Possible reaction approaches of CO<sub>2</sub> electrochemical reduction involving in MOF and MOFs derivatives catalysts.

Reactions	Theoretical potential [V vs. SHE]
CO <sub>2</sub> (g) + 2H <sub>2</sub> O(l) + 2e <sup>-</sup> ⇌ CO(g) + 2OH <sup>-</sup>	-0.93
CO <sub>2</sub> (g) + 2H <sup>+</sup> + 2e <sup>-</sup> ⇌ HCOOH(l)	-0.25
CO <sub>2</sub> (g) + H <sub>2</sub> O(l) + 2e <sup>-</sup> ⇌ HCOO <sup>-</sup> (aq) + OH <sup>-</sup>	-1.08
2CO <sub>2</sub> (g) + 2H <sup>+</sup> + 2e <sup>-</sup> ⇌ H <sub>2</sub> C <sub>2</sub> O <sub>4</sub> (aq)	-0.50
2CO <sub>2</sub> (g) + 2e <sup>-</sup> ⇌ C <sub>2</sub> O <sub>4</sub> <sup>2-</sup> (aq)	-0.59
CO <sub>2</sub> (g) + 6H <sup>+</sup> + 6e <sup>-</sup> ⇌ CH <sub>3</sub> OH(l) + H <sub>2</sub> O(l)	+0.02
CO <sub>2</sub> (g) + 5H <sub>2</sub> O(l) + 6e <sup>-</sup> ⇌ CH <sub>3</sub> OH(l) + 6OH <sup>-</sup>	-0.81
CO <sub>2</sub> (g) + 8H <sup>+</sup> + 8e <sup>-</sup> ⇌ CH <sub>4</sub> (g) + 2H <sub>2</sub> O(l)	+0.17
CO <sub>2</sub> (g) + 6H <sub>2</sub> O(l) + 8e <sup>-</sup> ⇌ CH <sub>4</sub> (g) + 8OH <sup>-</sup>	-0.66
2CO <sub>2</sub> (g) + 12H <sup>+</sup> + 12e <sup>-</sup> ⇌ C <sub>2</sub> H <sub>4</sub> (g) + 4H <sub>2</sub> O(l)	+0.06
2CO <sub>2</sub> (g) + 12H <sup>+</sup> + 12e <sup>-</sup> ⇌ CH <sub>3</sub> CH <sub>2</sub> OH(g) + 3H <sub>2</sub> O(l)	+0.08

derivatives for improving the faradaic efficiency and selectivity of CO<sub>2</sub> electrochemically converted to valued products.

CO has been widely used in a wide range of industries, such as chemicals, medicine and metallurgy, etc.<sup>[144]</sup> Besides, as the main components of syngas, CO plays a key role in the synthesis of various intermediates and organic chemical products. Development of highly efficient electrocatalysts for CO<sub>2</sub>-to-CO is of great significance.

Electroreduction of CO<sub>2</sub>-to-CO involving 2 electrons needs ≈ 137 kJ mol<sup>-1</sup>.<sup>[4,141]</sup> (Table 7) It contains three essential steps: (I) Capturing CO<sub>2</sub> on the catalysts surface accompanying with a proton/electron transfer process, to form \*COOH intermediate absorbed on catalysts surface. ("\*" represent the surface-coordinated state of the species.) (II) The absorbed \*COOH intermediates are further electrochemically reduced to \*CO based on another proton-coupled electron transfer process. (III) After that, the \*CO desorbed from the surface of the catalysts. Thus, the strategies for designing the idea catalysts will focus on the aspects of enhancing the capture and absorption of CO<sub>2</sub>, improve the proton and electron conductivity, and control the adsorption strength of the intermediates such as \*COOH and \*CO, which play key roles in the CO<sub>2</sub> activation. (Figure 18)

Metal-organic frameworks show a promising application in boosting the areal concentration of CO<sub>2</sub> reduction catalysts due to their high surface area (Table 8).<sup>[141,157]</sup> The porous and ordered characteristics of MOFs allow the electrolyte and dissolved CO<sub>2</sub> to permeate to the interior of the catalysts active

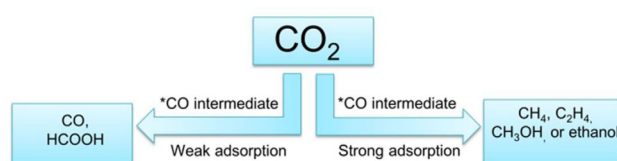


**Figure 18.** Possible mechanism which determines the products of CO<sub>2</sub> electrochemical reduction.

sites freely. By rationally incorporating the redox-active linker could also improve the charge transport of catalysts. (Figure 19) Taking advantages of the MOFs, Hupp and co-workers deposited Fe-based MOF-525 thin film on the conductive electrode for CO<sub>2</sub> electrochemical reduction.<sup>[145]</sup> The Fe-based MOF-525 film shows a highly effective catalyst surface concentration for CO<sub>2</sub> reduction due to the uniform distribution of Fe in MOFs film. The porphyrin linker improves the hopping charge transfer in the MOF film catalysts. Thus, the prepared Fe-based MOF-525 film demonstrated a ≈ 100% Faradaic efficiency. However, the selectivity of Fe-based MOF-525 film for CO is only 54 ± 2%. The low selectivity for CO is probably ascribed to the low local concentration of CO<sub>2</sub> and weak adsorption strength of MOF-525 film to \*COOH and \*CO. Thus, the new design for improving the CO<sub>2</sub> capture and adsorption strength of catalysts to intermediates is required.

Kang et al utilized ZIF-8, which has higher CO<sub>2</sub> capture ability than MOF-525, as catalysts for CO<sub>2</sub> electroreduction.<sup>[147]</sup> It

**Table 8.** MOF-based materials for electrochemical reduction of CO<sub>2</sub> to CO.

MOF	Main Product(s)	Selectivity for CO [%]	Medium	Total Faradaic Efficiency [%]	Ref.
MOF-525	CO	54	Acetonitrile	≈ 100	[145]
ZIF-8	CO	60	NaCl	95	[146]
Al <sub>2</sub> (OH) <sub>2</sub> TCPP-Co	CO	76	K <sub>2</sub> CO <sub>3</sub>	≈ 80	[147]
PCN-222(Fe)	CO	91	KHCO <sub>3</sub>	≈ 100	[148]
Ligand doping into ZIF-8	CO	90.57	KHCO <sub>3</sub>	-	[149]
Re-SURMOF	CO	93	KHCO <sub>3</sub>	-	[150]
NU-1000 (Cu)	CO	31		28	[151]
Ag-doped Co <sub>3</sub> O <sub>4</sub> derived from MOF	CO	55.6	KHCO <sub>3</sub>	≈ 100	[152]
Single Ni atoms derived from ZIF-8	CO	71.9	KHCO <sub>3</sub>	-	[153]
Pyrolysis ZIF-8	CO	78	KHCO <sub>3</sub>	≈ 100	[154]
C-AFC@ZIF-8	CO	93	KHCO <sub>3</sub>	≈ 100	[155]
Pyrolysis Co-ZIF-67	CO	94	KHCO <sub>3</sub>	≈ 100	[156]

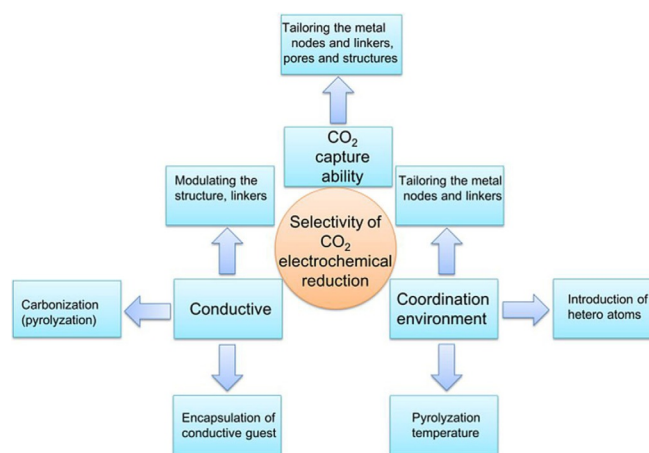


**Figure 19.** A schematic: Possible pathways for improving the electrochemical CO<sub>2</sub> reduction selectivity.

shows a faradaic efficiency of 60% for CO. In addition, Yaghi and Yang et al fabricate MOF- $\text{Al}_2(\text{OH})_2\text{TCCP-Co}$ , which incorporated catalytic cobalt center and porphyrin units, as thin films for selective reducing  $\text{CO}_2$  to CO.<sup>[158]</sup> The MOFs based modified metal center in ligand owns more catalytic active adsorption sites than those based on pristine ligands and thus enhances the adsorption of  $\text{CO}_2$ . It exhibits a high faradaic efficiency of 76%, contributed by modified catalytic Co center in porphyrin and the MOF frameworks. In situ spectroelectrochemical measurement was utilized to comprehensively study the redox catalytic centers in the MOFs and electronic structure of porphyrins. Similarly, Dong and co-workers employed Fe-metallated porphyrin-based PCN-222(Fe) for selective electrochemical conversion of  $\text{CO}_2$  to CO, showing a high faradaic efficiency of 91% for CO.<sup>[148]</sup> These results show the direction that modified catalytic metal center into porphyrin linker and incorporated them into MOF frameworks can optimize the selectivity of MOFs for electrochemical reduction of  $\text{CO}_2$ . Besides, rationally deposition of MOFs as oriented thin film via liquid-phase epitaxy layer-by-layer technique can also expose the active sites as much as possible. Liu and Sun et al reported Re-SURMOF for  $\text{CO}_2$  electrochemical reduction with a faradaic efficiency of 93% towards to CO.<sup>[150]</sup> The high faradaic efficiency of Re-SURMOF towards CO is ascribed to the oriented nature of SURMOFs, which facilitate charge transport from the electrode to the surface of the catalyst.

Although the porphyrin-based MOFs show a strong electron hopping for charge transfer and highly orientation of thin films offer the benefit for charge transfer, the conductivity of porphyrin-based MOFs is still unsatisfied. Tremendous efforts have been made to improve the charges transfer of the MOFs based materials. (Figure 20) Wang et al reported a strategy based doping electron-donating molecule of 1,10-phenanthroline into ZIF-8 frameworks as  $\text{CO}_2$  reduction electrocatalysts with a faradaic efficiency of 90.57% for CO generation.<sup>[149]</sup> The elec-

tron-donating nature of phenanthroline promotes the adjacent active sites of  $\text{sp}^2$  C atoms in imidazole ligand to have more electrons. These electrons enable the generation of  $^*\text{COOH}$ , which enhance the faradaic efficiency towards CO production.

Alternatively, the pyrolysis of MOFs to MOFs derivatives offers an opportunity for producing conductive carbon materials and keeping the high porosity of MOFs precursor, facilitating the charge transfer from the electrode to catalysts surface and expose the active sites as much as possible.<sup>[159]</sup> The catalytic hetero-atoms can be introduced onto the electrode by well-chosen of target MOFs and further improve the electrical, chemical and functional properties of the carbon materials by the pyrolytic process. In addition to that, the faradaic efficiency of  $\text{CO}_2$  electrochemical conversion to CO is enhanced.

There are three ways to introduce hetero atoms onto carbon matrix based on carbonization of MOFs: (I) The introduction of heteroatoms is based on metal nodes. Zheng et al pyrolyzed MOF  $[\text{AgCo}_2(\text{pyz})\text{PDC}_4][\text{Ag}_2\text{Co}(\text{pyz})_2\text{PDC}_2]$  into Ag-doped  $\text{Co}_3\text{O}_4$  catalyst.<sup>[152]</sup> The Ag-doped  $\text{Co}_3\text{O}_4$  catalyst shows a faradaic efficiency of 55.6%, which is superior than MOF-525 films. The main reasons are ascribed that the homogenous coved Ag and calcinated MOF itself improve the electron transport properties and further boost the catalytic efficiency. (II) The introduction of heteroatoms is based on organic ligands. Gascon et al reported that the calcination of ZIF-8 introduce the heteroatom N from the imidazole organic ligands to enhance the electrochemical reduction of  $\text{CO}_2$ -to-CO, showing a faradaic efficiency of 78% towards to CO.<sup>[154]</sup> Bao et al modified the ZIF-8 surface with ammonium ferric citrate and then pyrolyzed them into MOF derivatives.<sup>[155]</sup> The Fe-N active sites are found homogenous distributed and highly exposed to the porous carbon matrix. The introduction of heteroatoms Fe through surface modification increases the faradaic efficiency of CO from 78% to 93%. (III) The introduction of heteroatoms is based on the porosity of MOFs. The hetero active ions/atoms can load into the pores of MOFs before the composites were pyrolyzed. In this case, the location environment (e.g. distribution, exposure, and structure, etc.) can be controlled during the carbonization process. Li et al first synthesized ZIF-8 with a uniform rhombododecahedral shape and further encapsulated Ni precursor into the pores of ZIF-8.<sup>[153]</sup> Then, the composite was pyrolyzed at  $1000^\circ\text{C}$  to form Ni single atoms on carbon matrix with N hetero-atoms. The prepared Ni single atoms loaded on carbon matrix shows a CO faradaic efficiency of 71.9. These reports show that the rational production of heteroatoms from pyrolyzing MOFs is one of the promising ways to improve the selective electroreduction of  $\text{CO}_2$ -to-CO.

In addition, the pyrolysis of tailored MOFs can control the coordination number of the active sites in the catalysts. Wu et al first prepared bimetallic Co/Zn ZIFs as the precursor and afterwards evaporated the Zn and reduced the Co ions through pyrolysis process to form single Co atoms anchored on N-doped carbon matrix.<sup>[156]</sup> By changing the pyrolysis temperature, different coordination number of single Co atoms can be varying. For example, three atomically anchored Co catalysts with different Co-N number can be obtained at  $800^\circ\text{C}$  ( $\text{Co-N}_4$ ),  $900^\circ\text{C}$  ( $\text{Co-N}_3$ ), and  $1000^\circ\text{C}$  ( $\text{Co-N}_2$ ), respectively. The studies

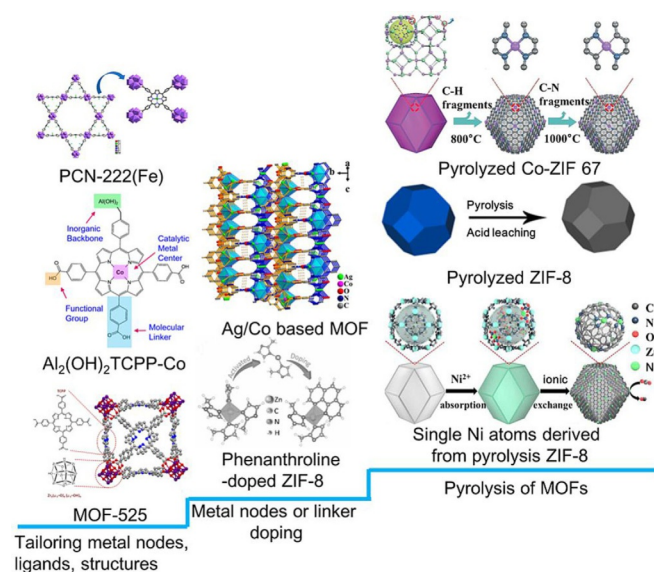


**Figure 20.** The developed strategies for the MOF-based materials for  $\text{CO}_2$  electrochemical reduction.

show that the low coordination number of catalysts has the fast dynamic in activation of CO<sub>2</sub> to the \*COOH and thus boost the CO<sub>2</sub> electroreduction activity. Thus, the Co-N<sub>2</sub> shows the highest selectivity of 94% CO productions Faradaic efficiency. (Figure 20)

Summarizing, achieving high Faradaic efficiency of electroreduction CO<sub>2</sub>-to-CO depends on the good balancing of the capture capacity, activation ability and adsorption strength of catalysts with CO<sub>2</sub> and the responded intermediates.

The electroreduction of CO<sub>2</sub>-to-CO is a simple 2 electrons transfer process. The high production of CO relies on the adsorption, reduction of \*COOH-to-\*CO and fast desorption of CO molecules. If the catalysts show weak stabilization of \*COOH (or \*COO<sup>-</sup>), another two-electron transfer products for generating formic acid or formate occurs. Kinogami and co-workers prepared copper rubeanate metal-organic framework (CR-MOF) for electrochemical reduction of CO<sub>2</sub> to formic acid (HCOOH) with a selectivity of ≈98% (Table 9).<sup>[160]</sup> The high se-

tion of catalyst surface to \*CO results in high production of CO. Whereas, the \*CO intermediates are strongly adsorbed on the catalyst surface. Then, the \*CO intermediates will be reacted with another CO<sub>2</sub> molecule to produce \*CO-CO<sub>2</sub><sup>-</sup> intermediate through C–O coupling. Furthermore, the formed \*CO-CO<sub>2</sub><sup>-</sup> intermediates can be further reduced and hydrogenated to CH<sub>4</sub>.

Han et al deposited Zn-BTC MOFs on carbon paper for electrochemical reduction of CO<sub>2</sub>-to-CH<sub>4</sub>.<sup>[163]</sup> By well control the morphology of Zn-BTC and chose of ionic liquids as electrolytes, Han and co-workers achieved a faradaic efficiency of 80% for CO<sub>2</sub>-to-CH<sub>4</sub>. The high faradaic efficiency is ascribed to the combination of Zn-BTC MOF electrode and ionic liquids. The Zn-BTC MOF has higher CO adsorption ability than CH<sub>4</sub>. Thus, the \*CO intermediates preferred to be adsorbed on Zn-BTC MOF electrode and further to be reduced to CH<sub>4</sub>. The ionic liquids can serve as a concentrator for storing CO<sub>2</sub>. Therefore, the Zn-BTC MOF electrode immersing in ionic liquids shows a promising way to produce CH<sub>4</sub> from CO<sub>2</sub> electrochemical reduction. Zhang et al also reported that depositing Cu<sub>3</sub>(BTC)<sub>2</sub> as electrode based on gas diffusion electrode (GDE) for electrochemical CO<sub>2</sub>-to-CH<sub>4</sub> shows 2–3 fold enhancement of faradaic efficiency for CH<sub>4</sub> comparing to blank GDE.<sup>[164]</sup> The increase of faradaic efficiency is ascribed to a high concentration of CO<sub>2</sub> adsorbed by Cu-MOF.

In addition, other hydrocarbons and alcohols such as ethylene, methanol, and ethanol can be produced via \*CO dimerization approaches. Sargent and co-workers synthesized Cu clusters with low coordination numbers based on the thermal distortion of HKUST-1 Cu dimer and showed a faradaic efficiency of 45% for C<sub>2</sub>H<sub>4</sub>, which is the highest reported value among Cu-based MOFs catalysts.<sup>[165]</sup> Pérez-Yáñez and co-workers introduced Ru<sup>III</sup>, Zn<sup>II</sup> and Pd<sup>II</sup> to the HKUST-1, which show a faradaic efficiency of 47.2% to methanol and ethanol.<sup>[162]</sup>

In summary, product selectivity of electrochemical CO<sub>2</sub> reduction is determined by the capture ability of CO<sub>2</sub> and adsorption ability of reaction intermediates, which are influenced by metal nodes, organic linkers,

grain boundaries, nanostructured morphology, vacancies, pore size, oxidation states, areal surface area, and surface structures. To enhance the faradaic efficiency of specific CO<sub>2</sub> electrochemical reduction products should be considered the overall parameters.

#### 4. MOF-based electrocatalysts for practical applications.

The as-studied electrocatalytic reactions are crucial for renewable technologies such as metal-air batteries and hydrogen production. For example, reactions such as ORR and OER are significant for metal-air batteries. MOF-based catalysts that show advanced bifunctional ORR and OER would be promising for such kind of metal-air batteries assembly. Besides, the assembly of HER and OER will be the technology as water electrolyz-

**Table 9.** MOF based materials for electrochemical reduction of CO<sub>2</sub> to other products.

MOF	Main Product(s)	Selectivity	Medium	Faradaic Efficiency [%]	Ref.
copper rubeanate	HCOOH	13.4%	KHCO <sub>3</sub>	13.4	[160]
Cu <sub>3</sub> (BTC) <sub>2</sub>	H <sub>2</sub> C <sub>2</sub> O <sub>4</sub>		DMF	51	[161]
Cu <sub>3</sub> (BTC) <sub>2</sub> doping with Ru	Methanol, Ethanol		KHCO <sub>3</sub>	47.2	[162]
Zn-BTC	CH <sub>4</sub>	85	ILs/CP	80.1	[163]
Cu <sub>3</sub> (BTC) <sub>2</sub>	CH <sub>4</sub>		NaHCO <sub>3</sub>	27	[164]
Calcinated HKUST-1	C <sub>2</sub> H <sub>4</sub>	–	KOH	45	[165]
HKUST-1	EtOH	–	KHCO <sub>3</sub>	10.3	[166]
Cu <sub>2</sub> [CuTCPP] nanosheet	HCOO <sup>-</sup>	–	MeCN with 1 M H <sub>2</sub> O and 0.5 M EMIMBF <sub>4</sub>	68.4	[167]
Cu-SIM NU-1000	HCOO <sup>-</sup>	–	NaClO <sub>4</sub>	28	[151]
Cu <sub>2</sub> O@Cu-MOF	CH <sub>4</sub>	–	KHCO <sub>3</sub>	63.2	[168]
OD-Cu/C	MeOH	–	KHCO <sub>3</sub>	43.2	[169]
MOF-derived Cu NPs	CH <sub>4</sub>	–	KHCO <sub>3</sub>	50	[170]

lectivity of electrochemical reduction of CO<sub>2</sub>-to-HCOOH is contributed to the proton conductivity, electronic conductivity, nanopores and isolated reaction sites. The formatted \*CO. is easily protonated by proton and further formation of HCOOH. In non-aqueous electrolytes, the format is possible to condense to oxalate. The results of CR-MOF for CO<sub>2</sub> electrochemical show that Cu-based MOFs may offer a feasible approach for the noteworthy production of HCOOH by rational design of the nanopores and frameworks.

By adjusting the adsorption capability of the catalysts towards to reaction intermediates such as \*COOH and \*CO, different products of CO<sub>2</sub> electrochemical reduction can be obtained. For example, \*COOH or \*COO<sup>-</sup> is formed through CO<sub>2</sub> adsorption and first electron reduction of CO<sub>2</sub>. If the \*COO<sup>-</sup> is strongly adsorbed on the catalyst surface, the \*CO intermediates is produced after gain another electron. The weak adsorp-



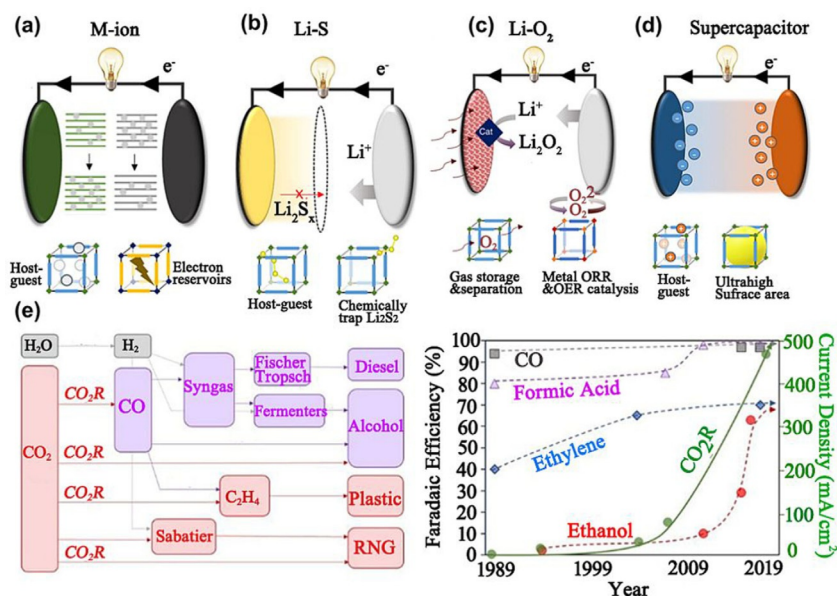


**Figure 21.** Scheme of MOF-based electrocatalysts for the potential application of devices and commodity chemicals. (a) Metal-ions batteries, (b) Li-sulfur batteries, (c) Li-O<sub>2</sub> batteries, (d) supercapacitors. (a)–(d), copyrights from reference [171], Copyright 2019, Nature Publishing Group. (e) Pathways and selectivities for renewable chemical synthesis. Copyrights from reference [172], Copyright 2019, AAAS.

er to generate clean hydrogen from water splitting. Exploration of MOF-based catalysts with excellent activity both in HER and OER could facilitate the production of hydrogen. Taking the advantages of high surface area and porous crystallinity, MOF-based materials exhibit their good performance on ion insertion and extraction as well as encapsulation of polysulfides. To this point, MOF-based materials will be developed as metal ions batteries, metal sulfur batteries (e.g. Li-S batteries, etc.) and supercapacitors. For the specific introduction of the strategies on bifunctional MOF-based catalysts and energy conversion and storage devices, we would like to guide the readers to the previous review.<sup>[29a, 43b, 171]</sup>

Electrochemically conversion of CO<sub>2</sub> to various products offer the technologies to produce many world's needed carbon-based commodity chemicals and turning the CO<sub>2</sub> wastes to high-value chemicals and feedstock (Figure 21). As discussed above, MOFs-based catalysts have shown their performance for converting CO<sub>2</sub> to different products. However, MOFs-based materials for electrochemical CO<sub>2</sub> reduction relevant to practical application is still challenging. For the details of the industrial application and marketing design of CO<sub>2</sub> electrocatalysts, we would like to guide the readers to the previous review.<sup>[172]</sup>

## 5. Summary, challenges and prospects

Many strategies have been developed to improve the efficiency and stability of MOF-based materials. These approaches should allow researchers to optimize new generations of the MOF-based electrocatalysts. Currently, the desired MOFs-based materials can be obtained by adjusting the compositions, tailoring the metal nodes and organic linkers, controlling the

morphology and rationally choosing substrates. The MOF-based materials with high selectivity of electrochemical CO<sub>2</sub> reduction to specific products can also be achieved by well controlling the synthesized engineering of MOF precursor preparation. These synthesized engineering concepts further can increase the number of active sites and improve the intrinsic characteristics of the catalysts, which in verse enhance the electrocatalytic activities or the faradaic efficiency of CO<sub>2</sub> electrochemical reduction. Based on the discussed strategies, some prepared MOF-based materials have shown better OER electrocatalytic activities than conventional noble metal-based materials. For CO<sub>2</sub> electrochemical reduction, the selectivity of the desired product can be improved. However, the electrocatalytic activities of MOF-based materials for the HER and ORR are still unsatisfied compared with the conventional Pt-based catalysts. The biggest obstacle, which impedes MOF-based for electrocatalysis systems, is their poor electric conductivity. Thus, exploring MOF-based materials with high electric conductivity is still demanding.

Currently, the MOF-based materials are usually utilized as a powder phase and drop-casted onto a substrate surface for electrocatalysis systems. In this case, the MOF-based materials and substrate surface usually show weak compatibility, hindering the charge transfer from the surface of the catalysts to the substrate surface and weakening the stability of electrocatalysts. The binder agents like Nafion solution are usually required, which would partially shield the active sites during the electron transfer process. Thus, it could be promising for future studies by growing the MOF-based materials as a thin film directly onto the substrates.<sup>[85b]</sup> Deposition the MOF directly onto the substrate surface could tailor the morphology and thickness of the film and maximize the active sites as much as

possible. Besides, the chemical bond, instead of physical packing, could anchor the MOF firmly onto the substrate and further facilitate the charge transfer and stability.

Additionally, the most used approaches for preparing MOF-derived materials is the pyrolysis process, which is energy and time-consuming. The facile one-step or in situ transformation of MOF into active electrocatalysts could be promising for future studies.<sup>[85b,92a]</sup> The facile one-step transformation or in situ transformation of MOFs could modulate the coordination environment by well controlling the parameters of compositions, structure and morphology, and substrates.

For practical use at the industrial scale, the current densities over 100 mAcm<sup>-2</sup> are necessary. This is one order of magnitude higher than those normally reported in the literature. Besides, the harsh conditions, such as strong alkaline environment and high temperature, are usually carried for the electrocatalysts in the industrial application. However, the catalysts' activity beyond these conditions and current density are scarcely addressed in laboratories fundamental research studies. At this point, it could be meaningful for testing the well-designed MOF-based electrode for real-life application. In order to avoid the macro gas bubbles, which could hinder the charge transfer and push the catalysts away from the substrate, microelectrode could be a promising candidate for future studies of MOF-based materials for industrial applications.<sup>[173]</sup>

## Acknowledgements

Juan Liu is grateful for Sino-Germany (CSC-DAAD) Post-doc Joint Scholarship. Shujin Hou is grateful for a PhD fellowship from the China Scholarship Council (CSC). Weijin Li is appreciated for the Alexander von Humboldt Research Fellowship for Postdoctoral Researchers. A.B. is thankful to Forschungsgemeinschaft (project BA 5795/4-1).

## Conflict of interest

The authors declare no conflict of interest.

**Keywords:** CO<sub>2</sub> reduction · derivatives · metal-organic frameworks · oxygen reduction reaction · water splitting

- [1] a) L. Yang, J. Shui, L. Du, Y. Shao, J. Liu, L. Dai, Z. Hu, *Adv. Mater.* **2019**, *31*, 1804799; b) Y. Zheng, Y. Jiao, A. Vasileff, S. Z. Qiao, *Angew. Chem. Int. Ed.* **2018**, *57*, 7568–7579; *Angew. Chem.* **2018**, *130*, 7690–7702.  
[2] F. A. L. Laskowski, M. R. Nellist, J. Qiu, S. W. Boettcher, *J. Am. Chem. Soc.* **2019**, *141*, 1394–1405.  
[3] S. Dey, B. Mondal, S. Chatterjee, A. Rana, S. Amanullah, A. Dey, *Nat. Rev. Chem.* **2017**, *1*, 0098.  
[4] X. Su, X. F. Yang, Y. Huang, B. Liu, T. Zhang, *Acc. Chem. Res.* **2019**, *52*, 656–664.  
[5] J. Liu, Q. Ma, Z. Huang, G. Liu, H. Zhang, *Adv. Mater.* **2019**, *31*, 1800696.  
[6] Y. Guo, T. Park, J. W. Yi, J. Henzie, J. Kim, Z. Wang, B. Jiang, Y. Bando, Y. Sugahara, J. Tang, Y. Yamauchi, *Adv. Mater.* **2019**, *31*, 1807134.  
[7] R. Francke, B. Schille, M. Roemelt, *Chem. Rev.* **2018**, *118*, 4631–4701.

- [8] N.-T. Suen, S.-F. Hung, Q. Quan, N. Zhang, Y.-J. Xu, H. M. Chen, *Chem. Soc. Rev.* **2017**, *46*, 337–365.  
[9] a) S.-N. Zhao, X.-Z. Song, S.-Y. Song, H.-j. Zhang, *Coord. Chem. Rev.* **2017**, *337*, 80–96; b) G. Li, S. Zhao, Y. Zhang, Z. Tang, *Adv. Mater.* **2018**, *30*, 1800702; c) P.-Q. Liao, J.-Q. Shen, J.-P. Zhang, *Coord. Chem. Rev.* **2018**, *373*, 22–48.  
[10] T. Qiu, Z. Liang, W. Guo, S. Gao, C. Qu, H. Tabassum, H. Zhang, B. Zhu, R. Zou, Y. Shao-Horn, *Nano Energy* **2019**, *58*, 1–10.  
[11] a) K. Jayaramulu, J. Masa, D. M. Morales, O. Tomanec, V. Ranc, M. Petr, P. Wilde, Y.-T. Chen, R. Zboril, W. Schuhmann, R. A. Fischer, *Adv. Sci.* **2018**, *5*, 1801029; b) L. Ye, J. Liu, Y. Gao, C. Gong, M. Addicoat, T. Heine, C. Wöll, L. Sun, *J. Mater. Chem. A* **2016**, *4*, 15320–15326.  
[12] C. Cao, D.-D. Ma, Q. Xu, X.-T. Wu, Q.-L. Zhu, *Adv. Funct. Mater.* **2019**, *29*, 1807418.  
[13] a) Q. Shao, P. Wang, X. Huang, *Adv. Funct. Mater.* **2019**, *29*, 1806419; b) L. Zhang, Z.-J. Zhao, J. Gong, *Angew. Chem. Int. Ed.* **2017**, *56*, 11326–11353; *Angew. Chem.* **2017**, *129*, 11482–11511.  
[14] a) X. Chen, K. Shen, J. Chen, B. Huang, D. Ding, L. Zhang, Y. Li, *Chem. Eng. J.* **2017**, *330*, 736–745; b) D. Ding, K. Shen, X. Chen, H. Chen, J. Chen, T. Fan, R. Wu, Y. Li, *ACS Catal.* **2018**, *8*, 7879–7888.  
[15] Z. Xue, Y. Li, Y. Zhang, W. Geng, B. Jia, J. Tang, S. Bao, H.-P. Wang, Y. Fan, Z.-w. Wei, Z. Zhang, Z. Ke, G. Li, C.-Y. Su, *Adv. Energy Mater.* **2018**, *8*, 1801564.  
[16] B. Y. Guan, Y. Lu, Y. Wang, M. Wu, X. W. Lou, *Adv. Funct. Mater.* **2018**, *28*, 1706738.  
[17] L. Sun, M. G. Campbell, M. Dincă, *Angew. Chem. Int. Ed.* **2016**, *55*, 3566–3579; *Angew. Chem.* **2016**, *128*, 3628–3642.  
[18] a) J. B. DeCoste, G. W. Peterson, H. Jasuja, T. G. Glover, Y.-g. Huang, K. S. Walton, *J. Mater. Chem. A* **2013**, *1*, 5642–5650; b) J. Canivet, A. Fateeva, Y. Guo, B. Coasne, D. Farrusseng, *Chem. Soc. Rev.* **2014**, *43*, 5594–5617; c) N. C. Burtch, H. Jasuja, K. S. Walton, *Chem. Rev.* **2014**, *114*, 10575–10612; d) K. Meyer, M. Ranocchiarì, J. A. van Bokhoven, *Energy Environ. Sci.* **2015**, *8*, 1923–1937.  
[19] Y. Wang, D. Yan, S. El Hankari, Y. Zou, S. Wang, *Adv. Sci.* **2018**, *5*, 1800064.  
[20] a) C. G. Morales-Guio, L.-A. Stern, X. Hu, *Chem. Soc. Rev.* **2014**, *43*, 6555–6569; b) S. Watzel, J. Fichtner, B. Garlyyev, J. N. Schwämmlein, A. S. Bandarenka, *ACS Catal.* **2018**, *8*, 9456–9462.  
[21] a) R. Paul, L. Zhu, H. Chen, J. Qu, L. Dai, *Adv. Mater.* **2019**, *31*, 1806403; b) Y. Yan, B. Y. Xia, B. Zhao, X. Wang, *J. Mater. Chem. A* **2016**, *4*, 17587–17603; c) J. Xie, Y. Xie, *Chem. Eur. J.* **2016**, *22*, 3588–3598.  
[22] a) J. Tymoczko, F. Calle-Vallejo, W. Schuhmann, A. S. Bandarenka, *Nat. Commun.* **2016**, *7*, 10990; b) M. D. Pohl, S. Watzel, F. Calle-Vallejo, A. S. Bandarenka, *ACS Omega* **2017**, *2*, 8141–8147.  
[23] W.-F. Chen, K. Sasaki, C. Ma, A. I. Frenkel, N. Marinkovic, J. T. Muckerman, Y. Zhu, R. R. Adzic, *Angew. Chem. Int. Ed.* **2012**, *51*, 6131–6135; *Angew. Chem.* **2012**, *124*, 6235–6239.  
[24] a) W.-F. Chen, J. T. Muckerman, E. Fujita, *Chem. Commun.* **2013**, *49*, 8896–8909; b) Z. Wang, Q. Li, H. Xu, C. Dahl-Petersen, Q. Yang, D. Cheng, D. Cao, F. Besenbacher, J. V. Lauritsen, S. Helveg, M. Dong, *Nano Energy* **2018**, *49*, 634–643.  
[25] Y. P. Zhu, C. Guo, Y. Zheng, S.-Z. Qiao, *Acc. Chem. Res.* **2017**, *50*, 915–923.  
[26] a) R. Aydin, F. Köleli, *Prog. Org. Coat.* **2006**, *56*, 76–80; b) B. Winther-Jensen, K. Fraser, C. Ong, M. Forsyth, D. R. MacFarlane, *Adv. Mater.* **2010**, *22*, 1727–1730.  
[27] a) W. Wang, X. Xu, W. Zhou, Z. Shao, *Adv. Sci.* **2017**, *4*, 1600371; b) J. Liu, D. Zhu, C. Guo, A. Vasileff, S.-Z. Qiao, *Adv. Energy Mater.* **2017**, *7*, 1700518; c) Z. Liang, C. Qu, W. Guo, R. Zou, Q. Xu, *Adv. Mater.* **2018**, *30*, 1702891.  
[28] a) K. Shen, X. Chen, J. Chen, Y. Li, *ACS Catal.* **2016**, *6*, 5887–5903; b) W. Chen, J. Pei, C.-T. He, J. Wan, H. Ren, Y. Wang, J. Dong, K. Wu, W.-C. Cheong, J. Mao, X. Zheng, W. Yan, Z. Zhuang, C. Chen, Q. Peng, D. Wang, Y. Li, *Adv. Mater.* **2018**, *30*, 1800396; c) S. Bhattacharyya, C. Das, T. K. Maji, *RSC Adv.* **2018**, *8*, 26728–26754.  
[29] a) H. B. Wu, X. W. Lou, *Sci. Adv.* **2017**, *3*, eaap9252; b) C. A. Downes, S. C. Marinescu, *ChemSusChem* **2017**, *10*, 4374–4392.  
[30] a) X. Wang, F. Li, W. Li, W. Gao, Y. Tang, R. Li, *J. Mater. Chem. A* **2017**, *5*, 17982–17989; b) Z.-F. Huang, J. Song, K. Li, M. Tahir, Y.-T. Wang, L. Pan, L. Wang, X. Zhang, J.-J. Zou, *J. Am. Chem. Soc.* **2016**, *138*, 1359–1365.

- [31] a) F. Yang, P. Zhao, X. Hua, W. Luo, G. Cheng, W. Xing, S. Chen, *J. Mater. Chem. A* **2016**, *4*, 16057–16063; b) W. Zhou, J. Lu, K. Zhou, L. Yang, Y. Ke, Z. Tang, S. Chen, *Nano Energy* **2016**, *28*, 143–150.
- [32] a) J. Duan, S. Chen, C. Zhao, *Nat. Commun.* **2017**, *8*, 15341; b) M. Zhai, F. Wang, H. Du, *ACS Appl. Mater. Interfaces* **2017**, *9*, 40171–40179.
- [33] a) L. Yan, L. Cao, P. Dai, X. Gu, D. Liu, L. Li, Y. Wang, X. Zhao, *Adv. Funct. Mater.* **2017**, *27*, 1703455; b) E. Zhang, Y. Xie, S. Ci, J. Jia, P. Cai, L. Yi, Z. Wen, *J. Mater. Chem. A* **2016**, *4*, 17288–17298.
- [34] a) T. Wang, Q. Zhou, X. Wang, J. Zheng, X. Li, *J. Mater. Chem. A* **2015**, *3*, 16435–16439; b) C. Sun, Q. Dong, J. Yang, Z. Dai, J. Lin, P. Chen, W. Huang, X. Dong, *Nano Res.* **2016**, *9*, 2234–2243.
- [35] a) F. Ming, H. Liang, H. Shi, X. Xu, G. Mei, Z. Wang, *J. Mater. Chem. A* **2016**, *4*, 15148–15155; b) L. Jiao, Y.-X. Zhou, H.-L. Jiang, *Chem. Sci.* **2016**, *7*, 1690–1695.
- [36] a) D. Sheberla, J. C. Bachman, J. S. Elias, C.-J. Sun, Y. Shao-Horn, M. Dincă, *Nat. Mater.* **2017**, *16*, 220–224; b) T. Kambe, R. Sakamoto, K. Hoshiko, K. Takada, M. Miyachi, J.-H. Ryu, S. Sasaki, J. Kim, K. Nakazato, M. Takata, H. Nishihara, *J. Am. Chem. Soc.* **2013**, *135*, 2462–2465; c) A. A. Talin, A. Centrone, A. C. Ford, M. E. Foster, V. Stavila, P. Haney, R. A. Kinney, V. Szalai, F. El Gabaly, H. P. Yoon, F. Léonard, M. D. Allendorf, *Science* **2014**, *343*, 66–69; d) J. Guo, Y. Xu, S. Jin, L. Chen, T. Kaji, Y. Honsho, M. A. Addicoat, J. Kim, A. Saeki, H. Ihee, S. Seki, S. Irie, M. Hiramoto, J. Gao, D. Jiang, *Nat. Commun.* **2013**, *4*, 2736.
- [37] A. J. Clough, J. W. Yoo, M. H. Mecklenburg, S. C. Marinescu, *J. Am. Chem. Soc.* **2015**, *137*, 118–121.
- [38] C. A. Downes, S. C. Marinescu, *ACS Catal.* **2017**, *7*, 848–854.
- [39] a) R. Dong, Z. Zheng, D. C. Tranca, J. Zhang, N. Chandrasekhar, S. Liu, X. Zhuang, G. Seifert, X. Feng, *Chem. Eur. J.* **2017**, *23*, 2255–2260; b) R. Dong, M. Pfeffermann, H. Liang, Z. Zheng, X. Zhu, J. Zhang, X. Feng, *Angew. Chem. Int. Ed.* **2015**, *54*, 12058–12063; *Angew. Chem.* **2015**, *127*, 12226–12231.
- [40] B. Nohra, H. El Moll, L. M. Rodriguez Albelo, P. Mialane, J. R. M. Marrot, C. Mellot-Draznieks, M. O’Keeffe, N. Ngo Biboum, J. L. Lemaire, B. Keita, L. Nadjo, A. Dolbecq, *J. Am. Chem. Soc.* **2011**, *133*, 13363–13374.
- [41] J.-S. Qin, D.-Y. Du, W. Guan, X.-J. Bo, Y.-F. Li, L.-P. Guo, Z.-M. Su, Y.-Y. Wang, Y.-Q. Lan, H.-C. Zhou, *J. Am. Chem. Soc.* **2015**, *137*, 7169–7177.
- [42] a) Q. Ren, H. Wang, X.-F. Lu, Y.-X. Tong, G.-R. Li, *Adv. Sci.* **2018**, *5*, 1700515; b) H. B. Aiyappa, J. Masa, C. Andronescu, M. Muhler, R. A. Fischer, W. Schuhmann, *Small Methods* **2018**, 1800415.
- [43] a) B. Zhu, R. Zou, Q. Xu, *Adv. Energy Mater.* **2018**, *8*, 1801193; b) B. Zhu, D. Xia, R. Zou, *Coord. Chem. Rev.* **2018**, *376*, 430–448; c) H. Zhang, X. Liu, Y. Wu, C. Guan, A. K. Cheetham, J. Wang, *Chem. Commun.* **2018**, *54*, 5268–5288; d) J. Li, X. Zhang, L. Han, D. Yan, S. Hou, T. Lu, Y. Yao, L. Pan, *J. Mater. Chem. A* **2018**, *6*, 24224–24231.
- [44] C. A. Downes, S. C. Marinescu, *Dalton Trans.* **2016**, *45*, 19311–19321.
- [45] W. Salomon, G. Paille, M. Gomez-Mingot, P. Mialane, J. Marrot, C. Roch-Marchal, G. Nocton, C. Mellot-Draznieks, M. Fontecave, A. Dolbecq, *Cryst. Growth Des.* **2017**, *17*, 1600–1609.
- [46] M. Jahan, Z. Liu, K. P. Loh, *Adv. Funct. Mater.* **2013**, *23*, 5363–5372.
- [47] a) J. Chen, Y. Yang, J. Su, P. Jiang, G. Xia, Q. Chen, *ACS Appl. Mater. Interfaces* **2017**, *9*, 3596–3601; b) A. Aijaz, J. Masa, C. Rösler, W. Xia, P. Weide, R. A. Fischer, W. Schuhmann, M. Muhler, *ChemElectroChem* **2017**, *4*, 188–193.
- [48] a) H. B. Wu, B. Y. Xia, L. Yu, X.-Y. Yu, X. W. Lou, *Nat. Commun.* **2015**, *6*, 6512; b) G. Liu, H. Bai, Y. Ji, L. Wang, Y. Wen, H. Lin, L. Zheng, Y. Li, B. Zhang, H. Peng, *J. Mater. Chem. A* **2019**, *7*, 12434–12439; c) Y. Zhang, X. Xia, X. Cao, B. Zhang, N. H. Tiep, H. He, S. Chen, Y. Huang, H. J. Fan, *Adv. Energy Mater.* **2017**, *7*, 1700220.
- [49] M. Xu, L. Han, Y. Han, Y. Yu, J. Zhai, S. Dong, *J. Mater. Chem. A* **2015**, *3*, 21471–21477.
- [50] W. He, R. Ifraemov, A. Raslin, I. Hod, *Adv. Funct. Mater.* **2018**, *28*, 1707244.
- [51] a) B. Chen, G. Ma, Y. Zhu, J. Wang, W. Xiong, Y. Xia, *J. Power Sources* **2016**, *334*, 112–119; b) Z. Wang, Q. Li, F. Besenbacher, M. Dong, *Adv. Mater.* **2016**, *28*, 10224–10229.
- [52] a) W. Chaikittisilp, K. Ariga, Y. Yamauchi, *J. Mater. Chem. A* **2013**, *1*, 14–19; b) S. Dou, C.-L. Dong, Z. Hu, Y.-C. Huang, J.-I. Chen, L. Tao, D. Yan, D. Chen, S. Shen, S. Chou, S. Wang, *Adv. Funct. Mater.* **2017**, *27*, 1702546.
- [53] a) M. Liu, J. Li, *ACS Appl. Mater. Interfaces* **2016**, *8*, 2158–2165; b) F. Ming, H. Liang, H. Shi, G. Mei, X. Xu, Z. Wang, *Electrochim. Acta* **2017**, *250*, 167–173.
- [54] a) C. Xuan, B. Hou, W. Xia, Z. Peng, T. Shen, H. L. Xin, G. Zhang, D. Wang, *J. Mater. Chem. A* **2018**, *6*, 10731–10739; b) Y. Wang, L. Tao, Z. Xiao, R. Chen, Z. Jiang, S. Wang, *Adv. Funct. Mater.* **2018**, *28*, 1705356.
- [55] C. Guan, X. Liu, A. M. Elshahawy, H. Zhang, H. Wu, S. J. Pennycook, J. Wang, *Nanoscale Horiz.* **2017**, *2*, 342–348.
- [56] a) Q. Shao, J. Yang, X. Huang, *Chem. Eur. J.* **2018**, *24*, 15143–15155; b) K. Jayaramulu, J. Masa, O. Tomanec, D. Peeters, V. Ranc, A. Schneemann, R. Zboril, W. Schuhmann, R. A. Fischer, *Adv. Funct. Mater.* **2017**, *27*, 1700451.
- [57] L. Ai, T. Tian, J. Jiang, *ACS Sustainable Chem. Eng.* **2017**, *5*, 4771–4777.
- [58] L. Li, X. Li, L. Ai, J. Jiang, *RSC Adv.* **2015**, *5*, 90265–90271.
- [59] X. Liang, B. Zheng, L. Chen, J. Zhang, Z. Zhuang, B. Chen, *ACS Appl. Mater. Interfaces* **2017**, *9*, 23222–23229.
- [60] T. Meng, J. Qin, S. Wang, D. Zhao, B. Mao, M. Cao, *J. Mater. Chem. A* **2017**, *5*, 7001–7014.
- [61] Y. Wang, W. Wu, Y. Rao, Z. Li, N. Tsubaki, M. Wu, *J. Mater. Chem. A* **2017**, *5*, 6170–6177.
- [62] Y. Pan, K. Sun, S. Liu, X. Cao, K. Wu, W.-C. Cheong, Z. Chen, Y. Wang, Y. Li, Y. Liu, D. Wang, Q. Peng, C. Chen, Y. Li, *J. Am. Chem. Soc.* **2018**, *140*, 2610–2618.
- [63] L. Yang, L. Zhang, G. Xu, X. Ma, W. Wang, H. Song, D. Jia, *ACS Sustainable Chem. Eng.* **2018**, *6*, 12961–12968.
- [64] H. Sun, Y. Lian, C. Yang, L. Xiong, P. Qi, Q. Mu, X. Zhao, J. Guo, Z. Deng, Y. Peng, *Energy Environ. Sci.* **2018**, *11*, 2363–2371.
- [65] Y. Jiao, Y. Zheng, M. Jaroniec, S. Z. Qiao, *Chem. Soc. Rev.* **2015**, *44*, 2060–2086.
- [66] a) S. Anantharaj, S. R. Ede, K. Sakthikumar, K. Karthick, S. Mishra, S. Kundu, *ACS Catal.* **2016**, *6*, 8069–8097; b) L. Han, S. Dong, E. Wang, *Adv. Mater.* **2016**, *28*, 9266–9291.
- [67] a) J. Suntivich, K. J. May, H. A. Gasteiger, J. B. Goodenough, Y. Shao-Horn, *Science* **2011**, *334*, 1383–1385; b) I. C. Man, H. Y. Su, F. Calle-Vallejo, H. A. Hansen, J. I. Martínez, N. G. Inoglu, J. Kitchin, T. F. Jaramillo, J. K. Nørskov, J. Rossmeisl, *ChemCatChem* **2011**, *3*, 1159–1165.
- [68] W. Lu, Z. Wei, Z.-Y. Gu, T.-F. Liu, J. Park, J. Tian, M. Zhang, Q. Zhang, T. Gentle, III, M. Bosch, H.-C. Zhou, *Chem. Soc. Rev.* **2014**, *43*, 5561–5593.
- [69] F.-L. Li, Q. Shao, X. Huang, J.-P. Lang, *Angew. Chem. Int. Ed.* **2018**, *57*, 1888–1892; *Angew. Chem.* **2018**, *130*, 1906–1910.
- [70] X.-F. Lu, P.-Q. Liao, J.-W. Wang, J.-X. Wu, X.-W. Chen, C.-T. He, J.-P. Zhang, G.-R. Li, X.-M. Chen, *J. Am. Chem. Soc.* **2016**, *138*, 8336–8339.
- [71] a) B. Zhang, X. Zheng, O. Voznyy, R. Comin, M. Bajdich, M. Garcia-Melchor, L. Han, J. Xu, M. Liu, L. Zheng, F. P. Garcia de Arquer, C. T. Dinh, F. Fan, M. Yuan, E. Yassitepe, N. Chen, T. Regier, P. Liu, Y. Li, P. De Luna, A. Janmohamed, H. L. Xin, H. Yang, A. Vojvodic, E. H. Sargent, *Science* **2016**, *352*, 333–337; b) Y.-T. Xu, Z.-M. Ye, J.-W. Ye, L.-M. Cao, R.-K. Huang, J.-X. Wu, D.-D. Zhou, X.-F. Zhang, C.-T. He, J.-P. Zhang, X.-M. Chen, *Angew. Chem. Int. Ed.* **2019**, *58*, 139–143; *Angew. Chem.* **2019**, *131*, 145–149; c) P. F. Liu, S. Yang, L. R. Zheng, B. Zhang, H. G. Yang, *Chem. Sci.* **2017**, *8*, 3484–3488; d) M. Y. Zu, C. Wang, L. Zhang, L. R. Zheng, H. G. Yang, *Mater. Horiz.* **2019**, *6*, 115–121.
- [72] S. Zhao, Y. Wang, J. Dong, C.-T. He, H. Yin, P. An, K. Zhao, X. Zhang, C. Gao, L. Zhang, J. Lv, J. Wang, J. Zhang, A. M. Khatkhat, N. A. Khan, Z. Wei, J. Zhang, S. Liu, H. Zhao, Z. Tang, *Nat. Energy* **2016**, *1*, 16184.
- [73] L. Wang, Y. Wu, R. Cao, L. Ren, M. Chen, X. Feng, J. Zhou, B. Wang, *ACS Appl. Mater. Interfaces* **2016**, *8*, 16736–16743.
- [74] L. Zhao, B. Dong, S. Li, L. Zhou, L. Lai, Z. Wang, S. Zhao, M. Han, K. Gao, M. Lu, X. Xie, B. Chen, Z. Liu, X. Wang, H. Zhang, H. Li, J. Liu, H. Zhang, X. Huang, W. Huang, *ACS Nano* **2017**, *11*, 5800–5807.
- [75] E. A. Flügel, V. W. H. Lau, H. Schlöberg, R. Glaum, B. V. Lotsch, *Chem. Eur. J.* **2016**, *22*, 3676–3680.
- [76] H. Wang, F.-X. Yin, B.-H. Chen, X.-B. He, P.-L. Lv, C.-Y. Ye, D.-J. Liu, *Appl. Catal. B* **2017**, *205*, 55–67.
- [77] J.-Q. Shen, P.-Q. Liao, D.-D. Zhou, C.-T. He, J.-X. Wu, W.-X. Zhang, J.-P. Zhang, X.-M. Chen, *J. Am. Chem. Soc.* **2017**, *139*, 1778–1781.
- [78] F. Dai, W. Fan, J. Bi, P. Jiang, D. Liu, X. Zhang, H. Lin, C. Gong, R. Wang, L. Zhang, D. Sun, *Dalton Trans.* **2016**, *45*, 61–65.
- [79] J. Jiang, L. Huang, X. Liu, L. Ai, *ACS Appl. Mater. Interfaces* **2017**, *9*, 7193–7201.



- [80] P. Manna, J. Debgupta, S. Bose, S. K. Das, *Angew. Chem. Int. Ed.* **2016**, *55*, 2425–2430; *Angew. Chem.* **2016**, *128*, 2471–2476.
- [81] B. Wurster, D. Grumelli, D. Hötger, R. Gutzler, K. Kern, *J. Am. Chem. Soc.* **2016**, *138*, 3623–3626.
- [82] X. He, F. Yin, G. Li, *Int. J. Hydrogen Energy* **2015**, *40*, 9713–9722.
- [83] a) S. Liu, Z. Wang, S. Zhou, F. Yu, M. Yu, C.-Y. Chiang, W. Zhou, J. Zhao, J. Qiu, *Adv. Mater.* **2017**, *29*, 1700874; b) Z. Tao, T. Wang, X. Wang, J. Zheng, X. Li, *ACS Appl. Mater. Interfaces* **2016**, *8*, 35390–35397.
- [84] a) L. Han, X.-Y. Yu, X. W. D. Lou, *Adv. Mater.* **2016**, *28*, 4601–4605; b) Y. Han, J. Zhai, L. Zhang, S. Dong, *Nanoscale* **2016**, *8*, 1033–1039.
- [85] a) K. He, Z. Cao, R. Liu, Y. Miao, H. Ma, Y. Ding, *Nano Res.* **2016**, *9*, 1856–1865; b) W. Li, S. Watzel, H. A. El-Sayed, Y. Liang, G. Kieslich, A. S. Bandarenka, K. Rodewald, B. Rieger, R. A. Fischer, *J. Am. Chem. Soc.* **2019**, *141*, 5926–5933.
- [86] a) J. Qian, T.-T. Li, Y. Hu, S. Huang, *Chem. Commun.* **2017**, *53*, 13027–13030; b) B. Y. Guan, L. Yu, X. W. Lou, *Energy Environ. Sci.* **2016**, *9*, 3092–3096.
- [87] a) M. Liu, W. Zheng, S. Ran, S. T. Boles, L. Y. S. Lee, *Adv. Mater. Interfaces* **2018**, *5*, 1800849; b) M. Shalom, D. Ressnig, X. Yang, G. Clavel, T. P. Fellinger, M. Antonietti, *J. Mater. Chem. A* **2015**, *3*, 8171–8177.
- [88] T. Wu, M. Pi, X. Wang, D. Zhang, S. Chen, *Phys. Chem. Chem. Phys.* **2017**, *19*, 2104–2110.
- [89] Q. Dong, Q. Wang, Z. Dai, H. Qiu, X. Dong, *ACS Appl. Mater. Interfaces* **2016**, *8*, 26902–26907.
- [90] Y. Xu, W. Tu, B. Zhang, S. Yin, Y. Huang, M. Kraft, R. Xu, *Adv. Mater.* **2017**, *29*, 1605957.
- [91] a) Y. Lee, J. Suntivich, K. J. May, E. E. Perry, Y. Shao-Horn, *J. Phys. Chem. Lett.* **2012**, *3*, 399–404; b) J. Zhou, Z. Wang, D. Yang, W. Zhang, Y. Chen, *Electrochim. Acta* **2019**, *317*, 408–415.
- [92] a) Q. Qian, Y. Li, Y. Liu, L. Yu, G. Zhang, *Adv. Mater.* **2019**, *31*, 1901139; b) A. Indra, U. Paik, T. Song, *Angew. Chem. Int. Ed.* **2018**, *57*, 1241–1245; *Angew. Chem.* **2018**, *130*, 1255–1259; c) J. Zhou, Y. Wang, X. Su, S. Gu, R. Liu, Y. Huang, S. Yan, J. Li, S. Zhang, *Energy Environ. Sci.* **2019**, *12*, 739–746; d) K. Rui, G. Zhao, Y. Chen, Y. Lin, Q. Zhou, J. Chen, J. Zhu, W. Sun, W. Huang, S. X. Dou, *Adv. Funct. Mater.* **2018**, *28*, 1801554.
- [93] T. Y. Ma, S. Dai, M. Jaroniec, S. Z. Qiao, *J. Am. Chem. Soc.* **2014**, *136*, 13925–13931.
- [94] X.-Y. Yu, Y. Feng, B. Guan, X. W. Lou, U. Paik, *Energy Environ. Sci.* **2016**, *9*, 1246–1250.
- [95] S. Hou, X. Xu, M. Wang, Y. Xu, T. Lu, Y. Yao, L. Pan, *J. Mater. Chem. A* **2017**, *5*, 19054–19061.
- [96] B. You, N. Jiang, M. Sheng, S. Gul, J. Yano, Y. Sun, *Chem. Mater.* **2015**, *27*, 7636–7642.
- [97] a) D. Kong, J. J. Cha, H. Wang, H. R. Lee, Y. Cui, *Energy Environ. Sci.* **2013**, *6*, 3553–3558; b) Y. Liu, H. Cheng, M. Lyu, S. Fan, Q. Liu, W. Zhang, Y. Zhi, C. Wang, C. Xiao, S. Wei, B. Ye, Y. Xie, *J. Am. Chem. Soc.* **2014**, *136*, 15670–15675.
- [98] J. Zhang, Q. Zhang, X. Feng, *Adv. Mater.* **2019**, *31*, 1808167.
- [99] a) X. Wang, J. Feng, Y. Bai, Q. Zhang, Y. Yin, *Chem. Rev.* **2016**, *116*, 10983–11060; b) Y. Qian, T. An, K. E. Birgersson, Z. Liu, D. Zhao, *Small* **2018**, *14*, 1704169.
- [100] Y. Hou, T. Huang, Z. Wen, S. Mao, S. Cui, J. Chen, *Adv. Energy Mater.* **2014**, *4*, 1400337.
- [101] T. Liu, P. Li, N. Yao, T. Kong, G. Cheng, S. Chen, W. Luo, *Adv. Mater.* **2019**, *31*, 1806672.
- [102] a) S. Liu, H. Zhang, Q. Zhao, X. Zhang, R. Liu, X. Ge, G. Wang, H. Zhao, W. Cai, *Carbon* **2016**, *106*, 74–83; b) X. Zhang, S. Liu, Y. Zang, R. Liu, G. Liu, G. Wang, Y. Zhang, H. Zhang, H. Zhao, *Nano Energy* **2016**, *30*, 93–102.
- [103] a) L. Li, P. Dai, X. Gu, Y. Wang, L. Yan, X. Zhao, *J. Mater. Chem. A* **2017**, *5*, 789–795; b) R. Bai, M. Yang, G. Hu, L. Xu, X. Hu, Z. Li, S. Wang, W. Dai, M. Fan, *Carbon* **2015**, *81*, 465–473; c) Y. Liu, X. Xu, M. Wang, T. Lu, Z. Sun, L. Pan, *Chem. Commun.* **2015**, *51*, 12020–12023.
- [104] Y. Qian, Z. Hu, X. Ge, S. Yang, Y. Peng, Z. Kang, Z. Liu, J. Y. Lee, D. Zhao, *Carbon* **2017**, *111*, 641–650.
- [105] S. Fu, C. Zhu, J. Song, D. Du, Y. Lin, *Adv. Energy Mater.* **2017**, *7*, 1700363.
- [106] a) K. Zhang, W. Guo, Z. Liang, R. Zou, *Sci. China Chem.* **2019**, *62*, 417–429; b) F. Sun, Q. Li, H. Xue, H. Pang, *ChemElectroChem* **2019**, *6*, 1273–1299.
- [107] a) X. Ge, A. Sumboja, D. Wu, T. An, B. Li, F. W. T. Goh, T. S. A. Hor, Y. Zong, Z. Liu, *ACS Catal.* **2015**, *5*, 4643–4667; b) A. Kulkarni, S. Siahrostami, A. Patel, J. K. Nørskov, *Chem. Rev.* **2018**, *118*, 2302–2312.
- [108] a) L. Li, J. He, Y. Wang, X. Lv, X. Gu, P. Dai, D. Liu, X. Zhao, *J. Mater. Chem. A* **2019**, *7*, 1964–1988; b) L. Yang, X. Zeng, W. Wang, D. Cao, *Adv. Funct. Mater.* **2018**, *28*, 1704537; c) Y. Qian, I. A. Khan, D. Zhao, *Small* **2017**, *13*, 1701143.
- [109] a) K. Zhang, X. Han, Z. Hu, X. Zhang, Z. Tao, J. Chen, *Chem. Soc. Rev.* **2015**, *44*, 699–728; b) J. Zhang, Z. Xia, L. Dai, *Sci. Adv.* **2015**, *1*, e1500564; c) J. Suntivich, H. A. Gasteiger, N. Yabuuchi, H. Nakanishi, J. B. Goodenough, Y. Shao-Horn, *Nat. Chem.* **2011**, *3*, 546.
- [110] a) H. — x. Zhong, J. Wang, Y.-w. Zhang, W.-l. Xu, W. Xing, D. Xu, Y.-f. Zhang, X.-b. Zhang, *Angew. Chem. Int. Ed.* **2014**, *53*, 14235–14239; *Angew. Chem.* **2014**, *126*, 14459–14463; b) P. Zhang, F. Sun, Z. Xiang, Z. Shen, J. Yun, D. Cao, *Energy Environ. Sci.* **2014**, *7*, 442–450; c) M. Zhang, Q. Dai, H. Zheng, M. Chen, L. Dai, *Adv. Mater.* **2018**, *30*, 1705431; d) L. Zhang, X. Wang, R. Wang, M. Hong, *Chem. Mater.* **2015**, *27*, 7610–7618.
- [111] J. Mao, L. Yang, P. Yu, X. Wei, L. Mao, *Electrochem. Commun.* **2012**, *19*, 29–31.
- [112] M. Jahan, Q. Bao, K. P. Loh, *J. Am. Chem. Soc.* **2012**, *134*, 6707–6713.
- [113] W.-H. Li, J. Lv, Q. Li, J. Xie, N. Ogiwara, Y. Huang, H. Jiang, H. Kitagawa, G. Xu, Y. Wang, *J. Mater. Chem. A* **2019**, *7*, 10431–10438.
- [114] E. M. Miner, T. Fukushima, D. Sheberla, L. Sun, Y. Surendranath, M. Dincă, *Nat. Commun.* **2016**, *7*, 10942.
- [115] a) I. Hod, P. Deria, W. Bury, J. E. Mondloch, C.-W. Kung, M. So, M. D. Sampson, A. W. Peters, C. P. Kubiak, O. K. Farha, J. T. Hupp, *Nat. Commun.* **2015**, *6*, 8304; b) J. Cao, C. Lei, J. Yang, X. Cheng, Z. Li, B. Yang, X. Zhang, L. Lei, Y. Hou, K. Ostrikov, *J. Mater. Chem. A* **2018**, *6*, 18877–18883.
- [116] H. Wang, F. Yin, B. Chen, G. Li, *J. Mater. Chem. A* **2015**, *3*, 16168–16176.
- [117] M. Jiang, L. Li, D. Zhu, H. Zhang, X. Zhao, *J. Mater. Chem. A* **2014**, *2*, 5323–5329.
- [118] S. Sohrabi, S. Dehghanpour, M. Ghalkhani, *ChemCatChem* **2016**, *8*, 2356–2366.
- [119] K. Cho, S.-H. Han, M. P. Suh, *Angew. Chem. Int. Ed.* **2016**, *55*, 15301–15305; *Angew. Chem.* **2016**, *128*, 15527–15531.
- [120] M. Lions, J. B. Tommasino, R. Chattot, B. Abeykoon, N. Guillou, T. Devic, A. Demessence, L. Cardenas, F. Maillard, A. Fateeva, *Chem. Commun.* **2017**, *53*, 6496–6499.
- [121] G. Chen, J. Zhang, F. Wang, L. Wang, Z. Liao, E. Zschech, K. Müllen, X. Feng, *Chem. Eur. J.* **2018**, *24*, 18413–18418.
- [122] a) X. Wang, J. Zhou, H. Fu, W. Li, X. Fan, G. Xin, J. Zheng, X. Li, *J. Mater. Chem. A* **2014**, *2*, 14064–14070; b) Q. Lai, L. Zheng, Y. Liang, J. He, J. Zhao, J. Chen, *ACS Catal.* **2017**, *7*, 1655–1663; c) T. Liu, P. Zhao, X. Hua, W. Luo, S. Chen, G. Cheng, *J. Mater. Chem. A* **2016**, *4*, 11357–11364; d) P. Yin, T. Yao, Y. Wu, L. Zheng, Y. Lin, W. Liu, H. Ju, J. Zhu, X. Hong, Z. Deng, G. Zhou, S. Wei, Y. Li, *Angew. Chem. Int. Ed.* **2016**, *55*, 10800–10805; *Angew. Chem.* **2016**, *128*, 10958–10963; e) Y. Chen, S. Ji, Y. Wang, J. Dong, W. Chen, Z. Li, R. Shen, L. Zheng, Z. Zhuang, D. Wang, Y. Li, *Angew. Chem. Int. Ed.* **2017**, *56*, 6937–6941; *Angew. Chem.* **2017**, *129*, 7041–7045; f) J. Guo, Y. Li, Y. Cheng, L. Dai, Z. Xiang, *ACS Nano* **2017**, *11*, 8379–8386; g) K. Strickland, E. Miner, Q. Jia, U. Tylus, N. Ramaswamy, W. Liang, M.-T. Sougrati, F. Jaouen, S. Mukerjee, *Nat. Commun.* **2015**, *6*, 7343.
- [123] a) S. Gadipelli, T. Zhao, S. A. Shevlin, Z. Guo, *Energy Environ. Sci.* **2016**, *9*, 1661–1667; b) J. Wang, W. Liu, G. Luo, Z. Li, C. Zhao, H. Zhang, M. Zhu, Q. Xu, X. Wang, C. Zhao, Y. Qu, Z. Yang, T. Yao, Y. Li, Y. Lin, Y. Wu, Y. Li, *Energy Environ. Sci.* **2018**, *11*, 3375–3379.
- [124] a) Y. He, S. Hwang, D. A. Cullen, M. A. Uddin, L. Langhorst, B. Li, S. Karakalos, A. J. Kropf, E. C. Wegener, J. Sokolowski, M. Chen, D. Myers, D. Su, K. L. More, G. Wang, S. Litster, G. Wu, *Energy Environ. Sci.* **2019**, *12*, 250–260; b) Q. Li, H. Pan, D. Higgins, R. Cao, G. Zhang, H. Lv, K. Wu, J. Cho, G. Wu, *Small* **2015**, *11*, 1443–1452; c) H. Zhang, S. Hwang, M. Wang, Z. Feng, S. Karakalos, L. Luo, Z. Qiao, X. Xie, C. Wang, D. Su, Y. Shao, G. Wu, *J. Am. Chem. Soc.* **2017**, *139*, 14143–14149.
- [125] a) T. Sun, S. Zhang, L. Xu, D. Wang, Y. Li, *Chem. Commun.* **2018**, *54*, 12101–12104; b) H. Hu, L. Han, M. Yu, Z. Wang, X. W. Lou, *Energy Environ. Sci.* **2016**, *9*, 107–111; c) B. Y. Xia, Y. Yan, N. Li, H. B. Wu, X. W. Lou, X. Wang, *Nat. Energy* **2016**, *1*, 15006.

- [126] a) H. Zhu, J. Yin, X. Wang, H. Wang, X. Yang, *Adv. Funct. Mater.* **2013**, *23*, 1305–1312; b) Y. J. Sa, C. Park, H. Y. Jeong, S.-H. Park, Z. Lee, K. T. Kim, G.-G. Park, S. H. Joo, *Angew. Chem. Int. Ed.* **2014**, *53*, 4102–4106; *Angew. Chem.* **2014**, *126*, 4186–4190; c) X. Liu, L. Dai, *Nat. Rev. Mater.* **2016**, *1*, 16064.
- [127] L. Zhang, Z. Su, F. Jiang, L. Yang, J. Qian, Y. Zhou, W. Li, M. Hong, *Nano-scale* **2014**, *6*, 6590–6602.
- [128] a) J.-S. Li, S.-L. Li, Y.-J. Tang, K. Li, L. Zhou, N. Kong, Y.-Q. Lan, J.-C. Bao, Z.-H. Dai, *Sci. Rep.* **2014**, *4*, 5130; b) J. Li, Y. Chen, Y. Tang, S. Li, H. Dong, K. Li, M. Han, Y.-Q. Lan, J. Bao, Z. Dai, *J. Mater. Chem. A* **2014**, *2*, 6316–6319; c) Y. A. Fu, Y. Huang, Z. Xiang, G. Liu, D. Cao, *Eur. J. Inorg. Chem.* **2016**, 2100–2105; d) Y. Zheng, Y. Jiao, L. Ge, M. Jaroniec, S. Z. Qiao, *Angew. Chem. Int. Ed.* **2013**, *52*, 3110–3116; *Angew. Chem.* **2013**, *125*, 3192–3198.
- [129] Y.-Z. Chen, C. Wang, Z.-Y. Wu, Y. Xiong, Q. Xu, S.-H. Yu, H.-L. Jiang, *Adv. Mater.* **2015**, *27*, 5010–5016.
- [130] L. Shang, H. Yu, X. Huang, T. Bian, R. Shi, Y. Zhao, G. I. N. Waterhouse, L.-Z. Wu, C.-H. Tung, T. Zhang, *Adv. Mater.* **2016**, *28*, 1668–1674.
- [131] B. You, N. Jiang, M. Sheng, W. S. Drisdell, J. Yano, Y. Sun, *ACS Catal.* **2015**, *5*, 7068–7076.
- [132] A. Aijaz, N. Fujiwara, Q. Xu, *J. Am. Chem. Soc.* **2014**, *136*, 6790–6793.
- [133] Y. Li, Z. Yan, Q. Wang, H. Ye, M. Li, L. Zhu, X. Cao, *Electrochim. Acta* **2018**, *282*, 224–232.
- [134] S. Pandiaraj, H. B. Aiyappa, R. Banerjee, S. Kurungot, *Chem. Commun.* **2014**, *50*, 3363–3366.
- [135] a) C. Mora, D. Spirandelli, E. C. Franklin, J. Lynham, M. B. Kantar, W. Miles, C. Z. Smith, K. Freel, J. Moy, L. V. Louis, E. W. Barba, K. Bettinger, A. G. Frazier, J. F. Colburn, N. Hanasaki, E. Hawkins, Y. Hirabayashi, W. Knorr, C. M. Little, K. Emanuel, J. Sheffield, J. A. Patz, C. L. Hunter, *Nat. Clim. Change* **2018**, *8*, 1062–1071; b) J. P. Gattuso, A. Magnan, R. Billé, W. W. L. Cheung, E. L. Howes, F. Joos, D. Allemand, L. Bopp, S. R. Cooley, C. M. Eakin, O. Hoegh-Guldberg, R. P. Kelly, H. O. Pörtner, A. D. Rogers, J. M. Baxter, D. Laffoley, D. Osborn, A. Rankovic, J. Rochette, U. R. Sumaila, S. Treyer, C. Turley, *Science* **2015**, *349*, aac4722.
- [136] a) S. C. Lewis, S. E. Perkins-Kirkpatrick, G. Althor, A. D. King, L. Kemp, *Geophys. Res. Lett.* **2019**, *46*, 3936–3943; b) A. K. Qaroush, H. S. Alshamaly, S. S. Alazzeq, R. H. Abeskhran, K. I. Assaf, A. A. F. Eftaiha, *Chem. Sci.* **2018**, *9*, 1088–1100.
- [137] D. F. Gao, R. M. Aran-Ais, H. S. Jeon, B. R. Cuenya, *Nat. Catal.* **2019**, *2*, 198–210.
- [138] T. Yu, Y. Chen, *Sci. Total Environ.* **2019**, *655*, 865–879.
- [139] Y. Kuramochi, O. Ishitani, H. Ishida, *Coord. Chem. Rev.* **2018**, *373*, 333–356.
- [140] D. Roman-Gonzalez, A. Moro, F. Burgoa, E. Pérez, A. Nieto-Márquez, Á. Martín, M. D. Bermejo, *J. Supercrit. Fluids* **2018**, *140*, 320–328.
- [141] F. N. Al-Rowaili, A. Jamal, M. S. Ba Shammakh, A. Rana, *ACS Sustainable Chem. Eng.* **2018**, *6*, 15895–15914.
- [142] a) C. A. Trickett, A. Helal, B. A. Al-Maythalyon, Z. H. Yamani, K. E. Cordova, O. M. Yaghi, *Nat. Rev. Mater.* **2017**, *2*, 17045.
- [143] a) W. Xia, A. Mahmood, R. Zou, Q. Xu, *Energy Environ. Sci.* **2015**, *8*, 1837–1866; b) H. Wang, Q.-L. Zhu, R. Zou, Q. Xu, *Chem* **2017**, *2*, 52–80; c) C. S. Diercks, Y. Liu, K. E. Cordova, O. M. Yaghi, *Nat. Mater.* **2018**, *17*, 301–307.
- [144] H. B. Gray, *Nat. Chem.* **2009**, *1*, 7.
- [145] I. Hod, M. D. Sampson, P. Deria, C. P. Kubiak, O. K. Farha, J. T. Hupp, *ACS Catal.* **2015**, *5*, 6302–6309.
- [146] Y. Wang, P. Hou, Z. Wang, P. Kang, *ChemPhysChem* **2017**, *18*, 3142–3147.
- [147] N. Kornienko, Y. Zhao, C. S. Kley, C. Zhu, D. Kim, S. Lin, C. J. Chang, O. M. Yaghi, P. Yang, *J. Am. Chem. Soc.* **2015**, *137*, 14129–14135.
- [148] B.-X. Dong, S.-L. Qian, F.-Y. Bu, Y.-C. Wu, L.-G. Feng, Y.-L. Teng, W.-L. Liu, Z.-W. Li, *ACS Appl. Energy Mater.* **2018**, *1*, 4662–4669.
- [149] S. Dou, J. Song, S. Xi, Y. Du, J. Wang, Z.-F. Huang, Z. J. Xu, X. Wang, *Angew. Chem. Int. Ed.* **2019**, *58*, 4041–4045; *Angew. Chem.* **2019**, *131*, 4081–4085.
- [150] See ref. 11b.
- [151] C.-W. Kung, C. O. Audu, A. W. Peters, H. Noh, O. K. Farha, J. T. Hupp, *ACS Energy Lett.* **2017**, *2*, 2394–2401.
- [152] S.-Y. Zhang, Y.-Y. Yang, Y.-Q. Zheng, H.-L. Zhu, *J. Solid State Chem.* **2018**, *263*, 44–51.
- [153] C. Zhao, X. Dai, T. Yao, W. Chen, X. Wang, J. Wang, J. Yang, S. Wei, Y. Wu, Y. Li, *J. Am. Chem. Soc.* **2017**, *139*, 8078–8081.
- [154] R. Wang, X. Sun, S. Ould-Chikh, D. Osadchii, F. Bai, F. Kapteijn, J. Gascon, *ACS Appl. Mater. Interfaces* **2018**, *10*, 14751–14758.
- [155] Y. Ye, F. Cai, H. Li, H. Wu, G. Wang, Y. Li, S. Miao, S. Xie, R. Si, J. Wang, X. Bao, *Nano Energy* **2017**, *38*, 281–289.
- [156] X. Wang, Z. Chen, X. Zhao, T. Yao, W. Chen, R. You, C. Zhao, G. Wu, J. Wang, W. Huang, J. Yang, X. Hong, S. Wei, Y. Wu, Y. Li, *Angew. Chem. Int. Ed.* **2018**, *57*, 1944–1948; *Angew. Chem.* **2018**, *130*, 1962–1966.
- [157] J. L. C. Rowsell, O. M. Yaghi, *Microporous Mesoporous Mater.* **2004**, *73*, 3–14.
- [158] See ref. 147.
- [159] Z.-X. Cai, Z.-L. Wang, J. Kim, Y. Yamauchi, *Adv. Mater.* **2019**, *31*, 1804903.
- [160] R. Hinogami, S. Yotsuhashi, M. Deguchi, Y. Zenitani, H. Hashiba, Y. Yamada, *ECS Electrochem. Lett.* **2012**, *1*, H17–H19.
- [161] R. Senthil Kumar, S. Senthil Kumar, M. Anbu Kulandainathan, *Electrochim. Commun.* **2012**, *25*, 70–73.
- [162] M. Perfecto-Irigaray, J. Albo, G. Beobide, O. Castillo, A. Irabien, S. Pérez-Yáñez, *RSC Adv.* **2018**, *8*, 21092–21099.
- [163] X. Kang, Q. Zhu, X. Sun, J. Hu, J. Zhang, Z. Liu, B. Han, *Chem. Sci.* **2016**, *7*, 266–273.
- [164] Y. L. Qiu, H. X. Zhong, T. T. Zhang, W. B. Xu, P. P. Su, X. F. Li, H. M. Zhang, *ACS Appl. Mater. Interfaces* **2018**, *10*, 2480–2489.
- [165] D. H. Nam, O. S. Bushuyev, J. Li, P. De Luna, A. Seifitokaldani, C. T. Dinh, F. P. Garcia de Arquer, Y. Wang, Z. Liang, A. H. Proppe, C. S. Tan, P. Todorovic, O. Shekhah, C. M. Gabardo, J. W. Jo, J. Choi, M. J. Choi, S. W. Baek, J. Kim, D. Sinton, S. O. Kelley, M. Eddaoudi, E. H. Sargent, *J. Am. Chem. Soc.* **2018**, *140*, 11378–11386.
- [166] J. Albo, D. Vallejo, G. Beobide, O. Castillo, P. Castaño, A. Irabien, *ChemSusChem* **2017**, *10*, 1100–1109.
- [167] J.-X. Wu, S.-Z. Hou, X.-D. Zhang, M. Xu, H.-F. Yang, P.-S. Cao, Z.-Y. Gu, *Chem. Sci.* **2019**, *10*, 2199–2205.
- [168] X. Tan, C. Yu, C. Zhao, H. Huang, X. Yao, X. Han, W. Guo, S. Cui, H. Huang, J. Qiu, *ACS Appl. Mater. Interfaces* **2019**, *11*, 9904–9910.
- [169] K. Zhao, Y. Liu, X. Quan, S. Chen, H. Yu, *ACS Appl. Mater. Interfaces* **2017**, *9*, 5302–5311.
- [170] M. K. Kim, H. J. Kim, H. Lim, Y. Kwon, H. M. Jeong, *Electrochim. Acta* **2019**, *306*, 28–34.
- [171] A. E. Baumann, D. A. Burns, B. Liu, V. S. Thoi, *Commun. Chem.* **2019**, *2*, 86.
- [172] P. De Luna, C. Hahn, D. Higgins, S. A. Jaffer, T. F. Jaramillo, E. H. Sargent, *Science* **2019**, *364*, eaav3506.
- [173] A. Ganassin, A. Maljusch, V. Colic, L. Spanier, K. Brandl, W. Schuhmann, A. Bandarenka, *ACS Catal.* **2016**, *6*, 3017–3024.

Manuscript received: May 31, 2019

Revised manuscript received: August 12, 2019

Version of record online: September 5, 2019